DISSERTATION ABSTRACT

The increasing concentration of heavy metals in the environment poses a threat due to the possibility of their migration along the levels of the food chain and, consequently, accumulation in the human body. Therefore, their recycling from aquatic environments has become a very important area a lot of scientific research.

An alternative to conventional purification technologies is the adsorption process, especially using magnetic nanoparticles Fe_3O_4, due to easy and quick isolation using an external magnetic field. Many functionalized $Fe_3O_4@SiO_2$ structures are known, but the search for new and selective composites for the heavy metal ions removal is still developed.

The main goal of the doctoral thesis research was to investigate the binding capacity towards selected heavy metal ions (Cd^{2+}, Pb^{2+}, Cu^{2+}) of a functionalized nanoparticles series based on the magnetic core, symbolised $Fe_3O_4@SiO_2$-R: $Fe_3O_4@SiO_2$-EDTA, $Fe_3O_4@SiO_2$-N_1, $Fe_3O_4@$ SiO_2-N_2, $Fe_3O_4@SiO_2$-N_3 and $Fe_3O_4@SiO_2$-cyclen.

During the doctoral thesis research tasks implementation, the synthesis of the indicated nanocomposites was carried out. Then, the obtained structures were characterized using techniques such as: SEM, TEM, XPS, XRD, FT-IR and zeta potential and WCA measurements. The results of the tests confirmed the effectiveness of the synthesis process and proved the presence of characteristic functional groups on the surface of the obtained nanomaterials. Moreover, the results of zeta potential measurements indicate that all analysed nanostructures are characterized by moderate stability of their colloid in water. Furthermore, the WCA measurement indicates that the tested nanoparticles form a hydrophilic film on the surface of the glass plate (WCA < 90º).

The binding capacity of nanoparticles was determined using the DPASV technique and HDME by stripping method. Electrochemical research has clearly shown that the external functional groups present on the nanocomposites surface are responsible for the ions binding, the nanoparticles lose their activity during storing in the electrolyte solution, and the time necessary to establish equilibrium in the solution after adding a portion of nanoparticles is approximately 20 minutes.

Determining the heavy metal ions binding capacity in the solution by $Fe_3O_4@SiO_2$-R nanoparticles showed that all the tested nanostructures can be used to bind selected ions. Nevertheless, $Fe_3O_4@SiO_2$-cyclen nanoparticles can be considered a

universal adsorbent because they showed a similar binding degree to all tested ions. While Fe_3O_4@SiO_2-N_3 nanoparticles showed selectivity towards Cu^{2+} ions. Additionally, the possibility of practical use of the tested nanomaterials for the isolation of metal ions from an aqueous solution was proven.

The implementation of the aim of the work and the doctoral thesis research tasks expanded the scope of useful knowledge necessary to design and obtain an effective nanoadsorbent based on magnetic iron oxide Fe_3O_4.

MATERIAŁY DODATKOWE

W materiałach dodatkowych, po każdym z załączników dołączono rysunki zawarte w publikacjach w oryginalnym rozmiarze, w celu lepszego uwidocznienia wyników pomiarowych.

1. Załącznik 1

Full Paper Wiley Online Library ELECTROANALYSIS

DOI: 10.1002/elan.201900616

Comparison of Cadmium Cd^{2+} and Lead Pb^{2+} Binding by Fe_2O_3@SiO_2-EDTA Nanoparticles – Binding Stability and Kinetic Studies

Amanda Kulpa,[a] Jacek Ryl,[b] Grzegorz Skowierzak,[a] Adrian Koterwa,[a] Grzegorz Schroeder,[c] Tadeusz Ossowski,[a] and Paweł Niedziałkowski*[a]

Abstract: This study describes the synthesis and characterization of ethylenediaminetetraacetic acid (EDTA) functionalized magnetic nanoparticles of 20 nm in size – Fe_3O_4@SiO_2-EDTA – which were used as a novel magnetic adsorbent for Cd(II) and Pb(II) binding in aqueous medium. These nanoparticles were obtained in two-stage synthesis: covering by tetraethyl orthosilicate and functionalization with EDTA derivatives. Nanoparticles were characterized using TEM, FT-IR, and XPS methods. Metal ions were detected under optimized experimental conditions using Differential Pulse Anodic Stripping Voltammetry (DPASV) and Hanging Mercury Drop Electrode (HDME) techniques. We compared the ability of Fe_3O_4@SiO_2-EDTA to bind cadmium and lead in concentration of 553.9 $\mu g L^{-1}$ and 647.5 $\mu g L^{-1}$, respectively. Obtained results show that the adsorption rate of cadmium binding was very high. The equilibrium for Fe_3O_4@SiO_2-EDTA-Cd(II) was reached within 19 min while for the Fe_3O_4@SiO_2-EDTA-Pb(II) was reached within 25 minutes. About 2 mg of nanoparticles was enough to bind 87.5 % Cd(II) and 54.1 % Pb(II) content. In the next step the binding capacity of Fe_3O_4@SiO_2-EDTA nanoparticles was determined. Only 1.265 mg of Fe_3O_4@SiO_2-EDTA was enough to bind 96.14 % cadmium ions while 5.080 mg of nanoparticles bound 40.83 % lead ions. This phenomenon proves that the studied nanoparticles bind Cd(II) much better than Pb(II). The cadmium ions binding capacity of Fe_3O_4@SiO_2-EDTA nanoparticles decreased during storage in 0.5 M KCl solution. Two days of Fe_3O_4@SiO_2-EDTA storage in KCl solution caused the 32 % increase in the amount of nanoparticles required to bind 60 % of cadmium while eight-days storage caused further increase to 328 %. The performed experiment confirmed that the storage of nanoparticles in solution without any surfactants reduced their binding capacity. The best binding capacity was observed for the nanoparticles prepared directly before the electrochemical measurements.

Keywords: Fe_3O_4 nanoparticles · EDTA · surface modification of Fe_3O_4 · silanization · cadmium determination

1 Introduction

Nowadays, environmental contamination by heavy metals has become one of the most important problems. Heavy metals are known as naturally occurring compounds, but the anthropogenic activities enhance their distribution in the environment. Undesirable human activity leads to their bioaccumulation in the food chains [1].

The most common heavy metal pollutants are lead, mercury, nickel, chromium, and zinc, but cadmium is regarded as the most widespread in the environment [2]. Cadmium and lead ions have negative influence on bones, liver, kidneys, lungs, brain, immunological and cardiovascular systems.

In human body, cadmium is accumulated in the kidneys and liver. Additionally, cadmium can also be found in the testes [3]. High level of cadmium concentration leads to the destruction of glomeruli and renal tubules, anaemia, bone diseases such as osteoporosis, disturbances of smell, and proteinuria [4]. Moreover, presence of cadmium ions reduces insulin secretion, affects the circulatory system, and increases lipid oxidation in the human body [5]. Cadmium induces cell death by apoptosis in the cerebral cortex [6].

In the body, lead is accumulated in soft tissues such as the liver, kidneys, lungs, brain, spleen, muscles, and heart by the blood transport. Lead is second in the list of toxic substances in the environment due to its wide distribution. Its accumulation in organism leads to saturnism [7] which causes the damage of liver and kidney [8] and reduces

[a] A. Kulpa, G. Skowierzak, A. Koterwa, T. Ossowski, P. Niedziałkowski
Department of Analytical Chemistry, Faculty of Chemistry, University of Gdansk, Wita Stwosza 63, 80-308 Gdansk, Gdansk (Poland)
E-mail: pawel.niedzialkowski@ug.edu.pl
[b] J. Ryl
Department of Electrochemistry, Corrosion and Materials Engineering, Faculty of Chemistry, Gdansk University of Technology, Narutowicza 11/12, 80-233 Gdansk, (Poland)
[c] G. Schroeder
Faculty of Chemistry, Adam Mickiewicz University in Poznan, University of Poznan 8, 61-614 Poznan, Poland

activities of glucose metabolism key enzymes in the brain [9].

Discovery of new, cheap, and waste-free analytical methods of determination and detection of cadmium ions in environmental samples is a great challenge. Many detection techniques have been developed for the heavy metal ion detection including: Atomic Absorption Spectroscopy (AAS) [10], Inductive Couple Plasma-Mass Spectroscopy (ICP-MS) [11], ion chromatography [12], neutron activation analysis [13], X-ray fluorescence spectroscopy (XRF) [14], and High Resolution Differential Surface Plasmon Resonance (SPR) [15].

Furthermore, electrochemical methods are often utilized for the measurement of heavy metal ions in the environment. The main advantages of these methods are simultaneous detection of multiple heavy metal ions and low detection limit capabilities [16].

The most common method used for the determination of cadmium is Differential Pulse Anodic Stripping Voltammetry (DPASV) using various electrodes such as: modified Glassy Carbon electrode (GC) [17], Hanging Mercury Drop Electrode (HMDE), a mercury film-coated electrode [18], or Boron Doped Diamond (BDD) electrode [19].

Recently, magnetic nanomaterials based on Fe_3O_4 have found many important applications in the industrial areas such as lithium-ion batteries [20,21], catalytic sorption [22] microwave absorption [23], or photocatalytic degradation [24,25]. Multifunctional magnetic nanomaterials are also extensively used in the biomedicine [23]. The most promising applications for these nanomaterials are photothermal killing of breast cancer cells [28], cell targeting and sorting [29,30], and drug delivery vehicles [31,32]. Additionally, these molecules are used in magnetic resonance [33,34] and fluorescence imaging [35,36].

Magnetic Fe_3O_4 nanoparticles can be obtained using different types of synthesis methods including: coprecipitation [37], sonochemical reaction [38], hydrothermal reaction [39], microemulsion and sol-gel synthesis [40,41], or cathodic electrochemical deposition [42]. An important characteristics of the magnetite nanoparticles is the capability of the surface modification with variety of functional groups, what enhances their applicability [43–45]. Modified surface magnetic iron oxide nanoparticles exhibit large surface area ratio toward volume and possess the ability to adsorb heavy metals in an aqueous medium throughout physical and chemical interactions [46].

Ethylenediaminetetraacetic acid (EDTA) in analytical chemistry is successfully used for the determination of many metal ions. EDTA can be also used to modify Fe_3O_4 nanoparticles to obtain superparamagnetic materials applicable for the studies on the adsorption of heavy metals [47]. Fe_3O_4@SiO_2-EDTA nanoparticles were previously obtained and they possess many advantages in comparison to EDTA. These superparamagnetic iron oxide nanoparticles have been applied as an efficient adsorbent for: methylene blue and brilliant green dyes removal from aqueous media [48], separation of rare earths [49], Cu(II), Ca(II) [50–52], Cd(II), Pb(II) [53,54], Ag(I), Mn(II), and Zn(II) [55] removal from an aqueous solution, and Hg(II) removal from an aqueous solution and crude petroleum samples [56].

In presented studies, we present a novel application approach of Fe_3O_4@SiO_2-EDTA for the cadmium detection in aqueous solution. We also compared the ability of Fe_3O_4@SiO_2-EDTA to bind cadmium and lead in minimum concentration.

The separation heavy metals with usage of magnetic nanomaterials predominant over non-magnetic materials due to the quickness and effectiveness of separation process from the medium. This work provide information about the ability of Fe_3O_4@SiO_2-EDTA to bind cadmium and lead in order to removal them from aqueous solution by application of external magnetic field.

According to our knowledge, our study reports the electroanalytical measurements including DPV method on Hanging Drop Mercury Electrode (HDME) for the first time in the literature. Regardless of the toxicity of mercury, HDME electrode is commonly accepted in the laboratory conditions due to the repeatable and reproducible measuring results. The main reason to use this electrode was its self-renewing surface which is not available in the case of solid electrodes. Moreover, there was no risk of the electrode surface modification during each measurement.

2 Experimental

2.1 Materials

The organic solvents, potassium chloride KCl (99.9 %), cadmium nitrate tetrahydrate $Cd(NO)_3 \cdot 4H_2O$ (99.9 %), and lead nitrate $Pb(NO_3)_2$ were purchased from POCh (Poland). All chemicals applied in electrochemical measurements were used as received without further purification. Tetraethyl orthosilicate (98 %) (TEOS) and N-[(3-Trimethoxysilyl)propyl] ethylenediamine triacetic acid trisodium salt (45 %) in water were purchased from Sigma-Aldrich. Aqueous solutions were prepared using ultra-pure deionized water.

2.2 Synthesis

2.2.1 Synthesis of Fe_3O_4@SiO_2

Fe_3O_4@SiO_2 nanoparticles were obtained in three steps of synthesis. In first stage, Fe_3O_4 nanoparticles were obtained using co-precipitation method without any surfactants [57]. Then, Fe_3O_4 surface was modified by tetraethyl orthosilicate and N-[(3-trimethoxysilyl)propyl]ethylenediamine according to the procedure described below.

The 15 mL mixture of 0.02 M $FeCl_2$ and 0.04 M $FeCl_3$ ($[Fe^{2+}]:[Fe^{3+}] = 1:2$) was stirred in a flask under nitrogen. This was followed by the addition of 0.6 mL of 28 % ammonia solution. Upon sonication for 10 min, the reaction mixture was heated to 80 °C for 60 min. Under a

neodymium magnet, the product was separated from the solution and washed until the solution reached neutral pH. In this method, Fe_3O_4 nanoparticles with a diameter of about 20 nm were obtained.

In the next process, the nanoparticles were silanized. Fe_3O_4@SiO_2 was prepared according to the Stöber method [58]. Tetraethyl orthosilicate (TEOS) was dissolved in ethanol (0.1 mL TEOS per 1 mL of ethanol). TEOS solution was slowly added to a stable suspension of Fe_3O_4 (15 mL per 1 g of Fe_3O_4), adjusted by ammonia solution to pH 11, and then the mixture was stirred overnight. The product Fe_3O_4@SiO_2 was magnetically collected, washed several times with water, and finally dried at 60 °C.

2.2.2 Synthesis of Fe_3O_4@SiO_2-EDTA Nanoparticles

1 g of Fe_3O_4@SiO_2 was added to 50 mL of water and the suspension was sonicated for 30 min. 0.4 g of N-[(3-Trimethoxysilyl)propyl] ethylenediamine triacetic acid trisodium salt (45 %) in water was added to the suspension and 0.5 mL of ammonia was slowly added. The suspension was then stirred for 24 h. The product Fe_3O_4@SiO_2-EDTA was magnetically collected, washed several times with water, 0.05 M HCl, water, ethanol, and finally dried at 40 °C. Modified Fe_3O_4@SiO_2-EDTA magnetite nanoparticles were obtained. The loading of carboxyl groups present in Fe_3O_4@SiO_2-EDTA nanoparticles were determined using acid-base titration method from 0.098 mmol/g to 0.110 mmol/g [59].

2.3 Fe_3O_4@SiO_2-EDTA Characterisation

Transmission electron microscopy (TEM) images of the Fe_3O_4@SiO_2-EDTA nanoparticles were obtained by Tecnai G2 Spirit BioTWIN FEI operating at 120 kV. All samples for TEM analysis were prepared by 30 min sonication of Fe_3O_4@SiO_2-EDTA nanoparticles in the absolute ethanol solution.

Fourier Transform Infrared Spectroscopy (FT-IR) spectra were obtained using Bruker FRA 106 spectrometer with the KBr pellet method.

X-ray Photoelectron Spectroscopy (XPS) was conducted using Escalab 250Xi multispectroscope (Thermo-Fisher Scientific, UK) utilizing monochromatic source with AlKα line at 1486.6 eV. The X-ray spot size was 250 µm. High-resolution measurements were carried out at 20 eV pass energy and 0.1 eV energy step size. Charge compensation was provided by means of a flood gun. Peak deconvolution was conducted using Avantage software provided by the spectroscope manufacturer.

2.4 Electrochemical Measurements

All electrochemical measurements were carried out using mercury electrode Metrohm 663 VA Stand connected with Autolab potentiostat/galvanostat PGSTAT-128 N controlled with NOVA 2.1.4 software. The three electrode cell system consisted of Static Drop Mercury Electrode (SDME) as a working electrode, Hg/Hg_2Cl_2/saturated KCl used as a reference electrode, and glassy carbon used as a counter electrode.

Differential pulse voltammetry (DPV) was utilized for the detection of Cd(II) and Pb(II) ions under optimized experimental conditions: deposition potential −0.9 V, deposition time 90 s, modulation amplitude 0.05 V, modulation time 0.07 s, interval time 1.85 s, and step potential 0.005 V.

The detection of Cd(II) ions was carried in a potential range of −0.8 V to −0.4 V, while for Pb(II) ions in a range of −0.65 V to −0.25 V. Metals ions solutions were prepared using cadmium and lead nitrate, pH 6.5 with potassium chloride as the supporting electrolyte. Fe_3O_4@SiO_2-EDTA nanoparticles before each measurement were prepared based on dispersion in electrolyte by sonication in ultrasonic bath for 30 min.

3 Results and Discussion

3.1 Synthesis of Fe_3O_4@SiO_2-EDTA

The magnetite derivatives called "core-shell" structures – Fe_3O_4@SiO_2-EDTA – were obtained by three-step reaction [50]. In the first step, the 20 nm magnetite nanoparticles Fe_3O_4 were obtained. In the second stage, the nanoparticles were covered with silica shell SiO_2 by reaction with tetraethyl orthosilicate (TEOS) [60]. Subsequently, their surface was modified in the reaction with N-[(3-Trimethoxysilyl)propyl]ethylenediamine tri-acetic and Fe_3O_4@SiO_2-EDTA nanoparticles were obtained (Figure 1).

3.2 TEM Analysis

The Fe_3O_4@SiO_2-EDTA nanoparticles were characterized using Transmission Electron Microscopy. TEM images of modified magnetite nanoparticles (Figure 2) showed that the nanostructures obtained by co-precipitation method

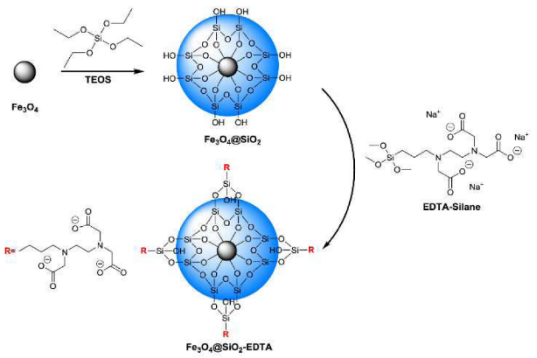

Fig. 1. Scheme of Fe3O4@SiO2-EDTA synthesis.

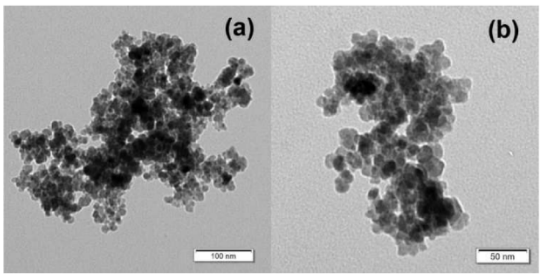

Fig. 2. TEM images of a), b) Fe_3O_4@SiO_2-EDTA nanoparticles.

are highly homogeneous in shape and size [50]. Figure 2 a and b shows the presence of small and spherical Fe_3O_4@SiO_2-EDTA nanoparticles. The structures indicate core-shell structures. The average size of Fe_3O_4@SiO_2-EDTA nanoparticles was found to be approximately 20 nm, what is comparable to core-shell nanostructures [61]. Examined nanoparticles were found to be in the agglomerated state. This is a very common observation for magnetic nanoparticles due to their natural tendency to form agglomerates based on their magnetic nature [47].

3.3 FT-IR Analysis

The FT-IR analysis was performed for uncoated Fe_3O_4 and coated Fe_3O_4@SiO_2, and functionalized Fe_3O_4@SiO_2-EDTA nanoparticles to compare their spectroscopic differences.

All spectra were obtained in KBr pellet. The spectra obtained for Fe_3O_4 and Fe_3O_4@SiO_2 are comparable with the IR spectra described previously [62–65]. Fe_3O_4@SiO_2 EDTA nanoparticles were brown, the spectrum is of high quality, is not ragged, and the characteristic signals are present in the spectrum (Figure 3. brown line).

Figure 3. presents the comparison of unmodified Fe_3O_4 and Fe_3O_4@SiO_2 and modified Fe_3O_4@SiO_2-EDTA nanoparticles. For all analysed nanoparticles, two characteristic absorption bands appear in the wavenumber range of 420 cm^{-1} to 780 cm^{-1} for metal-oxygen bond. Stretching vibration of tetrahedral site (Fe_{tetra}–O) and octahedral site (Fe_{octa}-O) bonds are observed at 448 cm^{-1} and 592 cm^{-1}, respectively [57, 62, 66]. We also observed the reduction in the intensity of Fe–O band for nanoparticles coated with silica and EDTA groups. The decrease in the band intensity confirms that the nanoparticles surface was successfully modified. [50]. The presence of band at 1090 cm^{-1} confirms that the silica shell was successfully coated on Fe_3O_4 surface forming Fe_3O_4@SiO_2. This band relates to Si–O–C and symmetric Si–O–Si stretching vibrations [46]. The signals observed for 1399 cm^{-1} and 1633 cm^{-1} correspond to the symmetrical and asymmetrical axial deformation group –COOH, which due to vibrational motions of C–O and C=O groups [44]. The two characteristics weak bands observed in the region of

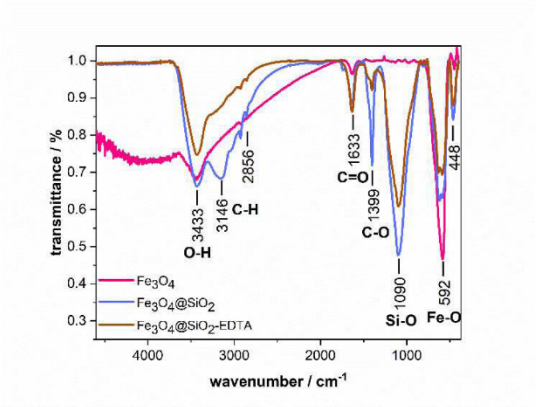

Fig. 3. The FT-IR spectra of Fe_3O_4, Fe_3O_4@SiO_2 and studied Fe_3O_4@SiO_2-EDTA nanoparticles.

2840 cm^{-1} 2950 and strong band at 3150 cm^{-1} are found in the IR spectra for Fe_3O_4@SiO_2 and Fe_3O_4@SiO_2-EDTA (Figure 3. blue and brown lines) and correspond to the C–H bond [55]. The broad strong band at 3433 cm^{-1} corresponds to the overlapping of –OH stretching bond. This band proves the formation of hydroxyl groups on the surface of magnetite [46]. The presence of all these bonds indicate the formation of silica shell on Fe_3O_4 nanoparticles. We can concluded that the synthesis procedure was conducted successfully. Additionally, FT-IR and XPS measurements independently confirmed the presence of the EDTA groups on the nanoparticles surface.

3.4 XPS Analysis

Survey XPS studies were conducted (see Figure 4a) followed by a detailed high-resolution spectral analysis in *C1s*, *O1s*, *N1s*, *Fe2p*, and *Si2p* binding energy (BE) range. The analysis to the large extent confirmed previously performed FT-IR studies. The detailed qualitative and quantitative analysis, based on high-resolution XPS spectra deconvolution, is shown in Table 1.

Peak deconvolution carried out in Fe2p binding energy range revealed presence of two oxidation states of iron, namely: Fe^{2+} ($Fe2p_{3/2}$ peak at 709.5 eV) and Fe^{3+} ($Fe2p_{3/2}$ at 711.8 eV), see Figure 4b [67,68]. The Fe^{2+}:Fe^{3+} ratio suggests the dominant presence of the lower oxidation state of iron, reaching approx. 81 %.

Furthermore, successful encapsulation of the nanoparticles with SiO_2 was confirmed by presence of the peak component in the energy range characteristic to silica at 103.5 eV [69].

The EDTA functionalization of the nanoparticles may be evaluated based on *C1s*, *O1s*, and *N1s* spectra. The nitrogen contribution is clearly visible both in survey as well as N1s spectra. A single form of nitrogen was

Table 1. Chemical analysis (in at.%) of Fe_3O_4@SiO_2-EDTA sample based on the high-resolution XPS spectra deconvolution.

Chemical state	C1s C–C	CO/CN	COOH	O1s Fe–O	SiO_2/CO	C=O	Fe2p$_{3/2}$ Fe^{2+}	Fe^{3+}	N1s C–N	Si2p$_{3/2}$ SiO_2
BE/eV	284.4	285.3	288.2	528.8	530.7	532.3	709.5	711.8	400.3	103.5
Fe_3O_4	9.9	14.1	4.9	15.6	25.1	7.3	6.3	1.5	2.7	12.6

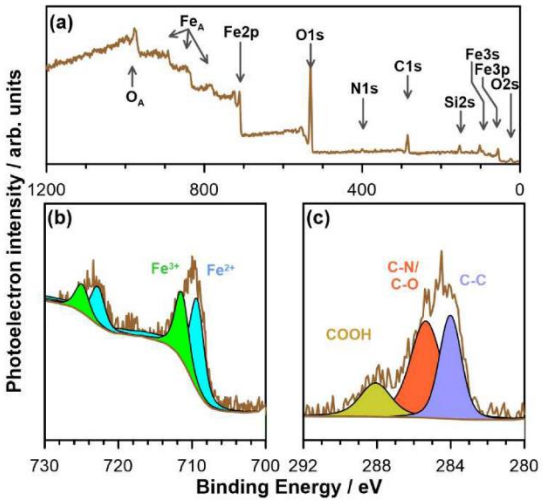

Fig. 4. XPS analysis of Fe_3O_4@SiO_2-EDTA sample: a) survey spectra; and high-resolution spectra in b) Fe2p and c) C1s binding energy range, subjected to peak deconvolution analysis.

observed peaking at 400.3 eV – a value characteristic for C–N bonds in EDTA [70].

The *C1s* spectrum was composed of three components, as presented in Figure 4c. The primary component located at 285.3 eV should be ascribed to either C–O or C–N bonds [70–72]. While the possible C–O interaction is testified by *O1s* peak at 530.7 eV, the BE mentioned above is also characteristic for SiO_2 species which are the primary source of signal taking into consideration the stoichiometry. Hence, it should be noted that the peak located at 285.3 eV for the nanoparticles is dominated by C–N interaction (8.1 at.% is estimated based on the nitrogen content: 2.7 at.%). Next, component located at 288.2 eV should be interpreted as carbon in carboxyl species [72–74].

One should also note that the *C1s* C–N:COOH rate of 0.6:1 corroborates the estimated 0.5:1 stoichiometry based on schematic functionalization process presented on Figure 1. The third *C1s* component ascribed as C–C originates from the C–C chain in Figure 1 but also adventitious carbon contaminating the nanoparticles in atmospheric air conditions [75].

The three components revealed in *O1s* spectra originate from various forms of oxygen: peaks at binding energies below 530 eV are typical for metal-oxygen interaction, here Fe–O. The peak at 530.7 eV primarily originates from SiO_2 but may also come from an organic carbon. Last but not least, the highest positive shift corresponds to C=O bonds, such as in carboxylic.

3.5 Electrochemical Behaviour of Fe_3O_4@SiO_2-EDTA Nanoparticles

The electrochemical properties of Fe_3O_4 nanoparticles were described previously. The modified Fe_3O_4 nanoparticles were used as modifiers of poly(vinyl)pyrrolidone (PVP) to obtain electrode meterial [76], platinum electrode for Hg(II) ions detection [56,77], carbon paste electrode detection of chlorite ions[78,79], Glassy Carbon (GC) electrode for Sudan I determination in food samples [80] or metal ions such as Cd(II), Pb(II), Cu(II) [81], and Boron Doped Diamond (BDD) electrode for the detection of a cancer biomarker [82].

The detailed binding mechanism of Fe_3O_4 modified by EDTA was described by Kataria et al. [54], while the binding mechanism of investigated ions was examined by Liu et al. and Xu et al. [50,51]. Based on this literature, all electrochemical experiments were performed in pH 6.5 due to the formation of $Cd(OH)_2$ and $Pb(OH)_2$/$Pb(OH)_4^{2-}$ hydroxides in pH higher than 7 from Cd(II) and Pb(II) ions, respectively. Furthermore, the adsorption of metal ions depends on the charge located on the nanoparticle surface [54] and the presence of EDTA groups (Figure 5). The interaction between Fe_3O_4@SiO_2-EDTA nanoparticles and metal ions involved both adsorption onto nanoparticles surface and complexation by EDTA ligand [50,53].

3.5.1 Stripping Voltammetry – Kinetics Examination

According to our knowledge, we present here the first study of Fe_3O_4@SiO_2- EDTA using Differential Pulse Voltammetry (DPV) in combination with Hanging Drop

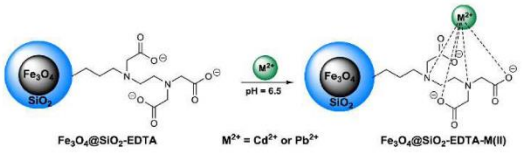

Fig. 5. Scheme of proposed mechanism of Cd(II) and Pb(II) ions binding by Fe_3O_4@SiO_2- EDTA nanoparticles.

Mercury Electrode (HDME) for binding of Cd(II) and Pb (II).

The main advantage usage of HDME is obtaining in each measurement the same repeatable results. Hanging Drop Mercury Electrode guarantee the possibility of receiving self-renewing surface of working electrode and in the same time prevents the electrode contamination by Fe_3O_4 derivatives and other ions present in solution.

Electrochemical measurements confirmed that Fe_3O_4@SiO_2-EDTA nanoparticles possess the ability to bind trace amounts of Cd(II)- and Pb(II) in an aqueous solution.

The utilisation of magnet and examined nanoparticles enable the 96.13 % removal of Cd(II) from the solution in and 54.1 % removal of Pb(II), what is confirmed with the results presented below.

Detection of Cd(II) and Pb(II) ions was carried out under optimized experimental conditions using DPASV and HDME due to reproducibility of the surface and speed of the measurement [83]. All measurements were performed in a scientific laboratory minimising the risk of the mercury environmental contamination. DPASV involves two steps including pre-concentration and metal ions stripping. The Cd(II) and Pb(II) ions are electrodeposited onto the working electrode firstly applying a negative potential (−0.9 V) and subsequently the faradic current obtained by oxidation is recorded when the potential sweeps toward the anodic direction (from −0.8 V to −0.4 V for Cd(II) and from −0.65 V to −0.2 V for Pb(II)).

To examine the binding abilities of Fe_3O_4@SiO_2-EDTA-Cd(II) and Fe_3O_4@SiO_2-EDTA-Pb(II) in time, a series of measurements were performed in the solution of 0.5 M KCl containing 553.9 $\mu g\,L^{-1}$ of Cd(II) ions and 647.5 $\mu g\,L^{-1}$ of Pb(II) ions, respectively. One well-defined peak at −0.62 V in anodic stripping voltammograms confirms the presence of Cd(II) ions in the solution without the nanoparticles (Figure 6 a). The peak in the potential of −0.4 V indicates the presence of lead ions in the solution (Figure 6 b). The longest of the binding stability experiment for the nanoparticles lasted 57 minutes. The cadmium and lead ions were bound by 1.87 mg and 1.86 mg of nanoparticles, respectively. The comparison of binding abilities for Fe_3O_4@SiO_2-EDTA nanoparticles with cadmium and lead ions are presented in Figure 6 a and b, respectively. After nanoparticles addition, the cadmium peak current intensity significantly decreased after first 7 minutes. Subsequently, its intensity slightly decreased in time (Figure 6 a). The changes recorded for lead binding measurements were not so prominent. Additionally, the intensity of peak current also decreased but then slightly increased and finally reached the equilibrium. (Figure 6 b). This phenomenon confirms that the addition of Fe_3O_4@SiO_2-EDTA nanoparticles led to the increased binding of cadmium and lead ions.

The degree of ions binding calculated for Fe_3O_4@SiO_2-EDTA confirms that the binding ability slightly increased

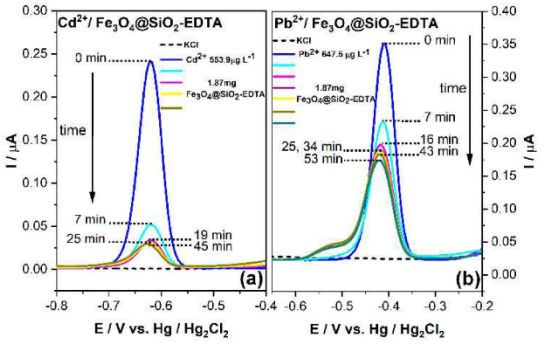

Fig. 6. Anodic stripping voltammograms for the peak intensity changes over time a) for Cd(II) ions (553.9 $\mu g\,L^{-1}$) bound by 1.87 mg of Fe_3O_4@SiO_2-EDTA and b) for Pb(II) ions (647.5 $\mu g\,L^{-1}$) bound by 1.86 mg of Fe_3O_4@SiO_2-EDTA.

and depends on time (Figure 7). The adsorption rate was high and the equilibrium was reached within 19 minutes and 25 minutes for cadmium ion and lead ion binding, respectively. The comparable amount of nanoparticles was used in these experiments. 1.87 mg of Fe_3O_4@SiO_2-EDTA was able to bind 87.5 % of Cd(II), while 1.86 mg of the nanoparticles bound 54.1 % of Pb(II). We found out that the larger amount of nanoparticles was needed to bind the lead ions. Therefore, the nanoparticles were subjected to further experiments to determine their capacity and stability in an aqueous solution.

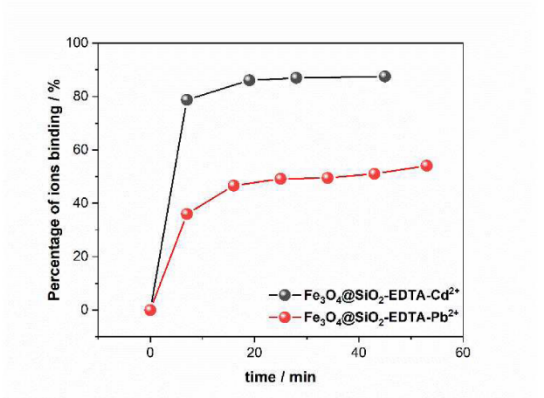

Fig. 7. Comparison of binding percentage of a) Cd(II) ions (553.9 $\mu g{\cdot}L^{-1}$) by 1.87 mg of Fe_3O_4@SiO_2-EDTA and b) Pb(II) ions (647.5 $\mu g\,L^{-1}$) by 1.86 mg of Fe_3O_4@SiO_2-EDTA nanoparticles.

3.5.2 Determination of Cd (II) and Pb(II) Binding Capacity

To determine the metal ions binding capacity of Fe_3O_4@SiO_2-EDTA nanoparticles, we performed the anodic stripping voltammetry in 0.5 M KCl solution containing 553.9 $\mu g L^{-1}$ Cd(II) and 647.5 $\mu g L^{-1}$ Pb(II) ions. The first measurement without nanoparticles gave one peak at −0.62 V in anodic stripping voltammograms for Cd(II) (Figure 8 a) and at −0.41 V for Pb(II) (Figure 8 b).

The cadmium peak intensity decreased during titration by Fe_3O_4@SiO_2-EDTA in eight steps in amount from 0.253 mg to 2.024 mg. The obtained results show the initial linear current peak decrease for each portion of nanoparticles. After addition of 1.265 mg of nanoparticles, the equilibrium was established and another portion of nanoparticles caused no changes in current peak intensity (Figure 8 a).

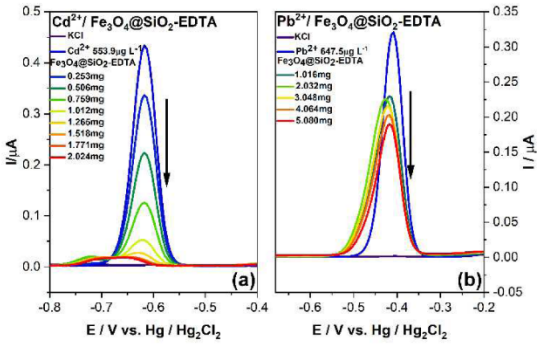

Fig. 8. Anodic stripping voltammogram for binding of a) Cd(II) ions (553.9 $\mu g L^{-1}$) and b) Pb(II) ions (647.5 $\mu g L^{-1}$) by Fe_3O_4@SiO_2-EDTA nanoparticles.

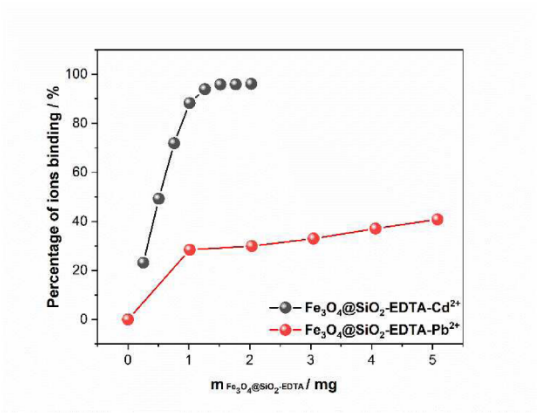

Fig. 9. Percentage of Cd(II) ions (553.9 $\mu g L^{-1}$) and Pb(II) ions 647.5 $\mu g L^{-1}$) binding by Fe_3O_4@SiO_2-EDTA nanoparticles.

A similar effect was achieved during addition of Fe_3O_4@SiO_2-EDTA nanoparticles to the Pb(II) solution. Nanoparticles were added in five steps in amount range of 1.016 mg to 5.080 mg. The Pb(II) peak intensity gently decreased after addition of each portion and after fifth step the equilibrium was not established. Due to the small changes of peak intensity and the addition of large amount of Fe_3O_4@SiO_2-EDTA nanoparticles, the measurements was stopped after the fifth step.

The gradual decrease in the peak intensity indicates the binding of the cadmium and lead ions by Fe_3O_4@SiO_2-EDTA nanoparticles. The established equilibrium proves a limited capacity of the given nanoparticles.

Figure 9 shows the binding percentage for Cd(II) ions (553.9 $\mu g L^{-1}$) and Pb(II) ions (969.0 $\mu g L^{-1}$) by Fe_3O_4@SiO_2-EDTA nanoparticles. Cd(II) binding increases the linearity observed during addition of the subsequent Fe_3O_4@SiO_2-EDTA portions. Addition of 1.265 mg of nanoparticles caused the capturing of 96.13 % Cd(II) ions and establishing of the equilibrium. Further addition of the increased amounts of nanoparticles does not cause any changes in the bounding level.

In the case of lead ions, the Fe_3O_4@SiO_2-EDTA nanoparticles binding intensity was much lower. Addition of 5.08 mg of nanoparticles results in binding of 40.83 % of lead ions. After this step, the degree of ions binding remains at the same level. This phenomenon proves that the studied nanoparticles bind Cd(II) much better than Pb(II).

3.5.3 Determination of Fe_3O_4@SiO_2-EDTA Activity

To test the activity of Fe_3O_4@SiO_2-EDTA nanoparticles, their binding capacity was determined in various time intervals: immediately after preparation, after two, and eight days. To obtain this goal, the nanoparticles were stored in a dark, cool place in the electrolyte solution (KCl 0.5 M). The experiment consisted of the anodic stripping voltammetry by addition of Fe_3O_4@SiO_2-EDTA nanoparticles portions to the cadmium solution (553.9 $\mu g L^{-1}$) measured previously. The obtained results of Cd(II) binding activity of directly prepared solution of nanoparticles is presented at Figure 8 A. The anodic stripping voltammograms of titrated solution containing Cd(II) ions by both nanoparticles stored 2 and 8 days is shown at (Figure 10). The addition of the next portions of titrant causes a decrease in the peak intensity. A decrease of peak intensity in this case was not so profound in comparison with the freshly prepared solution.

Figure 11. shows the percentage of cadmium binding for the freshly prepared solution of Fe_3O_4@SiO_2-EDTA, after 2 and 8 days of storage in the electrolyte. 2.024 mg of freshly prepared nanoparticles bound 96.13 % of Cd(II) ions from aqueous solution while after 2 days of storage 2.53 mg Fe_3O_4@SiO_2-EDTA nanoparticles is necessary to bind 95.53 % of Cd(II) ions. These results confirm that

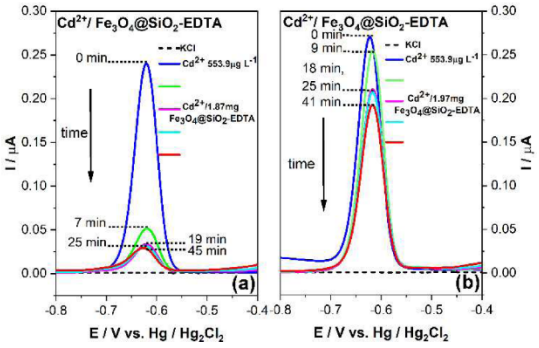

Fig. 10. Anodic stripping voltammograms for binding of Cd(II) ions (553.9 $\mu g L^{-1}$) by a) Fe_3O_4@SiO_2-EDTA after 2 days, b) Fe_3O_4@SiO_2-EDTA after 8 days of storage in the electrolyte (KCl 0.5 M) solution.

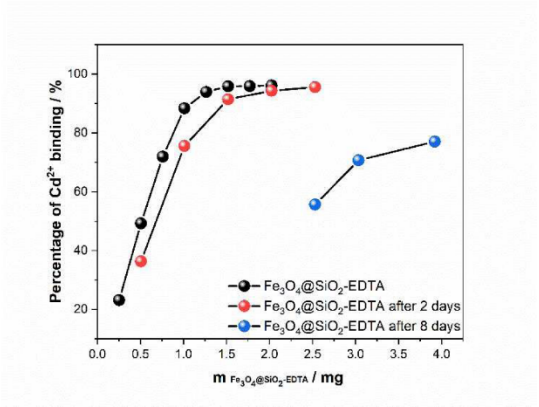

Fig. 11. Binding percentage plot of Cd(II) ions (553.9 $\mu g L^{-1}$) by Fe_3O_4@SiO_2-EDTA for the freshly prepared solution and after 2 and 8 days of its storage in the electrolyte solution.

after 2 days there is a need to use 25 % more nanoparticles to bound a similar amount of Cd(II) ions, while after 8 days the binding ability of nanoparticles is much lower. To bind 60 % of Cd(II) ions present in the solution, one should use 0.623 mg of the freshly prepared Fe_3O_4@SiO_2-EDTA.

After 2 days of storage the amount of nanoparticles increased to 31.6 %, with further increase to 328 % after 8 days of storage.

This experiment shows that the magnetite nanoparticles covered with EDTA groups lose their ion binding ability. This phenomenon can be associated with the strong agglomeration of Fe_3O_4@SiO_2-EDTA nanoparticles in the solution.

4 Conclusions

This study describes the preparation of Fe_3O_4 by co-precipitation method without any surfactants, by two-step modification by tetraethyl orthosilicate (TEOS), by N-[(3-Trimethoxysilyl)propyl] ethylenediamine and functionalization. Nanoparticles surface modification was confirmed by FT-IR spectra and XPS method. Additionally, the TEM characterization was performed for the obtained nanoparticles – we observed Fe_3O_4@SiO_2-EDTA nanoparticles of about 20 nm size.

Obtained nanoparticles were utilized as a Cd(II) and Pb(II) binding argent in aqueous solution. Binding ability of Fe_3O_4@SiO_2-EDTA-M(II) was conducted using DPASV method in combination with HDME in 0.5 M KCl solution. In the first stage, we compared the cadmium and lead ions binding properties of Fe_3O_4@SiO_2-EDTA. Nanoparticles showed the ability to bind both the Cd(II) and Pb(II) ions but not at the same level. For Fe_3O_4@SiO_2-EDTA-Cd(II) the adsorption rate was higher and the equilibrium was reached after 19 minutes, while in case of Fe_3O_4@SiO_2-EDTA-Pb(II) the equilibrium was not established even after 43 minutes. Binding of both cadmium and lead ions slightly depends on time. To compare these binding capacities, similar amounts of the nanoparticles were added to the Cd(II) (553.9 $\mu g L^{-1}$) and Pb(II) (647.5 $\mu g L^{-1}$) solutions. Electrochemical measurements results show that 87.5 % of Cd(II) ions and 54.12 % of Pb(II) ions was bound by 1.87 mg and 1.86 mg of Fe_3O_4@SiO_2-EDTA nanoparticles, respectively. We determined the binding capacity for Fe_3O_4@SiO_2-EDTA-Cd (II) and Fe_3O_4@SiO_2-EDTA-Pb(II). The experimental results indicate that only 1.265 mg and 5.080 mg of Fe_3O_4@SiO_2-EDTA is needed to bind 96.14 % of cadmium and 40.83 % of lead ions, respectively. This phenomenon proves that the studied nanoparticles bind Cd(II) much better than Pb(II).

The results of the Fe_3O_4@SiO_2-EDTA nanoparticles stability tests show that the storage in 0.5 M KCl solution in dark, cool place decreases their ion binding properties. The amount of Fe_3O_4@SiO_2-EDTA to bind 60 % of Cd (II) ions after 2 and 8 days of storage increases three times in comparison with the freshly prepared nanoparticles. We observed the best capacity for the nanoparticles prepared directly before the measurement. Furthermore, the storage of nanoparticles in potassium chloride solution significantly reduces their cadmium ions binding ability.

Acknowledgements

This study was financed by the University of Gdansk within the project supporting young scientists and PhD students (grant No. BMN 539–8210-B281-18). Authors would like to thank Alexander Company Gdynia for technical support.

References

[1] A. Butt, Qurat-ul-Ain, K. Rehman, M. X. Khan, T. Hesselberg, *Environ. Monit. Assess.* **2018**, 190.
[2] Z. L. He, X. E. Yang, P. J. Stoffella, *J. Trace Elem. Med. Biol.* **2005**, *19*, 125–140.
[3] W. R. García-Niño, J. Pedraza-Chaverrí, *Food Chem. Toxicol.* **2014**, *69*, 182–201.
[4] K. A. James, J. R. Meliker, *Int. J. Public Health* **2013**, *58*, 737–745.
[5] M. El Muayed, M. R. Raja, X. Zhang, K. W. MacRenaris, S. Bhatt, X. Chen, M. Urbanek, T. V. O'Halloran, W. L. Lowe, Jr., *Islets* **2012**, *4*, 405–416.
[6] J. Godt, F. Scheidig, C. Grosse-Siestrup, V. Esche, P. Brandenburg, A. Reich, D. A. Groneberg, *J. Occup. Med. Toxicol. Lond. Engl.* **2006**, *1*, 22.
[7] V. Balakumar, P. Prakash, K. Muthupandi, A. Rajan, *Sens. Actuators B* **2017**, *241*, 814–820.
[8] G. Hou, M. M. Surhio, H. Ye, X. Gao, Z. Ye, J. Li, M. Ye, *Int. J. Biol. Macromol.* **2019**, *124*, 716–723.
[9] S. Yun, Y. Wu, R. Niu, C. Feng, J. Wang, *Toxicol. Lett.* **2019**, *310*, 23–30.
[10] S. Radi, S. Tighadouini, M. Bacquet, S. Degoutin, F. Cazier, M. Zaghrioui, Y. Mabkhot, *Molecules* **2013**, *19*, 247–262.
[11] R. Sánchez, J. Snell, A. Held, H. Emons, *Anal. Bioanal. Chem.*, **2015**, *407*, 6569–6574.
[12] J. S. Rohrer, *Advances in Water Purification Techniques*, Elsevier, **2019**, ss. 115–134.
[13] T. Vasilopoulou, I. E. Stamatelatos, P. Batistoni, A. Colangeli, D. Flammini, N. Fonnesu, S. Loreti, B. Obryk, M. Pillon, R. Villari, *Fusion Eng. Des.* **2019**, *139*, 109–114.
[14] L. A. Hutton, G. D. O'Neil, T. L. Read, Z. J. Ayres, M. E. Newton, J. V. Macpherson, *Anal. Chem.* **2014**, *86*, 4566–4572.
[15] S. Wang, E. S. Forzani, N. Tao, *Anal. Chem.* **2007**, *79*, 4427–4432.
[16] C. Ariño, N. Serrano, J. M. Díaz-Cruz, M. Esteban, *Anal. Chim. Acta* **2017**, *990*, 11–53.
[17] M. Baghayeri, H. Alinezhad, M. Fayazi, M. Tarahomi, R. Ghanei-Motlagh, B. Maleki, *Electrochim. Acta* **2019**, *312*, 80–88.
[18] E. Fischer, *Anal. Chim. Acta* **1999**, *8*.
[19] K. E. Toghill, L. Xiao, G. G. Wildgoose, R. G. Compton, *Electroanalysis* **2009**, *21*, 1113–1118.
[20] S. Zhou, Y. Zhou, W. Jiang, H. Guo, Z. Wang, X. Li, *Appl. Surf. Sci.* **2018**, *439*, 927–933.
[21] L. Guo, H. Sun, C. Qin, W. Li, F. Wang, W. Song, J. Du, F. Zhong, Y. Ding, *Appl. Surf. Sci.* **2018**, *459*, 263–270.
[22] J. R. Rajabathar, J. J. Vijaya, A. Prabakaran, Z. A. Issa, A. M. Atta, A. O. Ezzat, A. M. Al-Mayouf, H. A. Al-Lohedan, *J. Alloys Compd.* **2017**, *698*, 1077–1085.
[23] M. Qiao, X. Lei, Y. Ma, L. Tian, W. Wang, K. Su, Q. Zhang, *J. Alloys Compd.* **2017**, *693*, 432–439.
[24] Q. Sun, Y. Hong, Q. Liu, L. Dong, *Appl. Surf. Sci.* **2018**, *430*, 399–406.
[25] Q. Zhang, L. Yu, C. Xu, J. Zhao, H. Pan, M. Chen, Q. Xu, G. Diao, *Appl. Surf. Sci.* **2019**, *483*, 241–251.
[26] A. Pariti, P. Desai, S. K. Y. Maddirala, N. Ercal, K. V. Katti, X. Liang, M. Nath, *Mater. Res. Express* **2014**, *1*, 35023.
[27] R. Hao, R. Xing, Z. Xu, Y. Hou, S. Gao, S. Sun, *Adv. Mater.* **2010**, *22*, 2729–2742.
[28] G. A. Sotiriou, F. Starsich, A. Dasargyri, M. C. Wurnig, F. Krumeich, A. Boss, J.-C. Leroux, S. E. Pratsinis, *Adv. Funct. Mater.* **2014**, *24*, 2818–2827.
[29] Z.-H. Sun, L.-H. Zhou, G.-J. Deng, M.-B. Zhegn, W.-Q. Yan, W.-J. Li, L.-T. Cai, P. Gong, *Chin. J. Anal. Chem.* **2017**, *45*, 1427–1433.
[30] R. Di Corato, N. C. Bigall, A. Ragusa, D. Dorfs, A. Genovese, R. Marotta, L. Manna, T. Pellegrino, *ACS Nano* **2011**, *5*, 1109–1121.
[31] C. Wang, L. Huang, S. Song, B. Saif, Y. Zhou, C. Dong, S. Shuang, *Appl. Surf. Sci.* **2015**, *357*, 2077–2086.
[32] G. Bao, S. Mitragotri, S. Tong, *Annu. Rev. Biomed. Eng.* **2013**, *15*, 253–282.
[33] J.-H. Liu, L. Wang, T.-Q. Zhang, J.-Q. Wang, X. Gong, F.-Z. Cui, J.-J. Zheng, B. Li, Z. Shi, *Chin. J. Anal. Chem.* **2019**, *47*, 678–685.
[34] J. Qin, H. Peng, J. Ping, Z. Geng, *Mater. Res. Bull.* **2019**, *114*, 90–94.
[35] N. Mir, P. Karimi, C. E. Castano, N. Norouzi, J. V. Rojas, R. Mohammadi, *Appl. Surf. Sci.* **2019**.
[36] C.-L. Huang, W.-J. Hsieh, C.-W. Lin, H.-W. Yang, C.-K. Wang, *Ceram. Int.* **2018**, *44*, 12442–12450.
[37] H. Meng, Z. Zhang, F. Zhao, T. Qiu, J. Yang, *Appl. Surf. Sci.* **2013**, *280*, 679–685.
[38] D. Ghanbari, M. Salavati-Niasari, M. Ghasemi-Kooch, *J. Ind. Eng. Chem.* **2014**, *20*, 3970–3974.
[39] V. Madhubala, T. Kalaivani, *Appl. Surf. Sci.* **2018**, *449*, 584–590.
[40] O. M. Lemine, K. Omri, B. Zhang, L. El Mir, M. Sajieddine, A. Alyamani, M. Bououdina, *Superlattices Microstruct.* **2012**, *52*, 793–799.
[41] D. Zhang, Z. Tong, S. Li, X. Zhang, A. Ying, *Mater. Lett.* **2008**, *62*, 4053–4055.
[42] M. Aghazadeh, I. Karimzadeh, M. R. Ganjali, *J. Magn. Magn. Mater.* **2017**, *439*, 312–319.
[43] F. Ke, J. Jiang, Y. Li, J. Liang, X. Wan, S. Ko, *Appl. Surf. Sci.* **2017**, *413*, 266–274.
[44] W. Cai, M. Guo, X. Weng, W. Zhang, Z. Chen, *Mater. Sci. Eng. C* **2019**, *98*, 65–73.
[45] X. Liu, J. Tian, Y. Li, N. Sun, S. Mi, Y. Xie, Z. Chen, *J. Hazard. Mater.* **2019**, *373*, 397–407.
[46] D. Chen, T. Awut, B. Liu, Y. Ma, T. Wang, I. Nurulla, *e-Polym.* **2016**, *0*.
[47] A. G. Magdalena, I. M. B. Silva, R. F. C. Marques, A. R. F. Pipi, P. N. Lisboa-Filho, M. Jafelicci, *J. Phys. Chem. Solids* **2018**, *113*, 5–10.
[48] N. Kataria, V. K. Garg, *Environ. Res.* **2019**, *172*, 43–54.
[49] D. Dupont, J. Luyten, M. Bloemen, T. Verbiest, K. Binnemans, *Ind. Eng. Chem. Res.* **2014**, *53*, 15222–15229.
[50] Y. Liu, R. Fu, Y. Sun, X. Zhou, S. A. Baig, X. Xu, *Appl. Surf. Sci.* **2016**, *369*, 267–276.
[51] M. Xu, Y. Zhang, Z. Zhang, Y. Shen, M. Zhao, G. Pan, *Chem. Eng. J.* **2011**, *168*, 737–745.
[52] Y. Liu, M. Chen, H. Yongmei, *Chem. Eng. J.* **2013**, *218*, 46–54.
[53] Y. Huang, A. A. Keller, *Water Res.* **2015**, *80*, 159–168.
[54] N. Kataria, V. K. Garg, *Chemosphere* **2018**, *208*, 818–828.
[55] E. Ghasemi, A. Heydari, M. Sillanpää, *Microchem. J.* **2017**, *131*, 51–56.
[56] U. Condomitti, A. Zuin, A. T. Silveira, K. Araki, H. E. Toma, *J. Electroanal. Chem.* **2011**, *661*, 72–76.
[57] C. A. Dinçer, N. Yıldız, N. Aydoğan, A. Çalımlı, *Appl. Surf. Sci.* **2014**, *318*, 297–304.
[58] W. Stöber, A. Fink, E. Bohn, *J. Colloid Interface Sci.* **1968**, *26*, 62–69.
[59] F. Nemati, M. M. Heravi, R. Saeedi Rad, *Chin. J. Catal.* **2012**, *33*, 1825–1831.

[60] D. Lewandowski, M. Cegłowski, M. Smoluch, E. Reszke, J. Silberring, G. Schroeder, *Microporous Mesoporous Mater.* **2017**, *240*, 80–90.
[61] Z. Chen, Z. Geng, Z. Zhang, L. Ren, T. Tao, R. Yang, Z. Guo, *Eur. J. Inorg. Chem.* **2014**, *2014*, 3172–3177.
[62] T. Q. Bui, H. T. M. Ngo, H. T. Tran, *J. Sci. Adv. Mater. Devices* **2018**, *3*, 323–330.
[63] M. Chellappa, U. Vijayalakshmi, *Mater. Today Proc.* **2019**, *9*, 371–379.
[64] L. Wang, C. Shen, Y. Cao, *J. Phys. Chem. Solids* **2019**, *133*, 28–34.
[65] M. Nasrollahzadeh, M. Sajjadi, H. A. Khonakdar, *J. Mol. Struct.* **2018**, *1161*, 453–463.
[66] B. Unal, M. S. Toprak, Z. Durmus, H. Sözeri, A. Baykal, *J. Nanopart. Res.* **2010**, *12*, 3039–3048.
[67] A. Mohammed, M. Saracoglu, N. El-Bagoury, T. Sharshar, M. Ibrahim, J. Wysocka, S. Krakowiak, J. Ryl, *Int. J. Electrochem. Sci.* **2016**, *11*, 1–23.
[68] D. Wilson, M. A. Langell, *Appl. Surf. Sci.* **2014**, *303*, 6–13.
[69] N. Koshizaki, H. Umehara, T. Oyama, *Thin Solid Films* **1998**, *325*, 130–136.
[70] S. Ravi, S. Zhang, Y.-R. Lee, K.-K. Kang, J.-M. Kim, J.-W. Ahn, W.-S. Ahn, *J. Ind. Eng. Chem.* **2018**, *67*, 210–218.
[71] M. C. Ortega-Liebana, N. X. Chung, R. Limpens, L. Gomez, J. L. Hueso, J. Santamaria, T. Gregorkiewicz, *Carbon*, **2017**, *117*, 437–446.
[72] J. Wysocka, M. Cieślik, S. Krakowiak, J. Ryl, *Electrochim. Acta*, **2018**.
[73] E. Johansson, L. Nyborg, *Surf. Interface Anal.* **2003**, *35*, 375–381.
[74] J. Ryl, R. Bogdanowicz, P. Slepski, M. Sobaszek, K. Darowicki, *J. Electrochem. Soc.* **2014**, *161*, H359–H364.
[75] S. Evans, *Surf. Interface Anal.* **1997**, *25*, 924–930.
[76] P. Tipsawat, U. Wongpratat, S. Phumying, N. Chanlek, K. Chokprasombat, S. Maensiri, *Appl. Surf. Sci.* **2018**, *446*, 287–292.
[77] L. Yang, X. Ren, F. Tang, L. Zhang, *Biosens. Bioelectron.* **2009**, *25*, 889–895.
[78] E. Al-Zahrani, M. T. Soomro, R. M. Bashami, A. U. Rehman, E. Danish, I. M. I. Ismail, M. Aslam, A. Hameed, *J. Environ. Chem. Eng.* **2016**, *4*, 4330–4341.
[79] H. Beitollahi, S. Tajik, S. Jahani, *Electroanalysis* **2016**, *28*, 1093–1099.
[80] H. Yin, Y. Zhou, X. Meng, T. Tang, S. Ai, L. Zhu, *Food Chem.* **2011**, *127*, 1348–1353.
[81] F. Bai, X. Zhang, X. Hou, H. Liu, J. Chen, T. Yang, *Electroanalysis* **2019**, *31*, 1448–1457.
[82] M. Braiek, Y. Yang, C. Farre, C. Chaix, F. Bessueille, A. Baraket, A. Errachid, A. Zhang, N. Jaffrezic-Renault, *Electroanalysis* **2016**, *28*, 1810–1816.
[83] A. Profumo, D. Merli, M. Pesavento, *Anal. Chim. Acta* **2005**, *539*, 245–250.

Received: October 14, 2019
Accepted: November 11, 2019
Published online on November 28, 2019

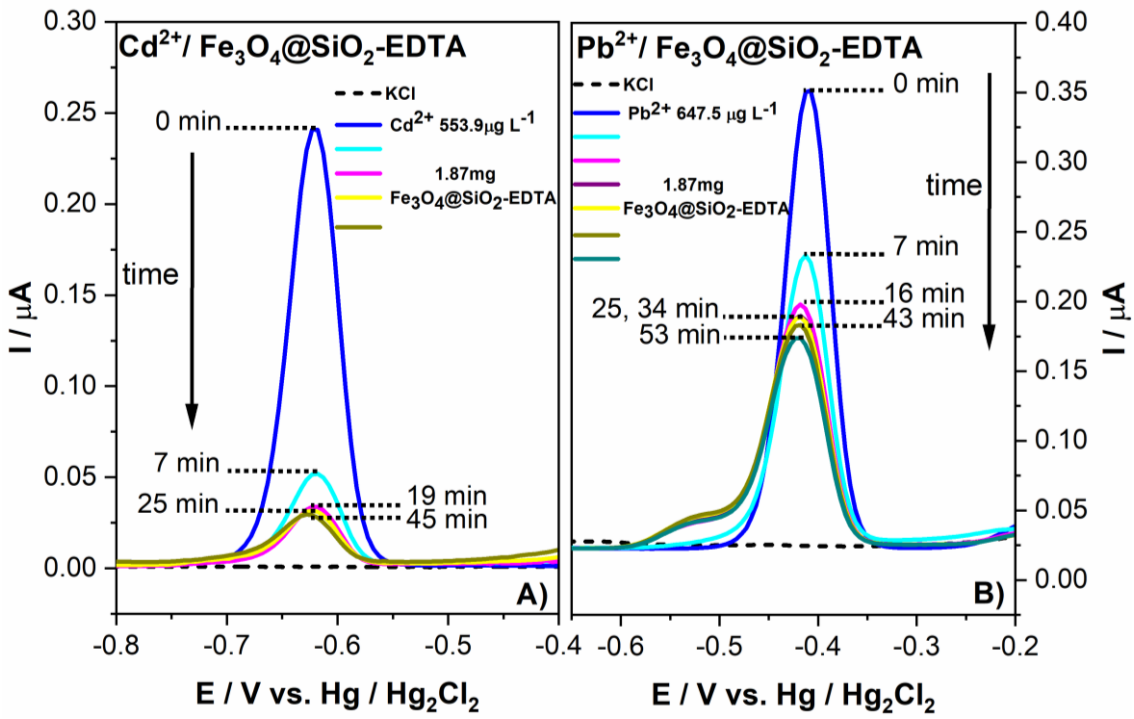

Fig. 6. Anodic stripping voltammograms for the peak intensity changes over time a) for Cd(II) ions (553.9 μg·L^{-1}) bound by 1.87 mg of Fe_3O_4@SiO_2-EDTA and b) for Pb(II) ions (647.5 μg·L^{-1}) bound by 1.86 mg of Fe_3O_4@SiO_2-EDTA.

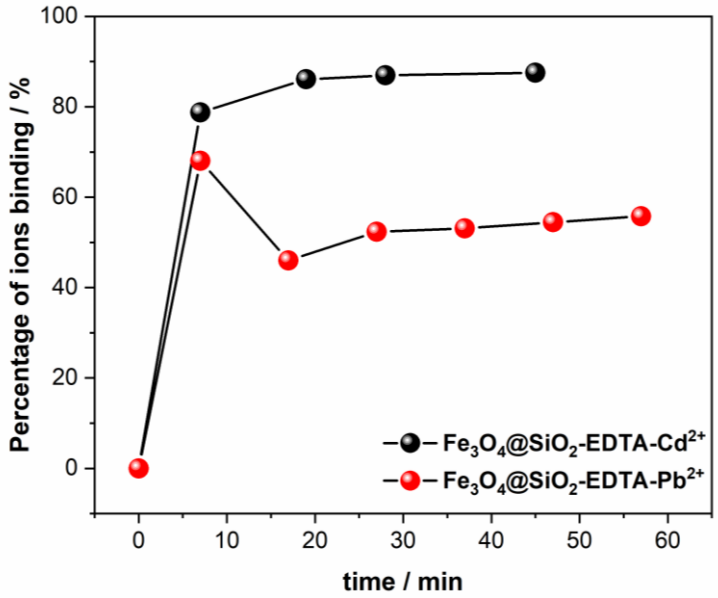

Fig. 7. Comparison of binding percentage of a) Cd(II) ions (553.9 μg·L^{-1}) by 1.87 mg of Fe_3O_4@SiO_2- EDTA and b) Pb(II) ions (647.5 μg·L^{-1}) by 1.86 mg of Fe_3O_4@SiO_2-EDTA nanoparticles.

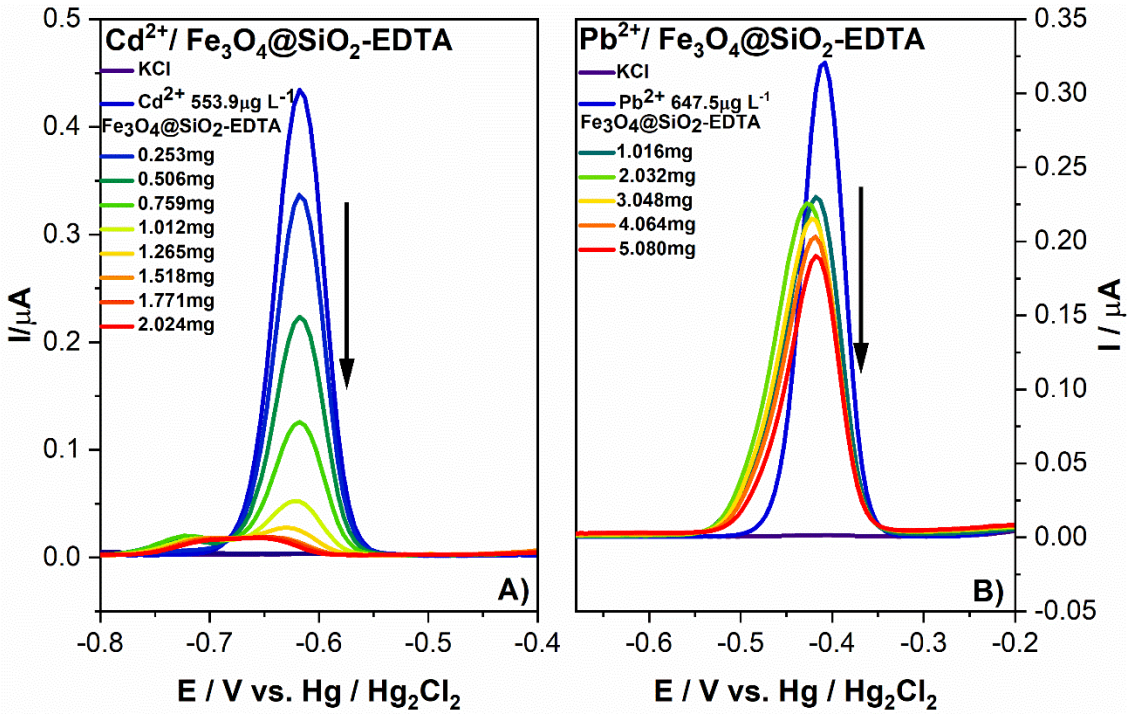

Fig. 8. Anodic stripping voltammogram for binding of a) Cd(II) ions (553.9 µg·L^{-1}) and b) Pb(II) ions (647.5 µg·L^{-1}) by Fe_3O_4@SiO_2-EDTA nanoparticles.

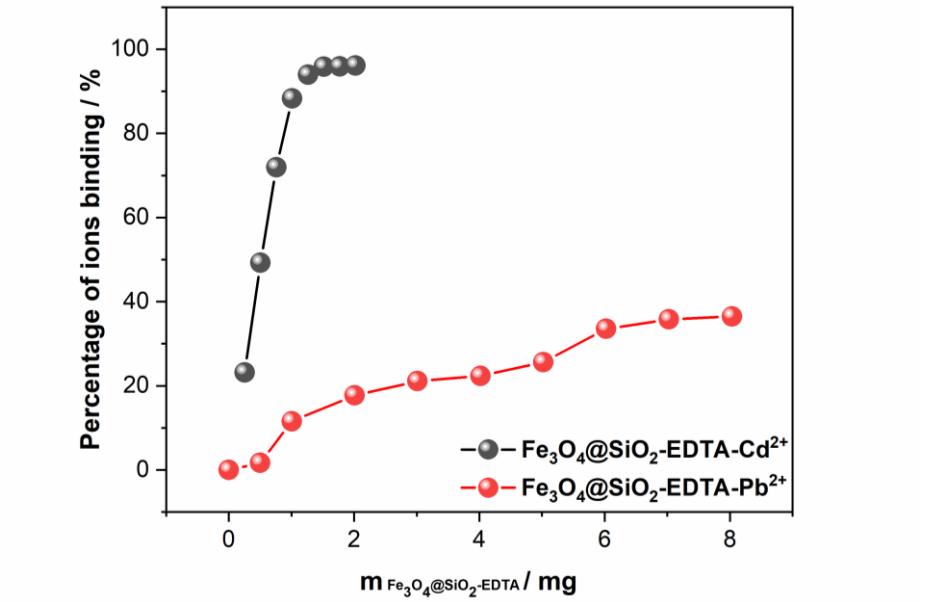

Fig. 9. Percentage of Cd(II) ions (553.9 µg·L^{-1}) and Pb(II) ions (647.5 µg·L^{-1}) binding by Fe_3O_4@SiO_2- EDTA nanoparticles.

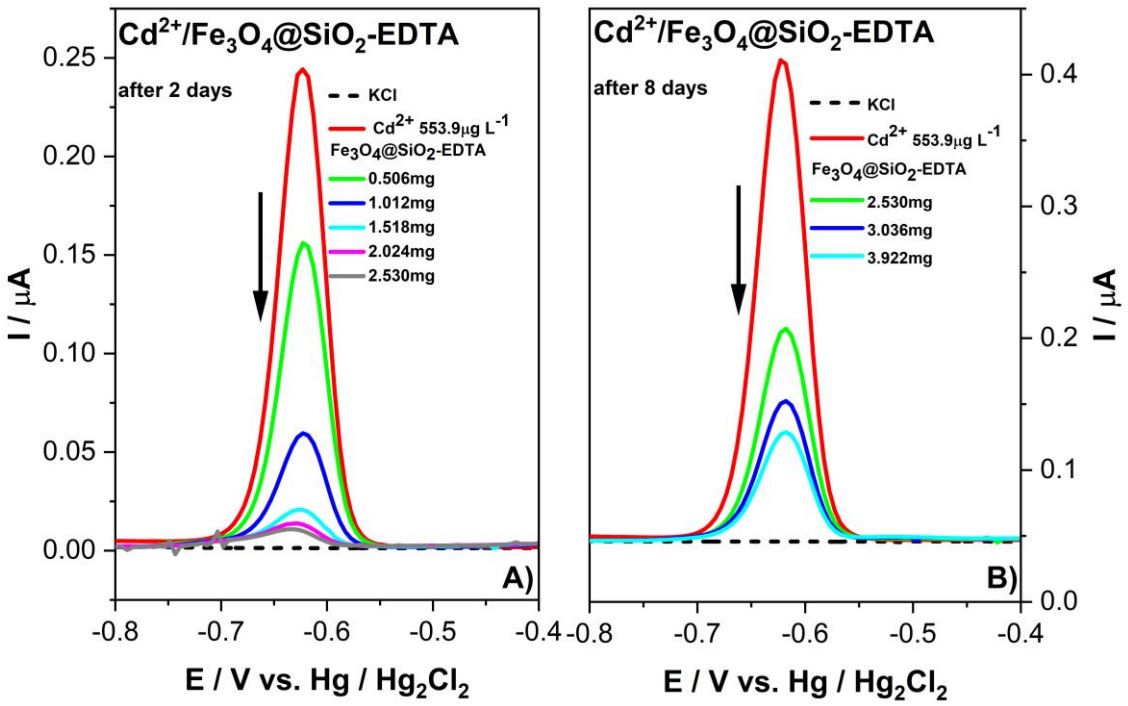

Fig. 10. Anodic stripping voltammograms for binding of Cd(II) ions (553.9 μg·L^{-1}) by a) Fe_3O_4@SiO_2-EDTA after 2 days, b) Fe_3O_4@SiO_2-EDTA after 8 days of storage in the electrolyte (KCl 0.5 M) solution.

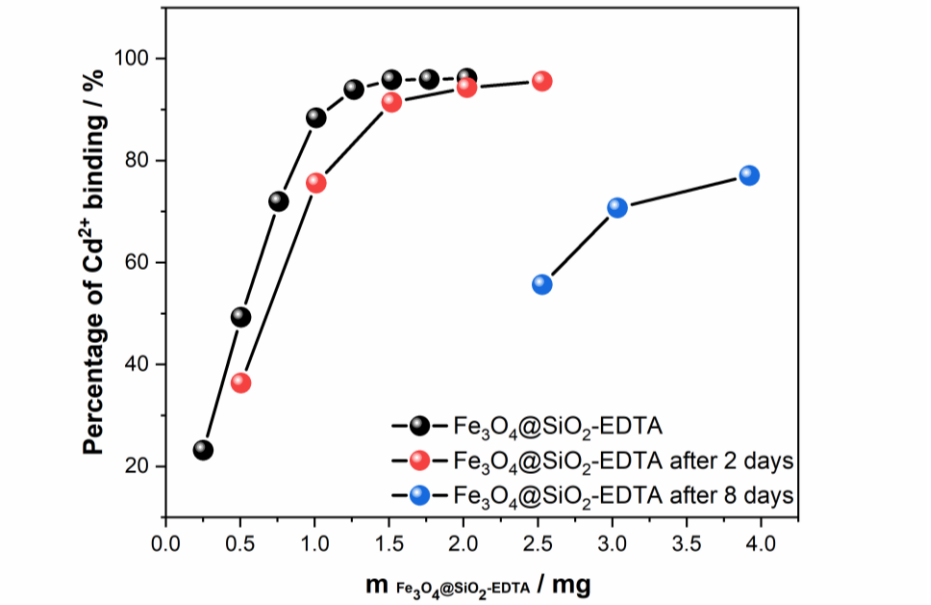

Fig. 11. Binding percentage plot of Cd(II) ions (553.9 μg·L^{-1}) by Fe_3O_4@SiO_2-EDTA for the freshly prepared solution and after 2 and 8 days of its storage in the electrolyte solution.

2. Załącznik 2

Journal of Molecular Liquids 314 (2020) 113677

Contents lists available at ScienceDirect

Journal of Molecular Liquids

journal homepage: www.elsevier.com/locate/molliq

Simultaneous voltammetric determination of Cd^{2+}, Pb^{2+}, and Cu^{2+} ions captured by $Fe_3O_4@SiO_2$ core-shell nanostructures of various outer amino chain length

A. Kulpa [a], J. Ryl [b], G. Schroeder [c], A. Koterwa [a], J. Sein Anand [d,e], T. Ossowski [a], P. Niedziałkowski [a,*]

[a] Department of Analytical Chemistry, Faculty of Chemistry, University of Gdansk, Wita Stwosza Str. 63, 80-308 Gdansk, Poland
[b] Department of Electrochemistry, Corrosion and Materials Engineering, Faculty of Chemistry, Gdansk University of Technology, Narutowicza 11/12, 80-233 Gdansk, Poland
[c] Faculty of Chemistry, Adam Mickiewicz University in Poznan, Uniwersytetu Poznańskiego Str. 8, 61-614 Poznan, Poland
[d] Department of Clinical Toxicology, Medical University of Gdansk, 4/6 Kartuska St., 80-104 Gdansk, Poland
[e] Pomeranian Center of Clinical Toxicology, 4/6 Kartuska St., 80-104 Gdansk, Poland

ARTICLE INFO

Article history:
Received 4 March 2020
Received in revised form 22 June 2020
Accepted 24 June 2020
Available online xxxx

Keywords:
Fe_3O_4 nanoparticles
Amino-modified $Fe_3O_4@SiO_2$ nanostructures
Cadmium
Lead and copper ions removal
Copper adsorption-desorption experiment

ABSTRACT

In the present study, we examined a novel functionalised magnetic nanoparticles $Fe_3O_4@SiO_2$-N_n as a nano adsorbent for binding of Cd^{2+}, Pb^{2+}, Cu^{2+} ions in an aqueous solution. First, we obtained the nanoparticles functionalised with various carbon chains containing different number of amino groups: (3-amino) propyltriethoxysilane ($Fe_3O_4@SiO_2$-N_1), N-(2-aminoethyl)-3-aminopropyltrimethoxysilane ($Fe_3O_4@SiO_2$-N_2) and N^1-(3-trimethoxysilylpropyl)diethylenetriamine ($Fe_3O_4@SiO_2$-N_3). In the next step, we conducted their characterisation using SEM, TEM, FT-IR, and XPS methods.
The detection of Cd^{2+}, Pb^{2+}, Cu^{2+} metal ions was performed under optimised experimental conditions using DPASV and HDME techniques. Using these methods we conducted the Cd^{2+}, Pb^{2+}, Cu^{2+} binding comparison in 4.5 μM concentration with 4 mg of $Fe_3O_4@SiO_2$-N_n. Obtained results show that the adsorption rate of each ion differs due to the nanoparticles modification.
The highest Pb^{2+} binding capacity was achieved using $Fe_3O_4@SiO_2$-N_1 and $Fe_3O_4@SiO_2$-N_2. The smallest binding capacity was observed for Cd^{2+} ions by $Fe_3O_4@SiO_2$-N_2 and $Fe_3O_4@SiO_2$-N_1.
The Cd^{2+} biding was not observed for both $Fe_3O_4@SiO_2$-N_2 and $Fe_3O_4@SiO_2$-N_3 nanoparticles. Additionally, Pb^{2+} was not bound by $Fe_3O_4@SiO_2$-N_3. The research results show that the $Fe_3O_4@SiO_2$-N_3 nanoparticles bind copper ions with high selectivity.
For the first time we performed the adsorption-desorption experiments using DPASV to prove the Cu^{2+} binding activity of $Fe_3O_4@SiO_2$-N_3 nanoparticles. Obtained results indicate that examined nanoparticles show strong binding capability. Additionally, we obtained 99.9% recovery of Cu^{2+} ions.

1. Introduction

In the last few decades we observed increasing heavy metal pollution generated by human activity - manufacturing processes such as refining and use of fertiliser and pesticides. Heavy metals have caused serious environmental concerns due to their low biodegradability, bioaccumulation tendency and mutagenicity [1,2]. Many heavy metals are regarded as carcinogens [3]. Due to the dissemination of lead in the environment and its increasing usage in industry, its carcinogenicity has been an object of interest of many research projects. Based on the experimental carcinogenicity results, the International Agency for Research on Cancer (IARC) commission classified lead and inorganic lead derivatives in 2B group, considered as possible carcinogenic to humans [4], while cadmium is classified as a human carcinogen [5]. Lead does not cause cancer, but it can contribute to its development [6,7]. Cadmium causes cancer by multiple mechanism based on, among others, inhibition of DNA damage repair and oxidative stress [5]. Recycling of heavy metals from wastewater has become essential field of scientific research and industry.

In recent years scientists utilised many metal ion separation and removal methods, including chemical co-precipitation [8], chemical coagulation process [9], flotation [10,11] and microflotation [12] techniques, ion removal by membrane filtration [13], osmosis [14], extraction with ionic liquids [15]. Adsorption methods predominate over traditional separation techniques due to their simplicity, easy handling and sludge-free operation, regeneration capacity, and cost-effectiveness [16]. Many metal ion adsorbents are known, including pumice [17], composite mineral adsorbents [18], pectin-based adsorbents [19], organic frameworks [20], and carbonaceous

* Corresponding author.
E-mail address: pawel.niedzialkowski@ug.edu.pl (P. Niedziałkowski).

https://doi.org/10.1016/j.molliq.2020.113677
0167-7322/

materials, such as activated carbon [21], biochar [22], carbon nanotubes [23], and graphene oxide [24].

Nowadays, the most popular agents for wastewater ion removal are the superparamagnetic modified nanoparticle adsorbents based on iron oxide Fe_3O_4 — imprinted magnetic biosorbent [25], copolymerized polyacrylamide cellulose modified nanomagnetite [26], sultone-modified magnetic activated carbon for Cd^{2+}, Pb^{2+}, and As^{3+} removal [27], and many magnetic materials used for dye remediation [28–30]. The superparamagnetic Fe_3O_4 nanoparticles with functionalised surface adsorbent have been successfully applied to remove variety of wastewater heavy metal ions, such as copper, zinc, mercury, chromium, lead, cadmium, manganese, uranium, or silver [31–35]. Among adsorbents utilised to remove both organic and inorganic wastewater compounds, magnetic nanoparticles with large surface area, facile maintenance, and high efficiency took a special place due to the simple, convenient, and fast separation using external magnetic field [36–40]. In comparison with the traditional solvent extraction, these superparamagnetic modified nanoparticle adsorption methods are more economic, more cost-effective, and environmentally friendly [41]. Many research groups focused on the amino-functionalised Fe_3O_4@SiO_2 core-shell magnetic nanocomposites as a novel adsorbent for the removal of aqueous pollutants [42,43].

Metals like, among others, gadolinum, technetium, iron, manganese, cobalt, gallium, play a crucial role in medicine. These elements are widely used in diagnostic procedures as, for example, radioisotope or contrast agents. Additionally, platinum, gold, silver, lithium, zinc, iron, or bismuth may also be used in a treatment of various diseases [44].

Metals can also be extremely toxic and cause life-threatening illnesses [45]. One of the most frequently occurring diseases is Wilson's disease.

Wilson's disease is a rare, autosomal recessive, and lethal-without-treatment genetic disorder caused by the excessive copper storage in various body tissues. In the case of healthy individuals, we can observe a balance between intestinal absorption of dietary copper and its hepatic excretion in bile. In Wilson's disease, hepatic copper is neither excreted in bile, nor incorporated into ceruloplasmin. This abnormality causes the accumulation of copper to toxic levels and its storage mainly in liver, brain, and cornea. The signs of Wilson's disease are associated with liver diseases and neurological symptoms. The diagnosis is based on the elevated urinary and hepatic copper and low ceruloplasmin levels. Management of Wilson's disease involves decreasing the excess levels of copper, chelation therapy, and oral zinc therapy. In some cases, liver transplantation may be necessary [46].

In this work, a series of silica-coated superparamagnetic Fe_3O_4@SiO_2 core-shell nanoparticles with modified surfaces differing in the number of amino groups in outer chains — Fe_3O_4@SiO_2-N_1, Fe_3O_4@SiO_2-N_2, Fe_3O_4@SiO_2-N_3 — (see, Fig. 1) was synthesised. The characterisation of the obtained structures was performed using SEM, TEM, FT-IR, and XPS method. Subsequently, the capability of functionalised nanoparticles concerning simultaneous Cd^{2+}, Pb^{2+}, and Cu^{2+} ion binding was studied using electrochemical techniques, such as DPV in combination with HMDE and preconcentration method. Finally, the adsorption-desorption experiments using DPASV method were performed for the first time to examine the Cu^{2+} binding by Fe_3O_4@SiO_2-N_3 nanoparticles in an aqueous solution.

2. Experimental

2.1. Reagents

All reagents, analytical grade, were purchased from the indicated suppliers and used without further purification. Aqueous solutions were prepared using ultra-pure deionised water. Ferric chloride hexahydrate ($FeCl_3 \cdot 6H_2O$) and ferrous chloride tetrahydrate ($FeCl_2 \cdot 4H_2O$), ammonia (25%), tetraethyl orthosilicate (98%) (TEOS), 3-(aminopropyl)triethoxysilane (APTES) (99%), N-(2-aminoethyl)-3-aminopropyltrimethoxysilane and N^1-(3-trimethoxysilylpropyl) diethylenetriamine were purchased from Sigma-Aldrich (Poland). The organic solvents, potassium chloride KCl (99.9%), cadmium nitrate tetrahydrate $Cd(NO_3)_2 \cdot 4H_2O$ (99.9%), lead nitrate $Pb(NO_3)_2$, and copper nitrate trihydrate $Cu(NO_3)_2 \cdot 3H_2O$ (99.9%) were purchased from POCh (Poland).

2.2. Synthesis of Fe_3O_4

Fe_3O_4 nanoparticles were obtained by the coprecipitation method in an aqueous solution according to the procedure described by Panta et al. [47]. The reaction was performed in non-oxidising conditions maintaining the precise 1 to 2 molar ratio of Fe^{2+}/Fe^{3+} in an alkaline solution. The advantages and disadvantages of the synthesis reducing conditions were previously described by Kim [48]. The Fe_3O_4 nanoparticles were obtained by dissolving 10.81 g (0.04 mol) of $FeCl_3 \cdot 6H_2O$ and 3.98 g (0.02 mol) of $FeCl_2 \cdot 4H_2O$ in 50 mL of deionised water. Next, argon was passed through the vigorously stirred solution to eliminate oxygen and then the reaction mixture was heated to 70 °C. When the set temperature was reached, 500 mL of ammonium hydroxide solution was added dropwise up to pH 11, what resulted in the formation of Fe_3O_4. Obtained nanoparticles were washed with water to neutralise pH, washed with methanol, and dried.

2.3. Synthesis of core-shell Fe_3O_4@SiO_2 nanoparticles

Synthesis of Fe_3O_4@SiO_2 was conducted according to Ströber procedure, which mechanism and optimisation were widely described in the literature [47,49–52]. 0.1 g of Fe_3O_4 nanoparticles was dispersed in the mixture of ethanol and water (60:10, v/v) using an ultrasonic bath for 15 min. Subsequently, 1 mL of ammonium hydroxide and 2 mL of tetraethyl orthosilicate (TEOS) were added dropwise to the stirring solution at room temperature. After 24 h, the obtained nanoparticles were washed with water and ethanol and dried in vacuum at 60 °C.

2.4. Modification of core-shell Fe_3O_4@SiO_2 nanoparticles by amine derivatives

The functionalisation of Fe_3O_4@SiO_2 nanoparticles by amine derivatives was performed in anhydrous toluene [53–55] to achieve optimal surface coverage. 4 mL of 3-amino propyl-triethoxysilane (APTES), N-(2-aminoethyl)-3-aminopropyl trimethoxysilane, or N^1-(3-trimethoxysilylpropyl)diethylenetriamine was added to 0.5 g of Fe_3O_4@SiO_2 nanoparticles dispersed in 100 mL of anhydrous toluene using ultrasonic bath. Then, the mixture was mechanically stirred for 12 h at 90 °C. After cooling to room temperature, the obtained Fe_3O_4@SiO_2-N_n amino derivatives (Fe_3O_4@SiO_2-N_1, Fe_3O_4@SiO_2-N_2, or Fe_3O_4@SiO_2-N_3) were magnetically collected, washed several times using absolute ethanol, and dried under vacuum at 50 °C (Fig. 1).

2.5. Methods

The images of all Fe_3O_4@SiO_2-N_n nanoparticles were obtained using the scanning electron microscope (SEM) — JEOL JSM7001F, operating at 9.5 kV — and transmission electron microscopy (TEM) — Tecnai G2 Spirit BioTWIN FEI, operating at 120 kV. All nanoparticles samples for TEM imagining were sonicated for 30 min in the absolute ethanol solution.

Fourier Transform Infrared Spectroscopy (FT-IR) spectra were obtained with the KBr pellet method using Bruker FRA 106 spectrometer.

X-Ray Photoelectron Spectroscopy (XPS) was utilised to evaluate the chemical composition of the investigated nanoparticles. For this purpose, the high-resolution scans were performed in Fe2p, C1s, O1s, N1s, and Si2p binding energy range. The measurements were carried out on Escalab 250Xi spectroscope, ThermoFisher Scientific. The monochromatic AlKα excitation source was used with a spot diameter of 250 μm. 10 eV pass energy and 0.05 eV energy step size were utilised. The charge

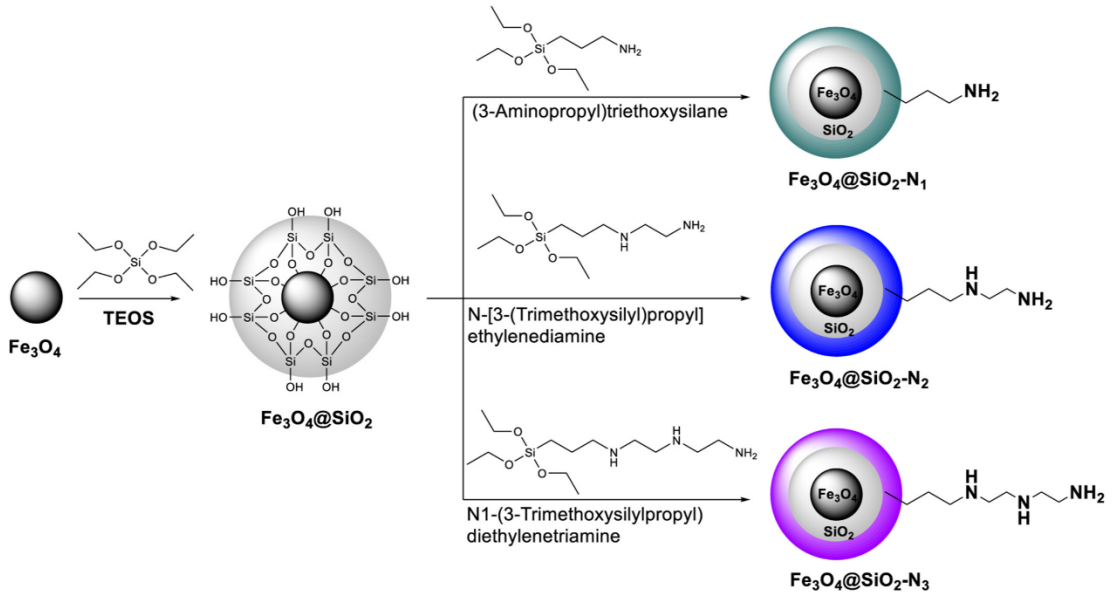

Fig. 1. Scheme of Fe_3O_4@SiO_2-N_n nanoparticles synthesis.

compensation was achieved through the low-energy electron and low-energy Ar^+ ions flow, with the final calibration of the XPS spectra for peak characteristics adventitious carbon C1s at 284.7 eV. The peak deconvolution was carried out using Avantage software provided by the spectroscope manufacturer.

All electrochemical measurements were carried out using Mercury Electrode Metrohm 663 VA Stand integrated with Autolab potentiostat/galvanostat PGSTAT-128 N controlled with NOVA 2.1.4 software. The three-electrode cell contained Static Drop Mercury Electrode (SDME) as a working electrode. Calomel $Hg|Hg_2Cl_2|KCl_{(saturated)}$ and glassy carbon (GC) were used as the reference and counter electrode, respectively.

Differential pulse voltammetry (DPV) was utilised for the detection of Cd^{2+}, Pb^{2+}, and Cd^{2+} ions under optimised experimental conditions: deposition potential −0.9 V, deposition time 90 s, modulation amplitude 0.05 V, modulation time 0.07 s, interval time 1.85 s, and step potential 0.005 V. All measurements were conducted in Teflon cell to avoid a sorption of metal ions on the glass surface.

The ion detection was performed in a potential range of −0.8 V to 0.0 V. The solutions of metal ions were prepared using potassium chloride KCl, pH 6.5 as the supporting electrolyte. Fe_3O_4@SiO_2-N_n nanoparticles were prepared by dispersion using the ultrasonic bath for 30 min before each measurement.

2.6. Determination of removal efficiency

The adsorption-desorption experiment was conducted to examine the efficiency of Cu^{2+} removal from an aqueous solution. The ion desorption process was investigated in 0.1 M HCl solution which was used as a desorbing agent. 5.08 mg of Fe_3O_4@SiO_2-N_3 was used to capture copper ions present in 10 mL of 4.3 μM Cu^{2+} solution. The solution was then left for 40 min at room temperature with shaking. Subsequently, all nanoparticles were collected magnetically and the supernatant was removed. Then, 10 mL of 0.1 M HCl was added to Fe_3O_4@SiO_2-N_3 nanoparticles with adsorbed Cu^{2+} and mixed with a stream of argon. The measurement of desorbed Cu^{2+} concertation was performed immediately using DPASV technique. The removal efficiency was calculated by the determination of the obtained voltammograms peak area for the standard solution and after desorption in 0.1 M HCl.

3. Results and discussion

3.1. SEM and TEM — morphology analysis

In the first step, the obtained Fe_3O_4@SiO_2-N_n nanoparticles were characterised using Scanning Electron Microscopy and Transmission Electron Microscopy (Fig. 2). SEM and TEM images of magnetite nanoparticles modified with different length of amino chains showed that the nanostructures received by co-precipitation method are highly homogeneous in shape and size. Fig. 3 confirms the presence of small and quasi-spherical core-shell structures. The average size of all Fe_3O_4@SiO_2-N_n nanoparticles was approximately 30–50 nm. All of the examined nanoparticles were in the agglomerated state due to their natural tendency to form agglomerates based on their magnetic nature.

3.2. FT-IR spectroscopy analysis

The FT-IR spectra were obtained to compare the spectroscopic differences and to validate the presence of functional groups on the nanomagnetite surface. Fig. 4a) shows the FT-IR spectra for pure Fe_3O_4 nanoparticles and silica-coated Fe_3O_4@SiO_2 as a reference and for nanoparticles functionalised by amino groups Fe_3O_4@SiO_2-N_1, Fe_3O_4@SiO_2-N_2, and Fe_3O_4@SiO_2-N_3. For all samples, two characteristic bands were shown at wavenumbers 453 cm^{-1} and 597 cm^{-1} from metal-oxygen stretching at Fe^{3+} site [56–58]. In all IR spectra, the decrease in the intensity of the Fe—O band for nanoparticles coated with silica and amino groups was observed. The decrease in the band intensity confirms that the nanoparticles surface was successfully functionalised [59]. Spectra for silica-coated nanoparticles showed a broad, strong band near 1096 cm^{-1} region assigned to symmetric and asymmetric

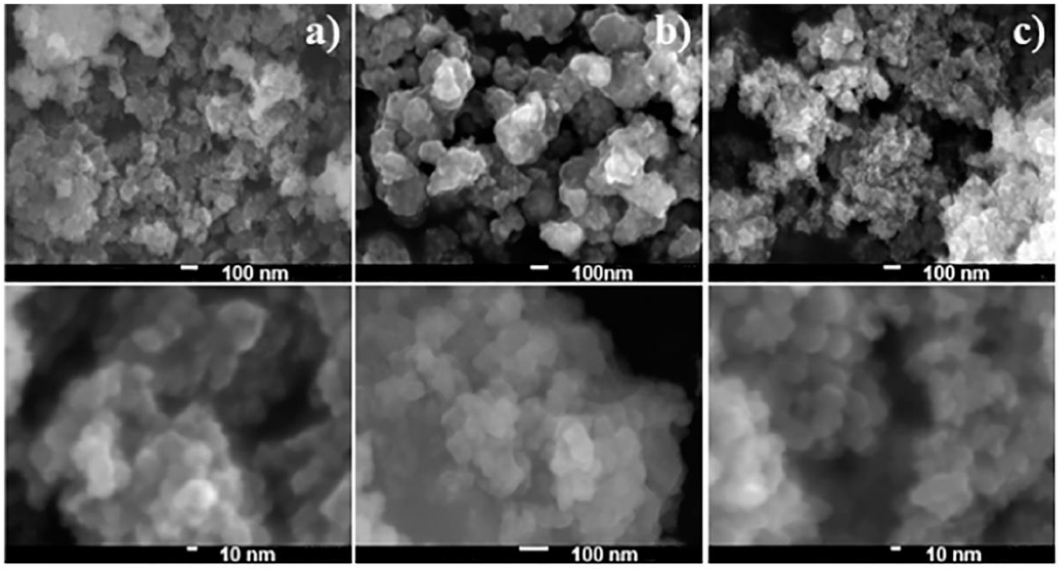

Fig. 2. SEM images of: column a) $Fe_3O_4@SiO_2$-N_1, column b) $Fe_3O_4@SiO_2$-N_2, and column c) $Fe_3O_4@SiO_2$-N_3.

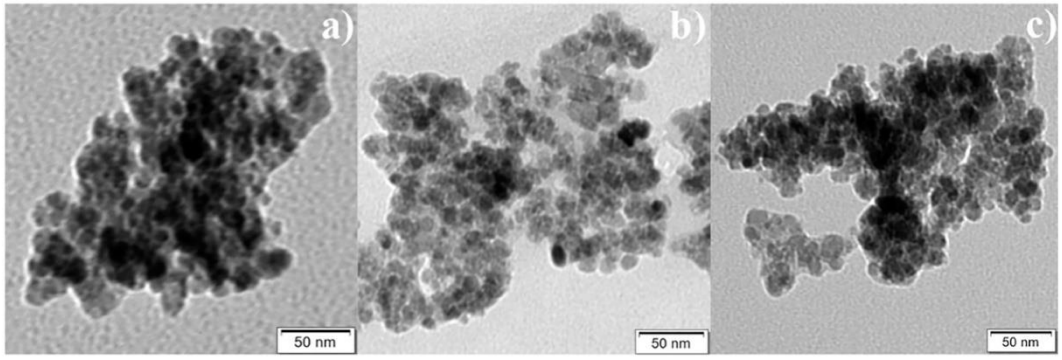

Fig. 3. TEM images of: a) $Fe_3O_4@SiO_2$-N_1, b) $Fe_3O_4@SiO_2$-N_2, and c) $Fe_3O_4@SiO_2$-N_3.

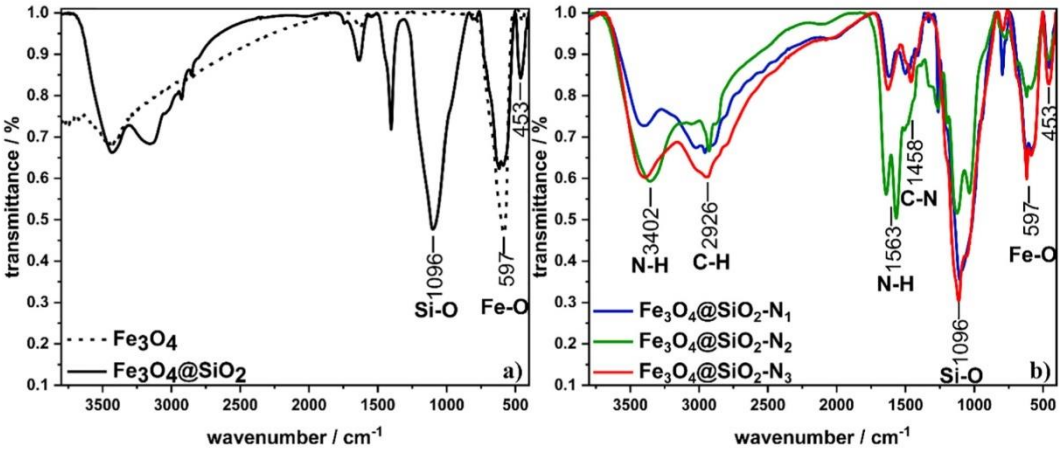

Fig. 4. FT-IR spectra for non-functionalised a) Fe_3O_4, $Fe_3O_4@SiO_2$ and b) functionalised $Fe_3O_4@SiO_2$-N_1, $Fe_3O_4@SiO_2$-N_2, and $Fe_3O_4@SiO_2$-N_3 nanoparticles.

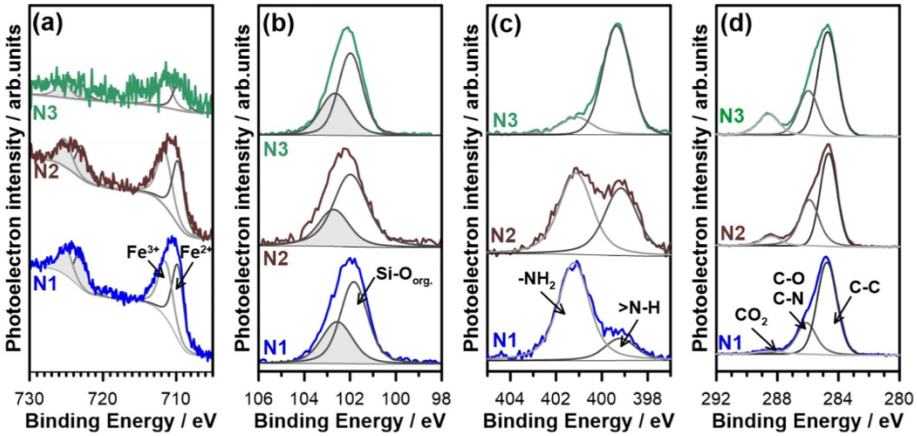

Fig. 5. High-resolution XPS spectra obtained for each investigated nanoparticle $Fe_3O_4@SiO_2$-N_1, $Fe_3O_4@SiO_2$-N_2, and $Fe_3O_4@SiO_2$-N_3 within the analysed binding energy range: (a) *Fe2p*, (b) *Si2p*, (c) *N1s*, and (d) *C1s* with superimposed deconvolution according to the model described below. The grey areas represent the $Fe2p_{1/2}$ and $Si2p_{1/2}$ peaks in *Fe2p* and *Si2p* peak doublets, respectively.

Si-O-Si stretching vibrations caused by the coating of silica shells on the magnetite surface [60].

On the spectra of all amino-modified nanoparticles (Fig. 4b) a new band appeared in the region of 1563 cm^{-1} and 3402 cm^{-1} attributed to N—H stretching vibrations of amino groups. These bands confirm the successful amino-functionalisation of the silica layer on $Fe_3O_4@SiO_2$ nanoparticles and the presence of terminal $–NH_2$ [61,62].

Additionally, a weak band at 1458 cm^{-1} attributed to the C—N stretch vibration was noticed [63]. The absorption bands at about 2930 cm^{-1} and 2850 cm^{-1} are the result of C—H stretching vibrations in the carbon chain [64].

These FT-IR spectra confirmed the formation of a silica shell on the surface of Fe_3O_4 and the amino-functionalisation of the $Fe_3O_4@SiO_2$ core-shell nanostructures.

3.3. XPS analysis

Moreover, we performed the XPS analyses for all obtained samples to confirm the structure of formed core-shell nanoparticles. The results of the high-resolution XPS analysis are collectively presented in Fig. 5 and Table 1 for each of the analysed samples.

The deconvolution in *Fe2p* binding energy (BE) range can be carried out with two spin-orbit doublets, characteristic for both Fe^{2+} and Fe^{3+}. Furthermore, *Fe2p* signal for $Fe_3O_4@SiO_2$-N_3 was barely detected [65–67]. The peak position remains unaltered for each studied compound, proving that modification of the organic chain does not influence the inner shell structure. Similar to the case of Fe_3O_4, the amount of silica is at its peak for $Fe_3O_4@SiO_2$-N_1 functionalisation. Moreover, the significant differences were not observed between $Fe_3O_4@SiO_2$-N_2 and $Fe_3O_4@SiO_2$-N_3 samples in this case, what may imply that the thickness of the organic amino shell is similar for both of these nanoparticles.

The shape of recorded *N1s* spectra reveal major differences between the analysed samples. Each of the nanoparticles contains nitrogen in two different chemical states, while their quantity differs significantly. Two deconvolution spectra used in the proposed model peak at 399.2 and 401.2 eV. The peak at higher BE's, dominant in the case of $Fe_3O_4@SiO_2$-N_1 sample, should represent the terminal amino-NH_2 functional groups in the compound. The presence of >N-H tertiary amino groups in $Fe_3O_4@SiO_2$-N_2 and $Fe_3O_4@SiO_2$-N_3 nanoparticles is reflected in *N1s* spectra with the increasing contribution of the component, located at lower binding energy range. Here, the share of terminal amino groups is reduced to 45% for $Fe_3O_4@SiO_2$-N_2 and to 18% for $Fe_3O_4@SiO_2$-N_3 samples. The aforementioned model finds a good correlation with the literature findings. The presence of N—H groups in $Fe_3O_4@SiO_2$-N_1 can be associated with the adsorption of CO_2 from the ambient atmosphere [68–70].

The presence of Si—O bonds with the organic chain was confirmed by a strong peak doublet at 101.7 eV. Similar values were previously reported for silicone groups in silanes and other organic, silicon-containing compounds [58,71]. Finally, the *C1s* peak region was analysed and deconvoluted in three different chemical states. The most significant component, detected at 284.7 eV, should be ascribed to C—C and C—H bonds in the functionalisation molecules forming the shell of the nanoparticles. Its total share in the analysed signal ranges between 33.3 and 36.8 at.%. Importantly, the presence of the component mentioned above may be caused by adventitious carbon from the air exposure [72]. The second notable component lies at 286.2 eV, an energy range typical for C—N bonds in amines and C—O bonds [73,74]. The share of the organic chain (measured as a sum of C—C and C—N components) is naturally the most prominent for the shortest amino chains with $Fe_3O_4@SiO_2$-N_1 molecule functionalisation. However, the significant differences were not observed between $Fe_3O_4@SiO_2$-N_2 and $Fe_3O_4@SiO_2$-N_3 samples, what is similar to the earlier conclusion regarding *Si2p* component. Finally, the last *C1s* peak emerges for both $Fe_3O_4@SiO_2$-N_2 and $Fe_3O_4@SiO_2$-N_3 samples, at energies exceeding 288 eV. This component is most often ascribed to carbon dioxide, which is probably adsorbed onto the nanoparticles surface [75]. Surface defects as well as structure modifications of the examined compounds influence the CO_2 adsorption [76,77]. Since its contribution is the highest for the $Fe_3O_4@SiO_2$-N_3 sample, it is suggested that its presence is connected with changes within >NH groups.

These analyses are confirmed in the distribution of various components in *O1s* spectra, which were deconvoluted in three peaks, connected with iron oxides (529.9 eV), silica, and possible C—O interaction (531.7 eV) and C═O bonds (533.5 eV). The Fe_3O_4 signal is the strongest for $Fe_3O_4@SiO_2$-N_1 sample and is up to four times weaker for $Fe_3O_4@SiO_2$-N_3, where, on the other hand, the signal from C═O bonds is more prominent. The two times higher contribution from silica in the *O1s* of $Fe_3O_4@SiO_2$-N_1 sample was also confirmed, strongly supporting the hypothesis regarding the smaller functionalisation thickness of these nanoparticles.

Table 1
Surface chemical composition of Fe_3O_4@SiO_2-N_1, Fe_3O_4@SiO_2-N_2, and Fe_3O_4@SiO_2-N_3 samples based on the deconvoluted high-resolution XPS spectra.

	Fe2p		*Si2p*	*N1s*		*C1s*			*O1s*		
	Fe^{2+}	Fe^{3+}	Si-O	>NH	-NH_2	C-C	CN	C=O	Fe-O	Si-O	C=O
BE/eV	709.8	711.4	101.7	399.2	401.2	284.7	286.1	288.5	529.9	531.7	533.5
N_1	1.1	1.0	13.0	1.3	5.7	33.3	12.8	1.3	4.0	25.3	1.2
N_2	0.7	0.7	7.9	2.8	3.4	34.2	22.0	4.4	2.6	16.9	4.3
N_3	0.1	0.1	7.9	8.2	1.7	36.8	16.1	8.0	0.9	17.0	3.1

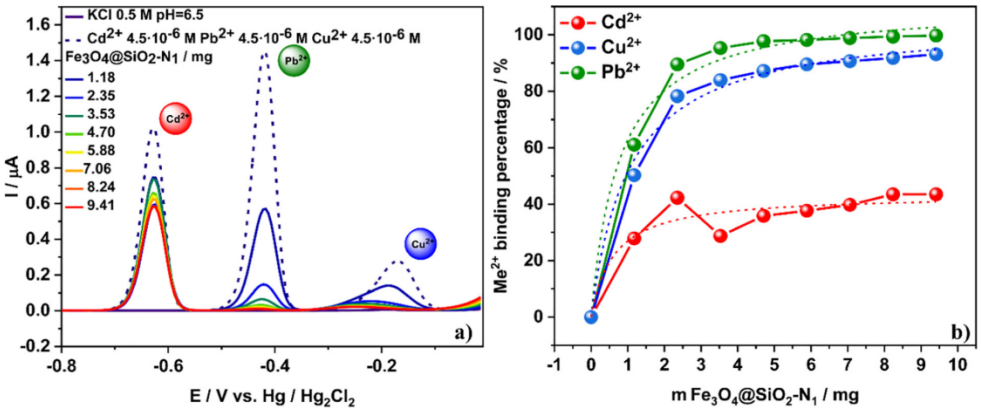

Fig. 6. a) Anodic stripping voltammograms and b) percentage of Cd^{2+} (4.5 μM), Pb^{2+} (4.5 μM) and Cu^{2+} (4.5 μM) binding by Fe_3O_4@SiO_2-N_1 nanoparticles.

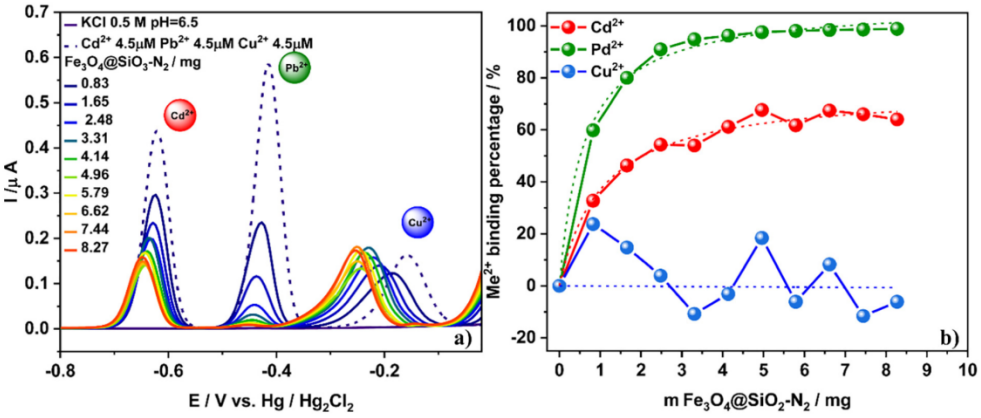

Fig. 7. a) Anodic stripping voltammograms and b) percentage of Cd^{2+} (4.5 μM), Pb^{2+} (4.5 μM), and Cu^{2+} (4.5 μM) binding by Fe_3O_4@SiO_2-N_2 nanoparticles.

3.4. Simultaneous electrochemical determination of Cd^{2+}, Pb^{2+}, and Cu^{2+}

The individual and simultaneous determination of Cd^{2+}, Cu^{2+}, and Pb^{2+} applying amino-functionalised Fe_3O_4@Carbon microspheres were previously measured by Bai et al. [78] using modified glassy carbon electrode.

In this work, the simultaneous detection of Cd^{2+}, Pb^{2+}, and Cu^{2+} was carried out under optimised experimental conditions using DPASV technique and HDM electrode. The main advantage of these electrodes, besides its surface reproducibility and fast measurement, [79] is the analysis of Fe_3O_4@SiO_2-N_n nanoparticles to assess their capability for binding the metal ions without electrode modification. We investigated three types of nanoparticles differing in the number of amino groups in the outer carbon chain — Fe_3O_4@SiO_2-N_1 with one amino group, Fe_3O_4@SiO_2-N_2 with two amino groups, and Fe_3O_4@SiO_2-N_3 with three amino groups.

To achieve this goal, all measurements were conducted under laboratory conditions to reduce the risk of environmental mercury contamination. Mercury from HDME can be reused after proper treatment. Two-stage DPASV analysis involved pre-concentration and metal ions

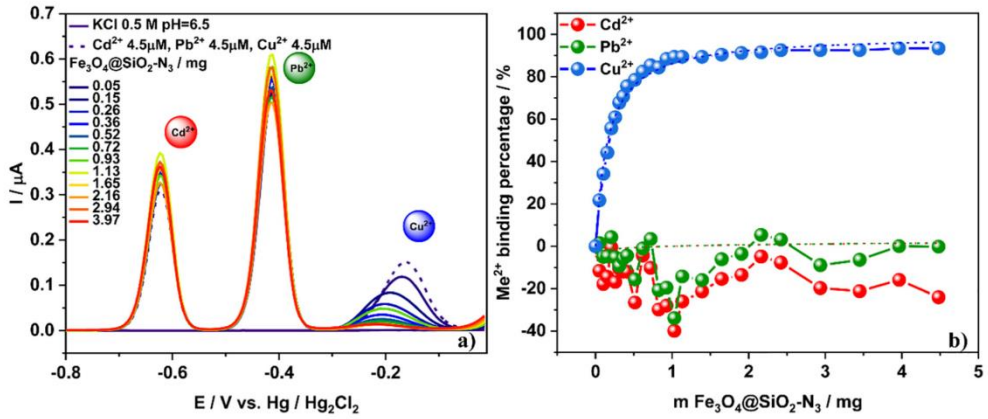

Fig. 8. a) Anodic stripping voltammograms and b) percentage of Cd^{2+} (4.5 µM), Pb^{2+} (4.5 µM), and Cu^{2+} (4.5 µM) binding by $Fe_3O_4@SiO_2$-N_3 nanoparticles.

stripping. First, the Cd^{2+}, Pb^{2+}, and Cu^{2+} ions were electrodeposited onto the working electrode by application of the negative potential (−0.9 V). Subsequently, the faradic current obtained by oxidation was recorded during the potential sweep toward the anodic direction (−0.8 V to 0.0 V).

To examine the selected ion binding abilities of $Fe_3O_4@SiO_2$-N_1, $Fe_3O_4@SiO_2$-N_2, and $Fe_3O_4@SiO_2$-N_3, series of measurements were performed in the solution containing Cd^{2+}, Pb^{2+}, and Cu^{2+}, 4.5 µM concentration. All electrochemical experiments were performed in 0.5 M KCl pH = 6.5 due to the formation of hydroxides of utilised metals at pH higher than 7 [58]. Furthermore, the adsorption of metal ions depends on the charge located on the nanocomposite surface and the number of functional groups [80].

Three well-defined peaks at −0.63 V, −0.42 V, and −0.17 V in anodic stripping voltammograms confirm the presence of Cd^{2+}, Pb^{2+}, and Cu^{2+} in the solution, respectively (see, Fig. 6). During the next portions of nanoparticles addition, a decrease in the intensity of the ions peaks was observed. The rate of peaks intensity change depended on the determined ion and used nanoparticles type. In all presented voltammograms, the dilution factor was expressed by the formula: $DF = \frac{V_0+V_s}{V_0}$, where V_0 is the initial volume and V_s is the step volume applied.

Fig. 6a) presents the voltammograms obtained during the titration of Cd^{2+}, Pb^{2+}, and Cu^{2+} by $Fe_3O_4@SiO_2$-N_1. The metal ion peaks intensity decreased during the addition of the next portions of nanoparticles in an amount of 1.18 mg to 9.41 mg, conducted in eight steps. The obtained results directly indicate that the initial linear current peak (blue intermittent line) decreases for Pb^{2+} and Cu^{2+} ions of each nanoparticles portion.

The intensity of Cd^{2+} peak decreased by a half and remained at this stable level. After the addition of 7.06 mg of nanoparticles, the equilibrium was established and the next portion of nanoparticles caused no changes in the current peak intensity. The $Fe_3O_4@SiO_2$-N_1 binding percentage was calculated (Fig. 6b) for Pb^{2+} and Cu^{2+} and reached 99.7% and 92.8%, respectively. However, the binding percentage for Cd^{2+} remained stable at the level of 40%. These results indicate that $Fe_3O_4@SiO_2$-N_1 nanoparticles express high sensitivity toward Pb^{2+} and Cu^{2+}, what is observed by binding of these ions in nearly 100%.

In the next step, we conducted the simultaneous experiments using Cd^{2+}, Pb^{2+} and Cu^{2+} to evaluate the $Fe_3O_4@SiO_2$-N_2 nanoparticles binding capacity. The titration of Cd^{2+}, Pb^{2+}, and Cu^{2+} was carried out in five steps using various amounts of $Fe_3O_4@SiO_2$-N_2 nanoparticles — 0.83 mg to 8.27 mg (Fig. 7a).

Surprisingly, besides a decrease in the peak intensity observed during Cd^{2+}, Pb^{2+} titration, we also detected a slight shift in the peaks toward lower potentials. Fig. 7a shows the voltammograms where a complete disappearance of Pb^{2+} peak and decrease in the Cd^{2+} peak intensity were observed.

In the case of Cu^{2+} titration (Fig. 7a), the effect of the signal decreasing is observed only in the first two steps, following a comparable signal level afterwards, shifted toward negative potentials. This phenomenon is probably associated with the adsorption of nanoparticles and their complexes to the mercury drop [81]. The irregular changes in the peak intensity clearly indicate that the equilibrium is not establishing.

After addition of 3.31 mg $Fe_3O_4@SiO_2$-N_2 no significant changes in the voltammogram were observed. Fig. 7b shows the binding percentage for $Fe_3O_4@SiO_2$-N_2 nanoparticles. The percentage of Pb^{2+} and Cd^{2+} ion binding by $Fe_3O_4@SiO_2$-N_2 was established at 98.5% and 66.6%, respectively. It is worth to notice that there was no ion binding

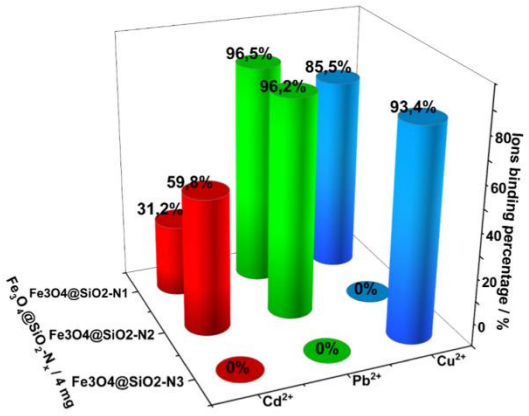

Fig. 9. Cd^{2+}, Pb^{2+}, Cu^{2+} ions binding percentage for $Fe_3O_4@SiO_2$-N_1, $Fe_3O_4@SiO_2$-N_2 and $Fe_3O_4@SiO_2$-N_3 nanoparticles.

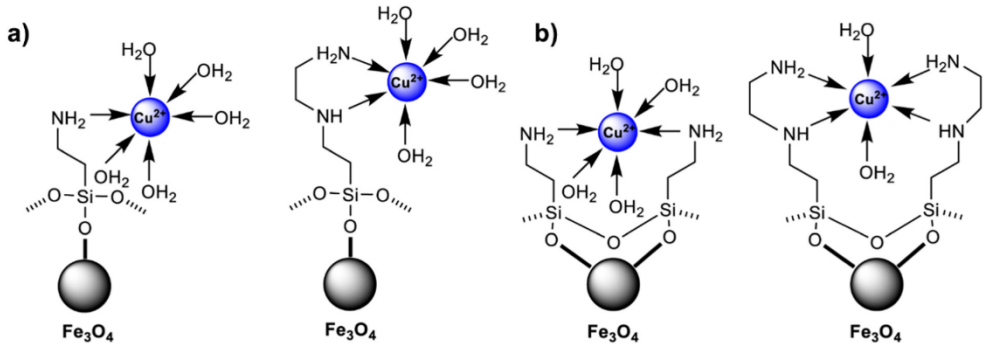

Fig. 10. Proposed structure of the two-type complexes a) 1:1 and b) 1:2 Fe_3O_4@SiO_2-N_n nanoparticles and ion metal interactions.

observed for Cu^{2+}. The percentage of Cu^{2+} binding by Fe_3O_4@SiO_2-N_2 remains at 0% even if nanoparticles were added in an excess. An average of obtained results and slight differences in Cu^{2+} peak intensity were regarded as measurement errors.

The voltammograms presented in Fig. 8a reveal the Cd^{2+}, Pb^{2+}, and Cu^{2+} titration by Fe_3O_4@SiO_2-N_3 in twelve steps in the nanoparticles amount range of 0.05 mg to 3.97 mg. The addition of the next nanoparticles portions led only to the disappearance of the Cu^{2+} peak. The Cd^{2+} and Pb^{2+} slight peak intensity changes were considered to be in the range of measurement error. For Fe_3O_4@SiO_2-N_3 nanoparticles, the Cu^{2+} binding percentage reached 92.5%, while 0% binding percentage was observed for Cd^{2+} and Pb^{2+} ions (Fig. 8b).

Fig. 9 presents the comparison of ion binding percentage for each Fe_3O_4@SiO_2-N_n nanoparticle. The binding percentage was recounted for 4 mg of nanoparticles added to the ion solution. The highest observed binding percentage for Pb^{2+} was over 96%, both for Fe_3O_4@SiO_2-N_1 and Fe_3O_4@SiO_2-N_2. The slightly smaller binding percentage was observed for Cu^{2+} binding by Fe_3O_4@SiO_2-N_3 and Fe_3O_4@SiO_2-N_1 resulting in 93.4% and 85.5%, respectively.

Furthermore, there was no Cd^{2+}, Pb^{2+}, and Cu^{2+} binding observed for Fe_3O_4@SiO_2-N_3, Fe_3O_4@SiO_2-N_3, and Fe_3O_4@SiO_2-N_2, respectively. These results directly indicate that the Fe_3O_4@SiO_2-N_3 nanoparticles bind Cu^{2+} with high selectivity.

On the basis of the structural characteristics of Cu (II) diamine complexes supported on silica gel and the distribution of these forms as a function of the pH solution described by Nowicki [82], the proposed structure of copper complex formation by Fe_3O_4@SiO_2-N_n is presented in Fig. 10. It seems that formation of complexes with metal ions with 1:1 and 1:2 stoichiometry is the key factor in the complexation of ions by amines in the hybrid material (Fig. 10).

The number of donor nitrogen atoms in the structure of the complexes, the size of the ions, the density of the charge of metal ions, and the number of water molecules that hydrate both the complexes and ligands significantly determine the stoichiometry and the process of complex formation by the hybrid material [83].

The differences in the binding selectivity for the examined metal ions by Fe_3O_4@SiO_2-N_n is probably related to the presence of intramolecular hydrogen bonds occurring both in the external and internal parts of the functional layer. The observation that Fe_3O_4@SiO_2-N_1 binds Cd^{2+}, Pb^{2+}, Cu^{2+}, Fe_3O_4@SiO_2-N_2 binds Cd^{2+}, Pb^{2+}, and Fe_3O_4@SiO_2-N_3 binds only Cu^{2+} results from these interactions. The aqua and amino complexes form between metal ions and amines with the deposition directly on a hybrid material. Subsequently, free electron pairs in this material, which come to varying degrees from nitrogen atoms of amines, determine the manner and selectivity of the ion binding with the studied material.

3.5. Cu^{2+} adsorption-desorption experiment using Fe_3O_4@SiO_2-N_3 nanoparticles

Based on the high selectivity of Fe_3O_4@SiO_2-N_3 for Cu^{2+} which was observed using electrochemical method, we decided to evaluate the adsorption-desorption properties only of this studied nanoparticle. It is worth to notice that, according to the authors' knowledge, this experiment using DPASV was performed for the first time. The procedure of Cu^{2+} adsorption was described in the experimental section. 5.08 mg of Fe_3O_4@SiO_2-N_3 was used to bind 43 nmol of Cu^{2+} in 0.5 M KCl solution. The adsorption process for nanoparticles containing an amino group is usually performed from a couple of minutes to hours [43,84–86]. In this work, the adsorption process was performed within 40 min incubation time at room temperature, with shaking. The desorption process was performed in 0.1 M HCl to obtain acidic pH and protonation of amino groups leading to the Cu^{2+} ions desorption. The desorption process was conducted using DPASV method directly after the addition of HCl. According to the previous research, the hydrochloric acid was selected as an optimal desorption agent [61,84]. In other study the desorption time ranged from 5 min to 40 min [43,85]. We, however, established the desorption time which was shorter than 5 min. Fig. 11 shows the voltammograms obtained for standard Cu^{2+} solution and after the nanoparticles regeneration. The peak shift is the consequence

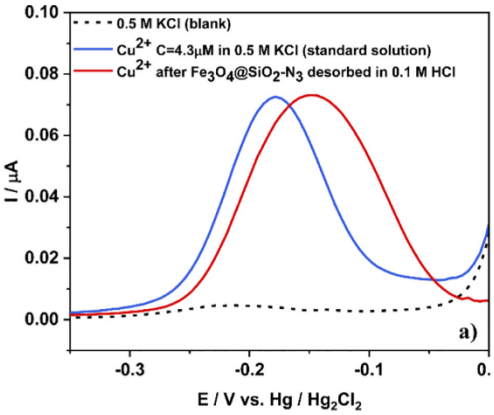

Fig. 11. Comparison of anodic stripping voltammograms of 0.5 M KCl electrolyte (blank), Cu^{2+} standard solution C = 4.3 μM, Cu^{2+} after Fe_3O_4@SiO_2-N_3 nanoparticles regeneration.

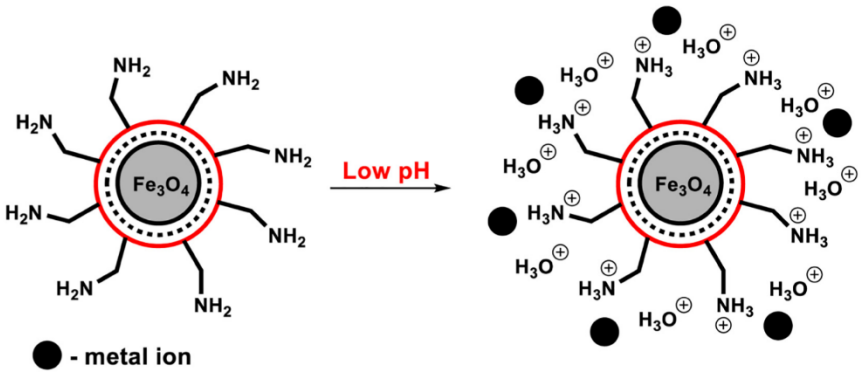

Fig. 12. Scheme of the proposed adsorption and desorption mechanism for the $Fe_3O_4@SiO_2$-N_n nanoparticles — metal ions interaction.

of different pH of the solution. The calculated Cu^{2+} removal efficiency was 99.9%.

Proper selection of pH range, which effects the behaviour of the nanoparticles, the form of determined metal ion, and its solubility, is the most important factor for the examination of the adsorption and desorption process efficiency [86]. The form of Cu^{2+} depends on the pH value of the solution. Cu^{2+} species occur at pH < 7 [84,87]. At pH > 7 different derivative products of Cu^{2+} hydrolysis — $Cu_2(OH)_2^{2+}$, $Cu(OH)^+$, $Cu(OH)_2$, $Cu(OH)_3^-$, $Cu(OH)_4^-$ — exist in the solution [88]. The Cu^{2+} quantity drops with the increasing pH value, what leads to the precipitation of various hydrolysis forms of Cu^{2+}. Due to this phenomenon, the adsorption process was performed at pH 6.5.

The adsorption and desorption process occurring for the studied nanoparticles is the consequence of the acid-base interactions. In an aqueous solution both H_3O^+ and metal ions undergo the adsorption processes onto amino groups present in $Fe_3O_4@SiO_2$-N_n nanoparticles (Fig. 12). Low pH value causes the increase of H_3O^+ species in a solution and the protonation of amino groups present on the nanoparticles surface. This, in consequence, leads to the decrease in the metal ion concentration due to the nanoparticle adsorption (Fig. 12). On the other hand, high pH value is associated with the elevated number of hydroxyl groups in the solution, what causes the amino groups deprotonation (Fig. 12). In consequence, the deprotonated amino groups increased the capability of the nanoparticles to bind metal ions [86].

4. Conclusions

In present work we examined a series of functionalised magnetite nanoparticles $Fe_3O_4@SiO_2$-N_n as a novel Cd^{2+}, Pb^{2+}, Cu^{2+} nano-adsorbent in KCl aqueous solution.

First, we synthetised the nanoparticles coated preliminary with SiO_2 using TEOS and then with various carbon chains containing a different number of amino groups — $Fe_3O_4@SiO_2$-N_1, $Fe_3O_4@SiO_2$-N_2, and $Fe_3O_4@SiO_2$-N_3. FT-IR and XPS spectra confirmed the presence of characteristic functional groups on the nanoparticles surface. Additionally, SEM and TEM analysis were utilised to confirm the homogenous spherical 30 to 50 nm nanostructures.

These three types of obtained nanoparticles were used as Cd^{2+}, Pb^{2+}, Cu^{2+} metal ion adsorbents. Metal ion binding ability of $Fe_3O_4@SiO_2$-N_n was measured using DPASV method in combination with HDME in 0.5 M KCl solution.

To compare binding capacity in 4.5 μM Cd^{2+}, Pb^{2+}, and Cu^{2+} solutions, the binding percentage was recalculated for 4 mg of used nanoparticles. Obtained results show that the adsorption rate is different for each ion depending on the nanoparticles type. The ion binding capacity and selectivity depends on the interactions occurring between the outer carbon amino chains and the metal ion.

The highest binding percentage — 96% — was observed for Pb^{2+} binding for both $Fe_3O_4@SiO_2$-N_1 and $Fe_3O_4@SiO_2$-N_2. Furthermore, slightly lower binding level of nearly 93% was observed for $Fe_3O_4@SiO_2$-N_3 Cu^{2+}. The middle value of the binding percentage — 85% — was observed for Cu^{2+} binding by $Fe_3O_4@SiO_2$-N_1. The lowest binding percentage was found in the case of $Fe_3O_4@SiO_2$-N_2 and $Fe_3O_4@SiO_2$-N_1 for Cd^{2+} at the level of 60% and 31%, respectively. Moreover, the binding was not observed for Cd^{2+} and Pb^{2+} by $Fe_3O_4@SiO_2$-N_3 and for Pb^{2+} by $Fe_3O_4@SiO_2$-N_3. The obtained results show that the nanoparticles with three amino groups in the outer chain — $Fe_3O_4@SiO_2$-N_3 — bind Cu^{2+} with high selectivity.

Furthermore, we used the adsorption and desorption experiment to analyse the Cu^{2+} binding selectivity of $Fe_3O_4@SiO_2$-N_3. The obtained results directly indicate that the recovery of Cu^{2+} from the aqueous solution is very high and reached 99.9%.

Examined series of amino functionalised $Fe_3O_4@SiO_2$-N_n nanoparticles are promising metal ion nano-adsorbents due to their high ion capacity, easy separation using magnetic field, and renewability based on the pH value control.

CRediT authorship contribution statement

A. Kulpa: Methodology, Formal analysis, Investigation, Visualization, Writing - original draft, Writing - review & editing, Project administration. **J. Ryl:** Formal analysis, Investigation, Writing - original draft. **G. Schroeder:** Formal analysis, Investigation. **A. Koterwa:** Formal analysis, Investigation, Visualization. **J. Sein Anand:** Writing - original draft, Software. **T. Ossowski:** Conceptualization, Supervision. **P. Niedziałkowski:** Conceptualization, Formal analysis, Writing - original draft, Writing - review & editing, Visualization, Supervision.

Declaration of competing interest

The authors declare that they have no known competing financial interests or persona l relationships that could have appeared to influence the work reported in this paper.

Acknowledgements

This study was financed by the University of Gdansk within the project supporting young scientists and PhD students (grant No. BMN 539-8210-B281-18 and 539-8210-B281-19). Authors are grateful to Alexander Company Gdynia for a technical support.

References

[1] N.K. Srivastava, C.B. Majumder, Novel biofiltration methods for the treatment of heavy metals from industrial wastewater, J. Hazard. Mater. 151 (2008) 1–8, https://doi.org/10.1016/j.jhazmat.2007.09.101.

[2] M. Noreen, M. Shahid, M. Iqbal, J. Nisar, Measurement of cytotoxicity and heavy metal load in drains water receiving textile effluents and drinking water in vicinity of drains, Measurement 109 (2017) 88–99, https://doi.org/10.1016/j.measurement.2017.05.030.

[3] H.S. Kim, Y.J. Kim, Y.R. Seo, An overview of carcinogenic heavy metal: molecular toxicity mechanism and prevention, Journal of Cancer Prevention 20 (2015) 232–240, https://doi.org/10.15430/JCP.2015.20.4.232.

[4] H. Fu, P. Boffetta, Cancer and occupational exposure to inorganic lead compounds: a meta-analysis of published data, Occup. Environ. Med. 52 (1995) 73–81, https://doi.org/10.1136/oem.52.2.73.

[5] P. Joseph, Mechanisms of cadmium carcinogenesis, Toxicol. Appl. Pharmacol. 238 (2009) 272–279, https://doi.org/10.1016/j.taap.2009.01.011.

[6] E.K. Silbergeld, M. Waalkes, J.M. Rice, Lead as a carcinogen: experimental evidence and mechanisms of action, Am. J. Ind. Med. 38 (2000) 316–323, https://doi.org/10.1002/1097-0274(200009)38:3<316::AID-AJIM11>3.0.CO;2-P.

[7] E.K. Silbergeld, Facilitative mechanisms of lead as a carcinogen, Mutation Research/Fundamental and Molecular Mechanisms of Mutagenesis 533 (2003) 121–133, https://doi.org/10.1016/j.mrfmmm.2003.07.010.

[8] V.N. Bulut, H. Demirci, D. Ozdes, A. Gundogdu, O. Bekircan, M. Soylak, C. Duran, A novel carrier element-free co-precipitation method for separation/preconcentration of lead and cadmium ions from environmental matrices, Environ. Prog. Sustain. Energy 35 (2016) 1709–1715, https://doi.org/10.1002/ep.12422.

[9] X. Tang, H. Zheng, H. Teng, Y. Sun, J.-S. Guo, W. Xie, Q. Yang, W. Chen, Chemical coagulation process for the removal of heavy metals from water: a review, Desalin. Water Treat. 57 (2014) 1–16, https://doi.org/10.1080/19443994.2014.977959.

[10] S.E. GHAZY, Separation of cadmium(II) from aqueous solutions by the precipitate flotation technique, Sep. Sci. Technol. 29 (1994) 935–941, https://doi.org/10.1080/01496399408006637.

[11] M.H. Salmani, M. Davoodi, M.H. Ehrampoush, M.T. Ghaneian, M.H. Fallahzadah, Removal of cadmium (II) from simulated wastewater by ion flotation technique, Iranian J Environ Health Sci Eng 10 (2013) 16–20, https://doi.org/10.1186/1735-2746-10-16.

[12] J.B. Melville, E. Matijevic, Removal of copper, lead, and cadmium ions by microflotation, J. Colloid Interface Sci. 57 (1976) 94–103, https://doi.org/10.1016/0021-9797(76)90179-X.

[13] H. Abu-Qudais, H. Moussa, Removal of heavy metals from wastewater by membrane processes: a comparative study, Desalination 164 (2004) 105–110, https://doi.org/10.1016/S0011-9164(04)00169-9.

[14] J. Kheriji, D. Tabassi, B. Hamrouni, Removal of Cd(II) ions from aqueous solution and industrial effluent using reverse osmosis and nanofiltration membranes, Water Sci. Technol. 72 (2015) 1206–1216, https://doi.org/10.2166/wst.2015.326.

[15] A.P. de los Ríos, F.J. Hernández-Fernández, L.J. Lozano, S. Sánchez, J.I. Moreno, C. Godínez, Removal of metal ions from aqueous solutions by extraction with ionic liquids, J. Chem. Eng. Data 55 (2010) 605–608, https://doi.org/10.1021/je9005008.

[16] G.K. Sarma, S. Sen Gupta, K.G. Bhattacharyya, Nanomaterials as versatile adsorbents for heavy metal ions in water: a review, Environ. Sci. Pollut. Res. 26 (2019) 6245–6278, https://doi.org/10.1007/s11356-018-04093-y.

[17] S.H. Khorzughy, T. Eslamkish, F.D. Ardejani, M.R. Heydartaemeh, Cadmium removal from aqueous solutions by pumice and nano-pumice, Korean J. Chem. Eng. 32 (2015) 88–96, https://doi.org/10.1007/s11814-014-0168-2.

[18] W.-R. Lim, S.W. Kim, C.-H. Lee, E.-K. Choi, M.H. Oh, S.N. Seo, H.-J. Park, S.-Y. Hamm, Performance of composite mineral adsorbents for removing Cu, Cd, and Pb ions from polluted water, Sci. Rep. 9 (2019) 1–10, https://doi.org/10.1038/s41598-019-49857-9.

[19] R. Wang, R. Liang, T. Dai, J. Chen, X. Shuai, C. Liu, Pectin-based adsorbents for heavy metal ions: a review, Trends Food Sci. Technol. 91 (2019) 319–329, https://doi.org/10.1016/j.tifs.2019.07.033.

[20] J. Li, X. Wang, G. Zhao, C. Chen, Z. Chai, A. Alsaedi, T. Hayat, X. Wang, Metal–organic framework-based materials: superior adsorbents for the capture of toxic and radioactive metal ions, Chem. Soc. Rev. 47 (2018) 2322–2356, https://doi.org/10.1039/C7CS00543A.

[21] S. Abdulrazak, K. Hussaini, H.M. Sani, Evaluation of removal efficiency of heavy metals by low-cost activated carbon prepared from African palm fruit, Appl Water Sci 7 (2017) 3151–3155, https://doi.org/10.1007/s13201-016-0460-x.

[22] L. Wang, Y. Wang, F. Ma, V. Tankpa, S. Bai, X. Guo, X. Wang, Mechanisms and reutilization of modified biochar used for removal of heavy metals from wastewater: a review, Sci. Total Environ. 668 (2019) 1298–1309, https://doi.org/10.1016/j.scitotenv.2019.03.011.

[23] S.S. Fiyadh, M.A. AlSaadi, W.Z. Jaafar, M.K. AlOmar, S.S. Fayaed, N.S. Mohd, L.S. Hin, A. El-Shafie, Review on heavy metal adsorption processes by carbon nanotubes, J. Clean. Prod. 230 (2019) 783–793, https://doi.org/10.1016/j.jclepro.2019.05.154.

[24] W. Peng, H. Li, Y. Liu, S. Song, A review on heavy metal ions adsorption from water by graphene oxide and its composites, J. Mol. Liq. 230 (2017) 496–504, https://doi.org/10.1016/j.molliq.2017.01.064.

[25] Y. He, P. Wu, W. Xiao, G. Li, J. Yi, Y. He, C. Chen, P. Ding, Y. Duan, Efficient removal of Pb(II) from aqueous solution by a novel ion imprinted magnetic biosorbent: adsorption kinetics and mechanisms, PLoS One 14 (2019), e0213377. , 1-17 https://doi.org/10.1371/journal.pone.0213377.

[26] I. Hasan, R.A. Khan, W. Alharbi, K.H. Alharbi, A. Alsalme, In situ copolymerized polyacrylamide cellulose supported Fe3O4 magnetic nanocomposites for adsorptive removal of Pb(II): artificial neural network modeling and experimental studies, Nanomaterials 9 (2019) 1687, https://doi.org/10.3390/nano9121687.

[27] V. Nejadshafiee, M.R. Islami, Adsorption capacity of heavy metal ions using sultone-modified magnetic activated carbon as a bio-adsorbent, Mater. Sci. Eng. C 101 (2019) 42–52, https://doi.org/10.1016/j.msec.2019.03.081.

[28] N.T. Abdel-Ghani, G.A. El-Chaghaby, E.-S.A. Rawash, E.C. Lima, Magnetic activated carbon nanocomposite from Nigella sativa L. waste (MNSA) for the removal of Coomassie brilliant blue dye from aqueous solution: statistical design of experiments for optimization of the adsorption conditions, J. Adv. Res. 17 (2019) 55–63, https://doi.org/10.1016/j.jare.2018.12.004.

[29] Y. Ji, C. Ma, J. Li, H. Zhao, Q. Chen, M. Li, H. Liu, A magnetic adsorbent for the removal of cationic dyes from wastewater, Nanomaterials 8 (710) (2018) 1–13, https://doi.org/10.3390/nano8090710.

[30] C. Jiang, X. Wang, D. Qin, W. Da, B. Hou, C. Hao, J. Wu, Construction of magnetic lignin-based adsorbent and its adsorption properties for dyes, J. Hazard. Mater. 369 (2019) 50–61, https://doi.org/10.1016/j.jhazmat.2019.02.021.

[31] E. Ghasemi, A. Heydari, M. Sillanpää, Superparamagnetic Fe3O4@EDTA nanoparticles as an efficient adsorbent for simultaneous removal of Ag(I), Hg(II), Mn(II), Zn (II), Pb(II) and Cd(II) from water and soil environmental samples, Microchem. J. 131 (2017) 51–56, https://doi.org/10.1016/j.microc.2016.11.011.

[32] S. Bao, L. Tang, K. Li, P. Ning, J. Peng, H. Guo, T. Zhu, Y. Liu, Highly selective removal of Zn(II) ion from hot-dip galvanizing pickling waste with amino-functionalized Fe 3 O 4 @SiO 2 magnetic nano-adsorbent, J. Colloid Interface Sci. 462 (2016) 235–242, https://doi.org/10.1016/j.jcis.2015.10.011.

[33] A. Dolgormaa, C. Lv, Y. Li, J. Yang, J. Yang, P. Chen, H. Wang, J. Huang, Adsorption of Cu(II) and Zn(II) ions from aqueous solution by gel/PVA-modified superparamagnetic Iron oxide nanoparticles, Molecules 23 (2018) 2982–2997, https://doi.org/10.3390/molecules23112982.

[34] H. Zheng, L. Zhou, Z. Liu, Z. Le, J. Ouyang, G. Huang, H. Shehzad, Functionalization of mesoporous Fe3O4@SiO2 nanospheres for highly efficient U(VI) adsorption, Microporous Mesoporous Mater. 279 (2019) 316–322, https://doi.org/10.1016/j.micromeso.2018.12.038.

[35] A. Tadjarodi, A. Abbaszadeh, M. Taghizadeh, N. Shekari, A.A. Asgharinezhad, Solid phase extraction of Cd(II) and Pb(II) ions based on a novel functionalized Fe3O4@SiO2 core-shell nanoparticles with the aid of multivariate optimization methodology, Mater. Sci. Eng. C 49 (2015) 416–421, https://doi.org/10.1016/j.msec.2015.01.013.

[36] F. Mohammadi, F. Mohammadi, A. Esrafili, H.R. Sobhi, M. Behbahani, M. Kermani, E. Asgari, Z.R. Fasih, Evaluation of adsorption and removal of methylparaben from aqueous solutions using amino-functionalized magnetic nanoparticles as an efficient adsorbent: optimization and modeling by response surface methodology (RSM), Desalin. Water Treat. 103 (2018) 248–260, https://doi.org/10.5004/dwt.2018.21781.

[37] A. Sheikhmohammadi, Z. Dahaghin, S.M. Mohseni, M. Sarkhosh, H. Azarpira, Z. Atafar, M. Abtahi, S. Rezaei, M. Sardar, H. Masoudi, M. Faraji, S. Nazari, R.H. Pouya, M. Almasian, The synthesis and application of the SiO 2 @Fe 3 O 4 @MBT nanocomposite as a new magnetic sorbent for the adsorption of arsenate from aqueous solutions: modeling, optimization, and adsorption studies, J. Mol. Liq. 255 (2018) 313–323, https://doi.org/10.1016/j.molliq.2018.01.164.

[38] A. Sheikhmohammadi, M. Safari, A. Alinejad, A. Esrafili, H. Nourmoradi, E. Asgari, The synthesis and application of the Fe3O4@SiO2 nanoparticles functionalized with 3-aminopropyltriethoxysilane as an efficient sorbent for the adsorption of Ethylparaben from wastewater: synthesis, kinetic, thermodynamic and equilibrium studies, Journal of Environmental Chemical Engineering 7 (2019), 103315. , 1–9 https://doi.org/10.1016/j.jece.2019.103315.

[39] R. Roto, Y. Yusran, A. Kuncaka, Magnetic adsorbent of Fe 3 O 4 @SiO 2 core-shell nanoparticles modified with thiol group for chloroauric ion adsorption, Appl. Surf. Sci. 377 (2016) 30–36, https://doi.org/10.1016/j.apsusc.2016.03.099.

[40] F. Ghorbani, S. Kamari, Core–shell magnetic nanocomposite of Fe3O4@SiO2@NH2 as an efficient and highly recyclable adsorbent of methyl red dye from aqueous environments, Environ. Technol. Innov. 14 (2019), 100333. , 1–16 https://doi.org/10.1016/j.eti.2019.100333.

[41] S. De Gisi, G. Lofrano, M. Grassi, M. Notarnicola, Characteristics and adsorption capacities of low-cost sorbents for wastewater treatment: a review, Sustain. Mater. Technol. 9 (2016) 10–40, https://doi.org/10.1016/j.susmat.2016.06.002.

[42] J. Wang, S. Zheng, Y. Shao, J. Liu, Z. Xu, D. Zhu, Amino-functionalized Fe3O4@SiO2 core–shell magnetic nanomaterial as a novel adsorbent for aqueous heavy metals removal, J. Colloid Interface Sci. 349 (2010) 293–299, https://doi.org/10.1016/j.jcis.2010.05.010.

[43] L. Sun, S. Hu, H. Sun, H. Guo, H. Zhu, M. Liu, H. Sun, Malachite green adsorption onto Fe3O4@SiO2-NH2: isotherms, kinetic and process optimization, RSC Adv. (2012) 11837–11844.

[44] M. Hanif, C.G. Hartinger, Anticancer metallodrugs: where is the next cisplatin? Future Med. Chem. 10 (2018) 615–617, https://doi.org/10.4155/fmc-2017-0317.

[45] T. Lazarević, A. Rilak, Ž.D. Bugarčić, Platinum, palladium, gold and ruthenium complexes as anticancer agents: current clinical uses, cytotoxicity studies and future perspectives, Eur. J. Med. Chem. 142 (2017) 8–31, https://doi.org/10.1016/j.ejmech.2017.04.007.

[46] P. Ferenci, Diagnosis of Wilson disease, Handbook of Clinical Neurology, Elsevier 2017, pp. 171–180, https://doi.org/10.1016/B978-0-444-63625-6.00014-8.

[47] P.C. Panta, C.P. Bergmann, Obtention by coprecipitation and magnetic characterization of Fe3o4 nanoparticles coated with surfactants, Nano Res. Appl. 1 (2015) 1–4.

[48] D.K. Kim, M. Mikhaylova, Y. Zhang, M. Muhammed, Protective coating of superparamagnetic iron oxide nanoparticles, Chem. Mater. 15 (2003) 1617–1627, https://doi.org/10.1021/cm021349j.

[49] Z. Lu, J. Dai, X. Song, G. Wang, W. Yang, Facile synthesis of Fe3O4/SiO2 composite nanoparticles from primary silica particles, Colloids Surf. A Physicochem. Eng. Asp. 317 (2008) 450–456, https://doi.org/10.1016/j.colsurfa.2007.11.020.
[50] D. Dupont, J. Luyten, M. Bloemen, T. Verbiest, K. Binnemans, Acid-stable magnetic core–shell nanoparticles for the separation of rare earths, Ind. Eng. Chem. Res. 53 (2014) 15222–15229, https://doi.org/10.1021/ie502546c.
[51] G.H. Bogush, C.F. Zukoski, Studies of the kinetics of the precipitation of uniform silica particles through the hydrolysis and condensation of silicon alkoxides, J. Colloid Interface Sci. 142 (1991) 1–18, https://doi.org/10.1016/0021-9797(91)90029-8.
[52] Y.A. Barnakov, M.H. Yu, Z. Rosenzweig, Manipulation of the magnetic properties of magnetite—silica nanocomposite materials by controlled stober synthesis, Langmuir 21 (2005) 7524–7527, https://doi.org/10.1021/la0508893.
[53] M. Zhu, M.Z. Lerum, W. Chen, How to prepare reproducible, homogeneous, and hydrolytically stable aminosilane-derived layers on silica, Langmuir 28 (2012) 416–423, https://doi.org/10.1021/la203638g.
[54] E.T. Vandenberg, L. Bertilsson, B. Liedberg, K. Uvdal, R. Erlandsson, H. Elwing, I. Lundström, Structure of 3-aminopropyl triethoxy silane on silicon oxide, J. Colloid Interface Sci. 147 (1991) 103–118, https://doi.org/10.1016/0021-9797(91)90139-Y.
[55] A. Bayat, M. Shakourian-Fard, N. Ehyaei, M.M. Hashemi, A magnetic supported iron complex for selective oxidation of sulfides to sulfoxides using 30% hydrogen peroxide at room temperature, RSC Adv. 4 (2014) 44274–44281, https://doi.org/10.1039/C4RA07356H.
[56] P. Arévalo-Cid, J. Isasi, F. Martín-Hernández, Comparative study of core-shell nanostructures based on amino-functionalized Fe3O4@SiO2 and CoFe2O4@SiO2 nanocomposites, J. Alloys Compd. 766 (2018) 609–618, https://doi.org/10.1016/j.jallcom.2018.06.246.
[57] H. Ciftci, B. Ersoy, A. Evcin, Synthesis, characterization and Cr(VI) adsorption properties of modified magnetite nanoparticles, Acta Phys. Pol. A 132 (2017) 564–569, https://doi.org/10.12693/APhysPolA.132.564.
[58] A. Kulpa, J. Ryl, G. Skowierzak, A. Koterwa, G. Schroeder, T. Ossowski, P. Niedziałkowski, Comparison of cadmium Cd2+ and lead Pb2+ binding by Fe2O3@SiO2-EDTA nanoparticles–binding stability and kinetic studies, Electroanalysis 32 (2020) 588–597, https://doi.org/10.1002/elan.201900616.
[59] Y. Liu, R. Fu, Y. Sun, X. Zhou, S.A. Baig, X. Xu, Multifunctional nanocomposites Fe 3 O 4 @SiO 2-EDTA for Pb(II) and cu(II) removal from aqueous solutions, Appl. Surf. Sci. 369 (2016) 267–276, https://doi.org/10.1016/j.apsusc.2016.02.043.
[60] S. Jin, B.C. Park, W.S. Ham, L. Pan, Y.K. Kim, Effect of the magnetic core size of amino-functionalized Fe3O4-mesoporous SiO2 core-shell nanoparticles on the removal of heavy metal ions, Colloids Surf. A Physicochem. Eng. Asp. 531 (2017) 133–140, https://doi.org/10.1016/j.colsurfa.2017.07.086.
[61] F. Liu, F. Niu, N. Peng, Y. Su, Y. Yang, Synthesis, characterization, and application of Fe3O4@SiO2–NH2 nanoparticles, RSC Adv. 5 (2015) 18128–18136, https://doi.org/10.1039/C4RA15968C.
[62] Y. Zhu, Y. Fang, S. Kaskel, Folate-conjugated Fe $_3$ O $_4$ @SiO $_2$ hollow mesoporous spheres for targeted anticancer drug delivery, J. Phys. Chem. C 114 (2010) 16382–16388, https://doi.org/10.1021/jp106685q.
[63] S. Shi, J. Yang, S. Liang, M. Li, Q. Gan, K. Xiao, J. Hu, Enhanced Cr(VI) removal from acidic solutions using biochar modified by Fe3O4@SiO2-NH2 particles, Sci. Total Environ. 628–629 (2018) 499–508, https://doi.org/10.1016/j.scitotenv.2018.02.091.
[64] M.E. Khosroshahi, L. Ghazanfari, Synthesis and functionalization of SiO2 coated Fe3O4 nanoparticles with amine groups based on self-assembly, Mater. Sci. Eng. C 32 (2012) 1043–1049, https://doi.org/10.1016/j.msec.2011.09.003.
[65] P.M. Dietrich, S. Glamsch, C. Ehlert, A. Lippitz, N. Kulak, W.E.S. Unger, Synchrotron-radiation XPS analysis of ultra-thin silane films: specifying the organic silicon, Appl. Surf. Sci. 363 (2016) 406–411, https://doi.org/10.1016/j.apsusc.2015.12.052.
[66] High resolution XPS of organic polymers: the scienta ESCA300 database (Beamson, G.; Briggs, D.), J. Chem. Educ. 70 (1993) A25, https://doi.org/10.1021/ed070pA25.5.
[67] S.R. Darmakkolla, H. Tran, A. Gupta, S.B. Rananavare, A method to derivatize surface silanol groups to Si-alkyl groups in carbon-doped silicon oxides, RSC Adv. 6 (2016) 93219–93230, https://doi.org/10.1039/C6RA20355H.
[68] A.K. Chauhan, D.K. Aswal, S.P. Koiry, S.K. Gupta, J.V. Yakhmi, C. Sürgers, D. Guerin, S. Lenfant, D. Vuillaume, Self-assembly of the 3-aminopropyltrimethoxysilane multilayers on Si and hysteretic current–voltage characteristics, Appl. Phys. A Mater. Sci. Process. 90 (2008) 581–589, https://doi.org/10.1007/s00339-007-4336-7.
[69] N. Graf, E. Yegen, T. Gross, A. Lippitz, W. Weigel, S. Krakert, A. Terfort, W.E.S. Unger, XPS and NEXAFS studies of aliphatic and aromatic amine species on functionalized surfaces, Surf. Sci. 603 (2009) 2849–2860, https://doi.org/10.1016/j.susc.2009.07.029.
[70] A. Elhambakhsh, P. Keshavarz, Investigation of carbon dioxide absorption using different functionalized Fe3O4 magnetic nanoparticles, Energy Fuel (2020)https://doi.org/10.1021/acs.energyfuels.0c00234.
[71] Q. Zhao, Y. Zhu, Z. Sun, Y. Li, G. Zhang, F. Zhang, X. Fan, Combining palladium complex and organic amine on graphene oxide for promoted Tsuji–Trost allylation, J. Mater. Chem. A 3 (2015) 2609–2616, https://doi.org/10.1039/C4TA05205F.
[72] T.L. Barr, S. Seal, Nature of the use of adventitious carbon as a binding energy standard, J. Vac. Sci. Technol. A 13 (1995) 1239–1246, https://doi.org/10.1116/1.579868.
[73] R. Bogdanowicz, M. Sawczak, P. Niedzialkowski, P. Zieba, B. Finke, J. Ryl, J. Karczewski, T. Ossowski, Novel functionalization of boron-doped diamond by microwave pulsed-plasma polymerized allylamine film, J. Phys. Chem. C 118 (2014) 8014–8025, https://doi.org/10.1021/jp5003947.
[74] P. Niedziałkowski, R. Bogdanowicz, P. Zięba, J. Wysocka, J. Ryl, M. Sobaszek, T. Ossowski, Melamine-modified boron-doped diamond towards enhanced detection of adenine, guanine and caffeine, Electroanalysis 28 (2016) 211–221, https://doi.org/10.1002/elan.201500528.
[75] F. Mirabella, E. Zaki, F. Ivars-Barcelo, S. Schauermann, S. Shaikhutdinov, H.-J. Freund, CO2 adsorption on magnetite Fe3O4(111), J. Phys. Chem. C 122 (2018) 27433–27441, https://doi.org/10.1021/acs.jpcc.8b08240.
[76] J. Pavelec, J. Hulva, D. Halwidl, R. Bliem, O. Gamba, Z. Jakub, F. Brunbauer, M. Schmid, U. Diebold, G.S. Parkinson, A multi-technique study of CO2 adsorption on Fe3O4 magnetite, J. Chem. Phys. 146 (2017) 014701 (1)–014701 (10), https://doi.org/10.1063/1.4973241.
[77] T. Yang, J. Liu, Y. Wang, X. Wen, B. Shen, Structures and energetics of CO2 adsorption on the Fe3O4 (111) surface, J. Fuel Chem. Technol. 46 (2018) 1113–1120, https://doi.org/10.1016/S1872-5813(18)30044-6.
[78] F. Bai, X. Zhang, X. Hou, H. Liu, J. Chen, T. Yang, Individual and simultaneous voltammetric determination of Cd(II), Cu(II) and Pb(II) applying amino functionalized Fe_3O_4 @carbon microspheres modified electrode, Electroanalysis 31 (2019) 1448–1457, https://doi.org/10.1002/elan.201900234.
[79] A. Profumo, D. Merli, M. Pesavento, Voltammetric determination of inorganic As(III) and total inorganic As in natural waters, Anal. Chim. Acta 539 (2005) 245–250, https://doi.org/10.1016/j.aca.2005.02.062.
[80] N. Kataria, V.K. Garg, Green synthesis of Fe3O4 nanoparticles loaded sawdust carbon for cadmium (II) removal from water: regeneration and mechanism, Chemosphere 208 (2018) 818–828, https://doi.org/10.1016/j.chemosphere.2018.06.022.
[81] W.H.M. Abdelraheem, Z.R. Komy, N.M. Ismail, Electrochemical determination of Cu2+ complexation in the extract of E. crassipes by anodic stripping voltammetry, Arab. J. Chem. 10 (2017) S1105–S1110, https://doi.org/10.1016/j.arabjc.2013.01.019.
[82] W. Nowicki, Structural studies of complexation of Cu(II) with aminosilane-modified silica surface in heterogeneous system in a wide range of pH, Appl. Surf. Sci. 469 (2019) 566–572, https://doi.org/10.1016/j.apsusc.2018.11.066.
[83] S.E. Lehman, I.A. Mudunkotuwa, V.H. Grassian, S.C. Larsen, Nano–bio interactions of porous and nonporous silica nanoparticles of varied surface chemistry: a structural, kinetic, and thermodynamic study of protein adsorption from RPMI culture medium, Langmuir 32 (2016) 731–742, https://doi.org/10.1021/acs.langmuir.5b03997.
[84] D. Chen, T. Awut, B. Liu, Y. Ma, T. Wang, I. Nurulla, Functionalized magnetic Fe3O4 nanoparticles for removal of heavy metal ions from aqueous solutions, E-Polymers (4) (2016) 313–322, https://doi.org/10.1515/epoly-2016-0043.
[85] M. Sun, P. Li, X. Jin, X. Ju, W. Yan, J. Yuan, X. Changrui, Heavy metal adsorption onto graphene oxide, amino group on magnetic nanoadsorbents and application for detection of Pb(II) by strip sensor, Food Agric. Immunol. 29 (2018) 1053–1073, https://doi.org/10.1080/09540105.2018.1509946.
[86] J. Zhang, S. Zhai, S. Li, Z. Xiao, Y. Song, Q. An, G. Tian, Pb(II) removal of Fe3O4@SiO2–NH2 core–shell nanomaterials prepared via a controllable sol–gel process, Chem. Eng. J. 215–216 (2013) 461–471, https://doi.org/10.1016/j.cej.2012.11.043.
[87] X.L. Wu, D. Zhao, S.T. Yang, Impact of solution chemistry conditions on the sorption behavior of Cu(II) on Lin'an montmorillonite, Desalination 269 (2011) 84–91, https://doi.org/10.1016/j.desal.2010.10.046.
[88] J. Vuceta, J.J. Morgan, Hydrolysis of Cu(II)1, Limnol. Oceanogr. 22 (1977) 742–746, https://doi.org/10.4319/lo.1977.22.4.0742.

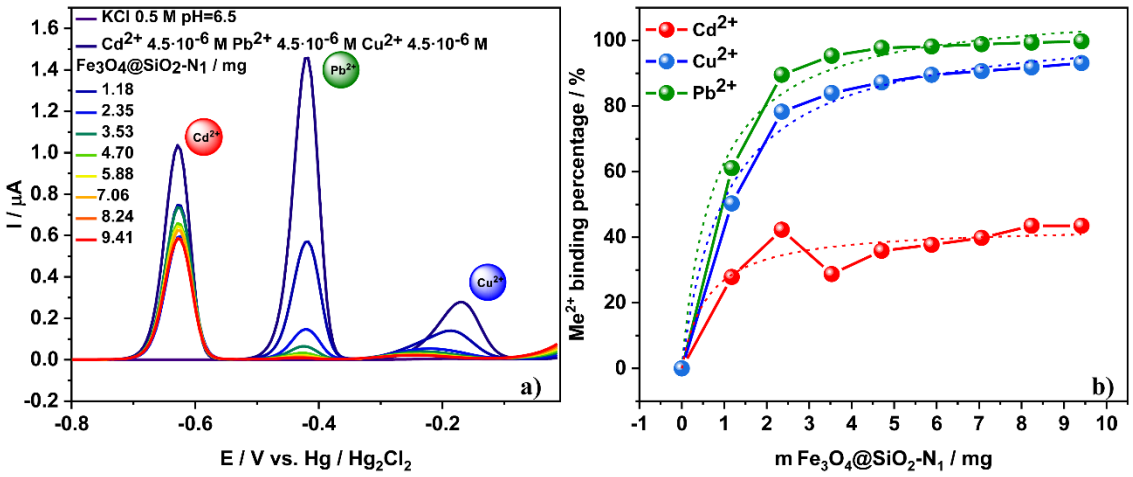

Fig. 6. a) Anodic stripping voltammograms and b) percentage of Cd^{2+} (4.5 µM), Pb^{2+} (4.5 µM) and Cu^{2+} (4.5 µM) binding by $Fe_3O_4@SiO_2$-N_1 nanoparticles.

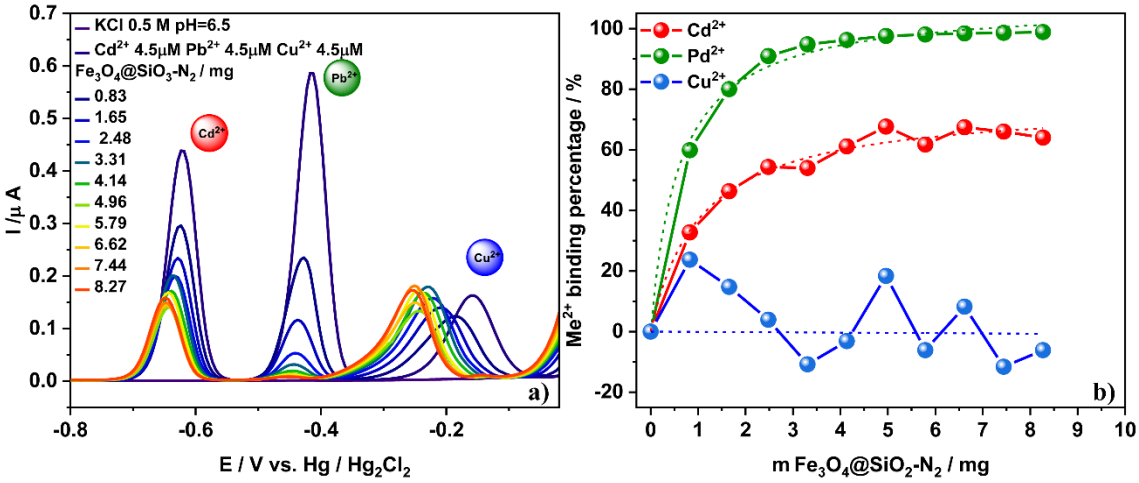

Fig. 7. a) Anodic stripping voltammograms and b) percentage of Cd^{2+} (4.5 µM), Pb^{2+} (4.5 µM), and Cu^{2+} (4.5 µM) binding by $Fe_3O_4@SiO_2$-N_2 nanoparticles.

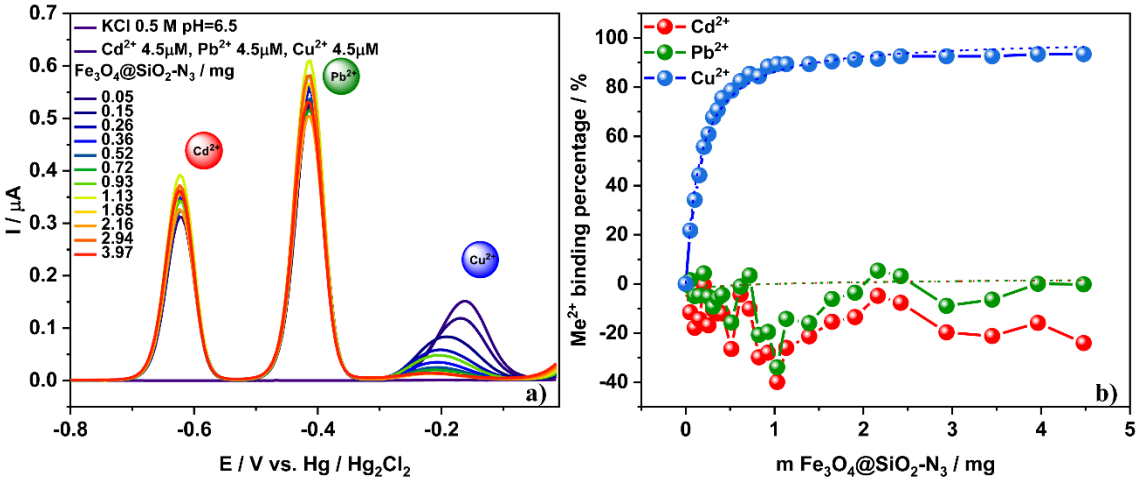

Fig. 8. a) Anodic stripping voltammograms and b) percentage of Cd^{2+} (4.5 µM), Pb^{2+} (4.5 µM), and Cu^{2+} (4.5 µM) binding by $Fe_3O_4@SiO_2$-N_3 nanoparticles.

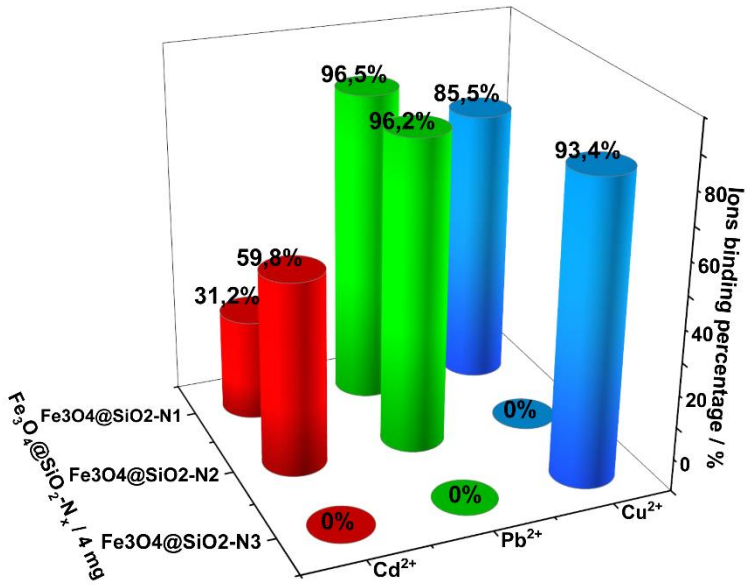

Fig. 9. Cd^{2+}, Pb^{2+}, Cu^{2+} ions binding percentage for $Fe_3O_4@SiO_2$-N_1, $Fe_3O_4@SiO_2$-N_2 and $Fe_3O_4@SiO_2$-N_3 nanoparticles.

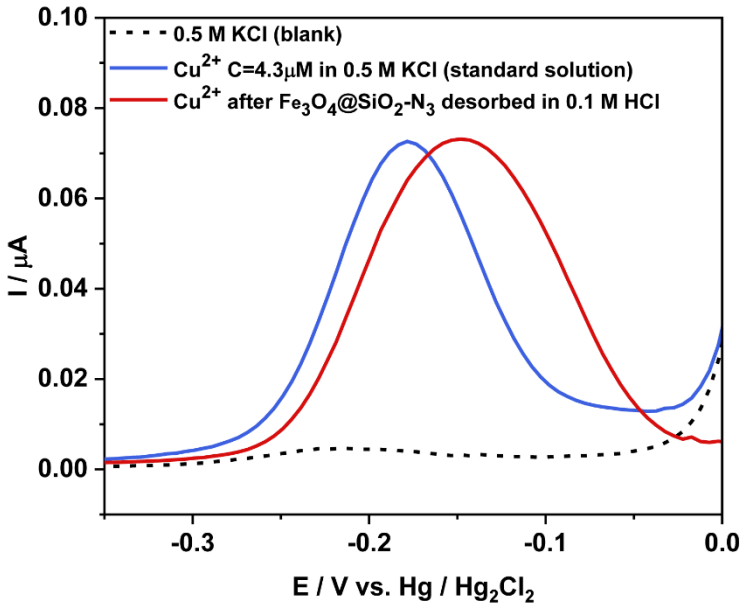

Fig. 11. Comparison of anodic stripping voltammograms of 0.5 M KCl electrolyte (blank), Cu^{2+} standard solution C = 4.3 μM, Cu^{2+} after $Fe_3O_4@SiO_2$-N_3 nanoparticles regeneration.

3. Załącznik 3

Journal of Molecular Liquids 368 (2022) 120710

Contents lists available at ScienceDirect

Journal of Molecular Liquids

journal homepage: www.elsevier.com/locate/molliq

New nanoadsorbent based on magnetic iron oxide containing 1,4,7, 10-tetraazacyclododecane in outer chain (Fe_3O_4@SiO_2-cyclen) for adsorption and removal of selected heavy metal ions Cd^{2+}, Pb^{2+}, Cu^{2+}

Amanda Kulpa-Koterwa [a], Jacek Ryl [b], Karolina Górnicka [c], Paweł Niedziałkowski [a,*]

[a] Department of Analytical Chemistry, Faculty of Chemistry, University of Gdansk, Wita Stwosza 63, 80-308 Gdańsk, Poland
[b] Division of Electrochemistry and Surface Physical Chemistry, Institute of Nanotechnology and Materials Engineering and Advanced Materials Center, Gdańsk University of Technology, Narutowicza 11/12, 80-233 Gdańsk, Poland
[c] Faculty of Applied Physics and Mathematics, Advanced Materials Center, Gdansk University of Technology, Narutowicza 11/12, 80-233 Gdansk, Poland

ARTICLE INFO

Article history:
Received 19 August 2022
Revised 26 October 2022
Accepted 28 October 2022
Available online 7 November 2022

Keywords:
Functionalised Fe_3O_4 nanoparticles
Stripping voltammetry
Cd^{2+}, Pb^{2+} and Cu^{2+} ions binding
Nanoadsorbent
1,4,7,10-tetraazacyclododecane
Heavy metal ions removal

ABSTRACT

Magnetic Fe_3O_4@SiO_2-cyclen nanoparticles were prepared and used as adsorbent for Cd^{2+}, Pb^{2+} and Cu^{2+} from aqueous solution removal process controlled with differential pulse anodic stripping voltammetry (DPASV) and hanging mercury drop electrode (HDME). Nanomaterial was synthesised in three-step process co-precipitation of Fe_3O_4 core, coating with silane and N-(3-(triethoxysilyl)propyl)-1,4,7,10-tetraaza cyclododecane-1-carboxamide silane functionalisation. The effectiveness of each step of the synthesis was confirmed using scanning electron microscopy (SEM), high-resolution X-ray photoelectron spectroscopy (XPS), powder X-ray diffraction (pXRD) and fourier-transform infrared spectroscopy (FT-IR) techniques. The Fe_3O_4@SiO_2-cyclen nanoparticles were employed for Cd^{2+}, Pb^{2+} and Cu^{2+} ions elimination from individual and mixed solutions by carrying out titration with a suspension of nanocomposites. The binding level for all ions both in the individual solutions and in the mixture was very similar at high levels. For Cd^{2+} and Cu^{2+} ions sorption efficiency level was from 83% to 89%, while for Pb^{2+} ions it was slightly lower at the level over 73%. In all cases, the equilibrium adsorption capacity parameter was over 1 mg/g and reached definitely higher values for individual ions solutions. The research results revealed that Fe_3O_4@SiO_2- cyclen nanoparticles can be a promising adsorbent for magnetic heavy metal ions water treatment agents.

1. Introduction

Over the last few decades, a significant increase has been observed in environmental pollution with heavy metal ions, which is a problem all over the world [1]. The increasing heavy metal ions concentration is generated mainly by technological and operational activities, production processes such as refining, power plants and combined heat and power plants, steel mills, coal and waste combustion, the chemical industry, the use of fertilisers and pesticides, and transport [2]. The presence of heavy metal ions in the environment constitutes a threat due to the possibility of their migration along the rungs of the trophic chain from soil, air, surface waters to plants, animals and in consequence to humans. Exposure to continuously increasing heavy metal ions concentrations lowers the action of biological barriers, which has a negative impact on human health due to their low biodegradability, bioaccumulation tendency, potential carcinogenic effect and mutagenicity [3]. Due to the danger posed by heavy metal ions environment contamination, the recycling of them from aquatic environments has become a very important area of scientific research and industry.

Until now, many methods of metal ions remediation from the environment have been used [4,5], particularly methods such as membrane filtration [6], osmosis [7], ion exchange [8], extraction with ionic liquids [9], photocatalysts [10], clays/layered double hydroxides [11], bioremediation [12], biomass and biosorption [13] phytoremediation [14], precipitation and coagulation [15,16] or electrocoagulation [17]. The conventional wastewater treatment technologies involving physical, chemical, and biological methods have their advantages but also disadvantages such as high costs,

* Corresponding author.
E-mail address: pawel.niedzialkowski@ug.edu.pl (P. Niedziałkowski).

https://doi.org/10.1016/j.molliq.2022.120710
0167-7322/

complex working operation, secondary pollutants production, low selectivity and many others [18]. To overcome these challenges, researchers used adsorption process as an alternative due to its wide working potentials, low price, simplicity in use, process efficiency, selectivity, capacity for material regeneration and pollutants trace concentration removal [19,20]. A wide range of materials have found application as heavy metal ions adsorbents e.g., chitosan and its functionalised forms [21], aerogels and their derivatives [22], based on cellulose [23], metal organic frameworks [24], carbon-based materials [25], polymers [26], dendrimers [27] and many others [28-31]. However, among many research groups, various nanoscale adsorbents became very popular due to their high surface area, high mobility in solution, reactivity, good adsorption capacity and in consequence efficiency [32]. A series of nanoparticles and their modification were investigated as heavy metal adsorbents but, in recent years, a particular interest was attached to nanoparticles with magnetic properties, especially magnetite Fe_3O_4 [33,34]. Magnetite nanoparticles occupy a special importance due to the possibility of easy and quick isolation with the use of an external magnetic field [35]. Furthermore, creating core–shell type structures with silica Fe_3O_4@SiO_2 provides a good basis for further functionalisation thus for obtaining a material with wide applicability and selectivity [36-38]. There are known plenty of Fe_3O_4@SiO_2 modified structures for heavy metal ions adsorption, however, the search for new and selective composites is still topical [39-41]. So far, there is lack of knowledge about crown ethers usage as surface nanocomposites modifiers. Qin et al. designed and synthesised silica gel bound di (aminobenzo)-18-crown-6(SGN18) for zirconium and hafnium adsorption [42]. Aza-crown ethers and derivatives in their heyday were widely used as complexation agents of metal ions in wide range of applications [43,44]. One of the well-known and widely used agent as a metal ions complexation was 1,4,7,10-tetraazacyclododecane [45-49].

In view of the fact that previously the authors used Fe_3O_4@SiO_2 nanoparticles containing nitrogen atoms in the outer chain as heavy metal ion adsorbent [50,51], they now decided to combine the excellent complexing properties of 1,4,7,10-tetraazacyclododecane and the possibility of pollutants magnetic isolation. In this work, magnetic core–shell nanoparticles functionalised with 1,4,7,10-tetraazacyclododecane Fe_3O_4@SiO_2-cyclen were designed, synthesised and used as heavy metal Cd^{2+}, Pb^{2+}, and Cd^{2+} ions adsorbent for the first time. The newly obtained nanomaterial was characterised at every stage of synthesis using SEM, FT-IR, pXRD and (XPS) methods. Furthermore, the ions binding kinetics studies was performed and the binding capacity of nanoparticles was investigated using the differential pulse anodic stripping voltammetry (DPASV) method coupled with hanging mercury drop electrode (HDM) electrode. It is worth mentioning that the application of electrochemical detection skips conventional techniques' limitations in heavy metal detection and offers the same sensitivity with a lower cost, less complex operational procedures and fast on-site detection [52].

2. Experimental

2.1. Reagents

All analytical grade reagents were purchased from the indicated suppliers and used without further purification. All inorganic salts – ferric chloride hexahydrate ($FeCl_3{\cdot}6H_2O$), ferrous chloride tetrahydrate ($FeCl_2{\cdot}4H_2O$), potassium chloride KCl (99.9%), cadmium nitrate tetrahydrate $Cd(NO_3)_2{\cdot}4H_2O$ (99.9%), lead nitrate Pb $(NO_3)_2$, and copper nitrate trihydrate $Cu(NO_3)_2{\cdot}3H_2O$ (99.9%) – were purchased from POCh (Poland). The organic solvents, ammonia (25%), tetraethylorthosilicate (98%) (TEOS), triethoxy(3-isocyanatopropyl)silane were purchased from Sigma-Aldrich (Poland). 1,4,7,10-tetraazacyclododecane was bought from Strem Chemicals. Aqueous solutions were prepared using ultra-pure deionised water.

2.2. Synthesis of core–shell Fe_3O_4@SiO_2-cyclen nanostructures

New functionalised nanocomposites were obtained in the three-steps synthesis process (see Fig.1). In the first stage, a magnetic Fe_3O_4 core was received by the co-precipitation method. The mixture of Fe^{2+}($FeCl_2{\cdot}4H_2O$) and Fe^{3+} ($FeCl_3{\cdot}6H_2O$) in aqueous solution using a three-neck flask was stirred under nitrogen conditions. Then the 25% ammonia solution was dripped into the reaction until the pH reached 11. Then the reaction mixture was heated to 60 °C for 3 h to complete precipitation of the magnetite. The obtained nanoparticles were separated by a magnet and washed with distilled water several times.

The second stage of the synthesis involved the nanomagnetite coating with silica forming Fe_3O_4@SiO_2, which was used for further modification. 16 g of Fe_3O_4 nanoparticles obtained in the previous stage was dispersed in a mixture of 240 mL EtOH and 60 mL H_2O. Then 3 mL of TEOS was added into reaction and the reaction was heated overnight to 50 °C. After this time, the obtained nanoparticles were magnetically collected and washed with distilled water several times.

In next stage of synthesis it was necessary to synthesise a modifier of the obtained nanoparticles Fe_3O_4@SiO_2 due to the fact that the silane derivatives containing 1,4,7,10-tetraazacyclododecane are not a commercially available.

The reaction of 1,4,7,10-tetraazacyclododecane with triethoxy(3-isocyanatopropyl)silane was performed according to the modified procedure described previously [53] to obtain N-(3-(triethoxy silyl)propyl)-1,4,7,10-tetraazacyclododecane-1-carboxamide.

To the solution of 1,4,7,10-tetraazacyclododecane (4.179 g, 24,256 mmol) dissolved in 200 mL dichloromethane 6 mL of triethoxy(3-isocyanatopropyl)silane (24,256 mmol) was dropwise added and the reaction was carried out overnight at 40 °C under a reflux condenser. Then the solvent was evaporated under reduced pressure. The obtained colourless oil was dried in a vacuum desiccator over P_2O_5 to obtain 2.159 g of colourless solid with a yield of 21.33%.

MALDI-TOF MS: m/z 419,29 $[M + H]^+$, (MW = 420.31).

IR (KBr) (cm^{-1}): 3291, 2972, 2926, 2886, 2735, 1627, 1536, 1478, 1444, 1391, 1365, 1254, 1189, 1165, 1103, 1078, 955, 784.

^{1}H NMR ($CDCl_3$): 0.538–0.572 (t, 2H, $(CH_3\text{-}CH_2)_3SiO\text{-}\underline{CH_2}\text{-}CH_2\text{-}CH_2\text{-}HN$-, J_1 = 7 Hz; J_1 = 10,0 Hz; J_2 = 8,5 Hz); 1.135–1.165 (dt, 9H, $(\underline{CH_3}\text{-}CH_2)_3SiO\text{-}CH_2\text{-}CH_2\text{-}CH_2\text{-}HN$-, J_1 = 1 Hz; J_1 = 1,5 Hz; J_1 = J_2 = 7.0 Hz); 1.479–1.623 (m, 2H, $(CH_3\text{-}CH_2)_3SiO\text{-}CH_2\text{-}\underline{CH_2}\text{-}CH_2\text{-}HN$-); 2.564–3.652 (m, 18H, $(CH_3\text{-}CH_2)_3SiO\text{-}CH_2\text{-}CH_2\text{-}\underline{CH_2}\text{-}HN$- -H-$\underline{CH_2}\text{-}\underline{CH_2}\text{-}N$-,); 3.734–3.754 (q, 6H, $(CH_3\text{-}\underline{CH_2})_3SiO\text{-}CH_2\text{-}CH_2\text{-}CH_2\text{-}HN$-, J_1 = 3 Hz; J_1 = 4 Hz; J_3 = J_4 = 3.0 Hz);

The third stage consisted of Fe_3O_4@SiO_2 modification to obtain Fe_3O_4@SiO_2-cyclen. 1.593 g of Fe_3O_4@SiO_2 was added to a solution of (3.324 g, 7,928 mmol) N-(3-(triethoxysilyl)propyl)-1,4,7,10-tetraazacyclododecane-1-carboxamide dissolved in 150 mL toluene. Then the reaction mixture was stirred for 12 h at 120 °C. After cooling to room temperature the obtained product was magnetically collected and washed several times with toluene and then with methanol. The resulting product was air-dried.

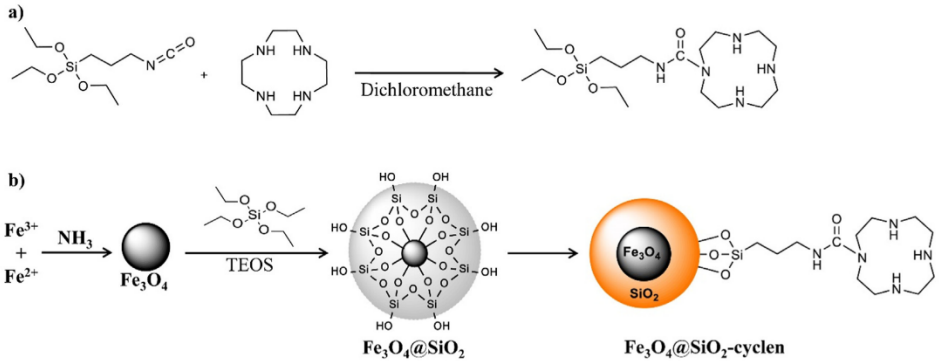

Fig. 1. Scheme of a) nanoparticles modifier N-(3-(triethoxysilyl)propyl)-1,4,7,10-tetraazacyclododecane-1-carboxamide and b) functionalised Fe_3O_4@SiO_2-cyclen nanocomposite synthesis.

2.3. The Cd^{2+}, Pb^{2+} and Cu^{2+} ions removal experiments from aqueous solutions by Fe_3O_4@SiO_2-cyclen binding

The removal experiments of Cd^{2+}, Pb^{2+} and Cu^{2+} ions from aqueous solutions were performed by titration with Fe_3O_4@SiO_2-cyclen nanoparticles. The ions-binding abilities of Fe_3O_4@SiO_2-cyclen were studied in the solutions containing both individual ion or the mixture of Cd^{2+}, Pb^{2+} and Cu^{2+} ions in concentration level $4.5{\cdot}10^{-6}$ M. Before starting (DPASV) measurement a 0.25 mg of Fe_3O_4@SiO_2- cyclen nanoparticles was added into ion solution at each titration step and then mixed for 20 min All measurements were performed in 0.5 M KCl pH 6.00.

2.4. Methods

Fourier Transform Infrared Spectroscopy (FT-IR) spectra were obtained were recorded on a Perkin Elmer Spectrum™ 3 FT-IR spectrometer with the KBr pellet technique.

Maldi-Tof mass spectra was performed on autoflex maX Brucker using α-cyano-4-hydroxycinnamic acid (CCA) as a matrix.

^{1}H NMR spectra were recorded in $CDCl_3$ on a Bruker Advance III 500 MHz, where tetramethylsilane (TMS) was used as the internal standard. The chemical shifts are reported in ppm, while the signal patterns are given as follows: triplet (t), doublet of triplets (dt), quartet (q) and multiplet (m).

The scanning electron microscopy (SEM) images were captured with an FEI Quanta 250 FEG (ThermoFisher Scientific) microscope, equipped with a Schottky field emission gun. The microscope was operating at 20 kV accelerating voltage in high vacuum mode.

High-resolution X-ray Photoelectron Spectroscopy (XPS) analysis was carried out using Escalab 250Xi multispectroscope (ThermoFisher Scientific). The spectroscope is equipped with an AlKα x-ray source; the pass energy through the hemispherical analyser was 20 eV. The measurement was assisted with low-energy electron and low-energy Ar^+ ion bombardment for charge compensation. The measurements were carried out in C 1 s, Fe 2p, Si 2p and N 1 s core-level binding energy range, where the adventitious C 1 s spectra (284.6 eV) was used for final peak calibration. Peak deconvolution was performed using Avantage v5.9921 (ThermoFisher Scientific).

The crystalline phases and crystallite size were determined by room-temperature powder x-ray diffraction (pXRD). The pXRD patterns were collected on D2 Phaser (Brucker) diffractometer, using CuKα radiation (λ = 1.54056 Å) with a scanning angle 2⊖ = 5–90° and a step size 0.01°. LeBail refinement of the pXRD pattern was performed to determine the lattice parameters, using the DIFFRAC.SUITE TOPAS.

All differential pulse anodic stripping voltammetry (DPASV) measurements were performed using an Autolab potentiostat/galvanostat (PGSTAT-128N, Methrom), equipped with NOVA 2.1.4 software. Three electrode Teflon electrochemical cell was used in all experiments to avoid metal ions sorption on the glass surface. A Static Drop Mercury Electrode (SDME) 663 VA Stand Metrohm was used as a working electrode. The reference electrode was calomel electrode $Hg|Hg_2Cl_2|KCl_{(saturated)}$ and platinum wire (Pt) were used as the counter electrode.

The detection of Cd^{2+}, Pb^{2+}, and Cd^{2+} by DPASV method was performed using the following conditions: deposition time 90 s, deposition potential –0.9 V, modulation amplitude 0.05 V, modulation time 0.07 s, interval time 1.85 s, and step potential 0.003 V. The simultaneous Cd^{2+}, Pb^{2+}, and Cd^{2+} ions was performed in a potential range of −0.8 V to −0.04 V, while the individual detection of ions was performed in potential range of −0.8 V to −0.5 V, −0.6 V to −0.3 V and −0.4 V to −0.04 V for Cd^{2+}, Pb^{2+}, Cu^{2+} detection, respectively.

The metal ions solutions were prepared in the supporting electrolyte, which was potassium chloride KCl 0.5 M, pH 6.0. The Fe_3O_4@SiO_2-cyclen nanoparticles suspension in supporting electrolyte solution before each measurement was freshly prepared by using ultrasonic bath for 30 min.

3. Results and discussion

3.1. XPS and SEM analysis

The high-resolution XPS analysis was performed to evaluate the efficiency of consecutive Fe_3O_4 nanoparticles functionalisation steps. The XPS spectra of each studied sample are presented in Fig. 2.

Fig. 2A shows iron chemistry. The spectra obtained for the Fe_3O_4 sample may be deconvoluted into two Fe $2p_{3/2}$ features, peaking at 708.6 and 710.8 eV, which is characteristic of Fe^{2+} and Fe^{3+} in Fe_3O_4, respectively [54]. The calculated Fe^{2+}:Fe^{3+} ratio is 2:1. Importantly, upon the formation of Fe_3O_4@SiO_2 core–shell structure, the peak position as well as the Fe^{2+}:Fe^{3+} ratio remains unchanged, testifying to unchanged iron chemistry and structure within the nanoparticles. Nevertheless, the Fe 2p spectra intensity weakens upon the NP coverage with an SiO_2 shell, and eventually becomes indistinguishable for Fe_3O_4@SiO_2-cyclen, due to the limited depth of the XPS signal origin (approx. 3–5 nm).

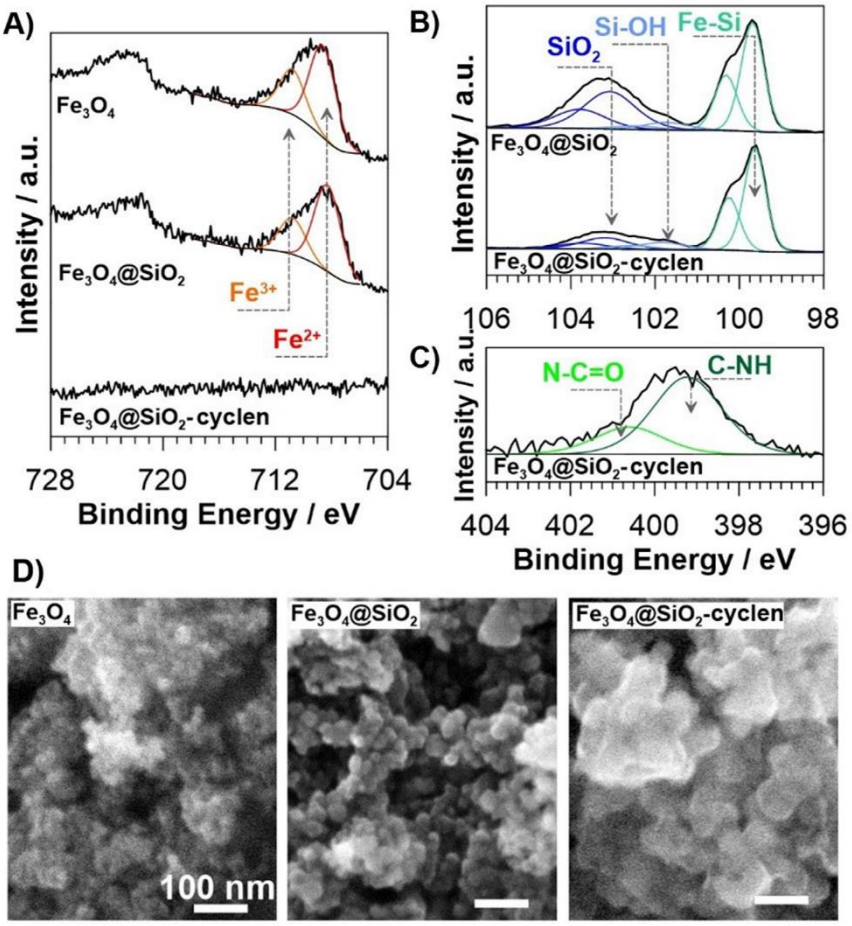

Fig. 2. High-resolution XPS analysis of the studied Fe_3O_4, Fe_3O_4@SiO_2 and Fe_3O_4@SiO_2- cyclen samples in the binding energy range of: A) Fe 2p, B) Si 2p and C) N 1 s peak with spectral deconvolution. D) SEM micrographs of studied materials. The scale bar marks 100 nm.

The Si 2p spectra shows more complex character, with not less than three deconvolution peak doublets to be distinguished in Fig. 2B. The characteristic component at 103.2 eV is attributed to SiO_2 while the second, smaller component negatively shifted at 0.9 eV may correspond to Si-OH bonds [55]. The third, notable component with Si $2p_{3/2}$ at 99.8 eV may have multiple origins, including Si-Fe bonds [56] or even Si-C bonds [57]. Adventitious carbon contribution in Fe_3O_4@SiO_2 NP powder is a relevant source for Si-C. After further modification with N-(3-(triethoxysilyl)propyl)-1,4,7,10-tetraazacyclododecane-1-carboxamide the share of 99.8 eV feature rises by 35%. This modification is assisted with two time decreases of the SiO_2 share, again due to the restricted depth of the XPS analysis. The detailed information are presented in Table 1.

While the N-(3-(triethoxysilyl)propyl)-1,4,7,10-tetraazacyclodo decane-1-carboxamide compounds do not introduce C 1 s features that can be easily differentiated from the surface-adsorbed adventitious carbon under air exposure, the successful

Table 1
The chemical composition (in at.%) using XPS analysis by peak deconvolution.

Sample	Fe 2p		Si 2p			N 1 s	
	Fe^{2+}	Fe^{3+}	SiO_2	Si-OH	Si-(Fe/C)	NH-C	NC = O
BE / eV	708.6	710.8	103.2	102.3	99.8	399.3	400.6
Fe_3O_4	67.1	32.9	–	–	–	–	–
Fe_3O_4@SiO_2	1.3	0.6	40.2	6.9	50.0	–	–
Fe_3O_4@SiO_2-cyclen	–	–	16.4	9.7	67.4	4.8	1.7

Fe_3O_4@SiO_2-cyclen synthesis may be confirmed tracking N 1 s spectral shape. As seen in Fig. 2C this peak was deconvoluted using two separate components. The first, and more notable, at 399.3 eV is characteristic of NH-C bonds [58], while the latter, at 400.6 eV, was assigned to NC = O [59].

The morphology of each studied nanomaterial was revealed by SEM micrographs as seen in Fig. 2D. The size of the Fe_3O_4 nanoparticles is below 20 nm, thus making it impossible for accurate estimation. Such small particle size is reported as sufficient to achieve superparamagnetism in Fe_3O_4 NPs [60]. Further encapsulation in SiO_2 by TEOS allows for full NP contours to be recognised and increasing the average size to approx. 34 ± 5 nm. This result suggests the SiO_2 thickness to exceed 5 nm, testifying for nearly the entire removal of the high resolution Fe 2p signal. The final functionalisation notably enlarges the Fe_3O_4@SiO_2-cyclen dimensions, which now reach 50 to as much as 100 nm. The less regular size introduced by Sil- Prop- cyclen is the probable explanation behind a significant share of Si still to be recognised by XPS.

3.2. pXRD analysis

The pXRD analysis was used to investigate the crystallinity nature, and size of crystallites of bare Fe_3O_4 nanoparticles and after each functionalisation steps. The XRD patterns of a) bare Fe_3O_4, b) silica-coated Fe_3O_4@SiO_2,and c) functionalised Fe_3O_4@SiO_2-cyclen nanoparticles together with the LeBail refinement (solid red line) are presented in Fig. 3. A difference plot (between experimental and fitted data) and the Bragg positions are also shown in Fig. 3.

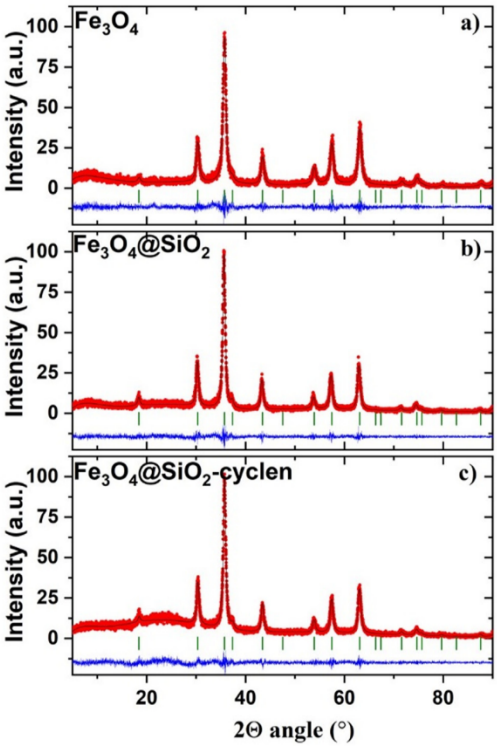

Fig. 3. Powder x-ray diffraction pattern (pXRD) (red points) together with the LeBail refinement profile (solid black line) for a) bare Fe_3O_4, b) silica coated Fe_3O_4@SiO_2 and c) functionalized Fe_3O_4@SiO_2-cyclen. The green vertical bars indicate the expected Bragg peak positions for Fe_3O_4 (JCPDS card PDF 00–065-0731).

Our pXRD analysis confirms that for each studied sample all the diffraction peaks correspond to the cubic crystal structure (space group *Fd-3 m*, no. 227). Estimated lattice parameters for the Fe_3O_4 phase do not differ much and are a = 8.329(1) Å for bare Fe_3O_4, a = 8.3521(6) Å for Fe_3O_4@SiO_2, and a = 8.3462(6) Å for Fe_3O_4@SiO_2-cyclen nanoparticles. The average crystallite size of the Fe_3O_4 phase was estimated from the Scherrer formula based on the line broadening at half the maximum intensity of the reflection (220). The estimated crystallite sizes are 14, 19 and 18 nm for Fe_3O_4, Fe_3O_4@SiO_2, and Fe_3O_4@SiO_2-cyclen samples, respectively. The obtained results are in agreement with SEM micrographs.

3.3. FT-IR spectroscopy analysis

FT-IR analysis was performed to identify the appropriate functional groups present in the Fe_3O_4 nanoparticles at each functionalisation steps.

The Fe_3O_4 spectrum (Fig. 4 a) shows strong stretching vibration Fe–O band at 576 cm^{-1} typical for iron oxide [61]. Also observed was the reduction in the Fe–O band intensity for coated nanoparticles with silica and functional group. The band intensity decrease confirms the success in the surface functionalisation process [50]. After silica coating of nanomagnetite the intense Si–O band appeared at 1077 cm^{-1}. It is associated with stretching vibrations of Si–O–Si and O–Si–O on the surface of the magnetic core at 968 cm^{-1} and 1077 cm^{-1}, respectively [62,63]. The broad strong band at 3433 cm^{-1} is related to the overlapping of O–H stretching bond, which proves hydroxyl groups formation on the magnetite surface [64]. Fig. 4 b blue line shows spectra for nanoparticles modifier N-(3-(triethoxysilyl)propyl)-1,4,7,10-tetraazacyclododecane-1-carboxamide for comparison. A 780 cm^{-1} weak band and a two headed band about 1536 cm^{-1} and 1624 cm^{-1} characteristic for N–H vibrations are observed. Furthermore, there are bands that appeared at 1359 cm^{-1} and about 2900 cm^{-1} corresponding to C–N and N–H stretching vibrations, respectively. The same characteristic bands for the spectrum for the functionalised nanoparticles Fe_3O_4@SiO_2-cyclen (Fig. 4 b orange line) are observed, which proves the success of the nanomaterials synthesis process. In addition, there is a bandwidth extension at 3283 cm^{-1} which probably corresponds to overlapping O–H and N–H bands. On the basis of SEM, XPS and FT-IR analysis it can be concluded that the functionalised core–shell nanoparticles formation was conducted successfully.

3.4. Electrochemical analysis

In this work, the independent and simultaneous determination of Cd^{2+}, Pb^{2+} and Cu^{2+} ions was performed under optimised experimental conditions using the DPASV method and HDM electrode. 1,4,7,10-tetraazacyclododecane functionalised magnetite nanoparticles Fe_3O_4@SiO_2-cyclen were investigated as a new heavy metal ions adsorbent. To examine the ions-binding abilities of Fe_3O_4@SiO_2-cyclen, a series of measurements were performed in the solutions containing Cd^{2+}, Pb^{2+} and Cu^{2+} ions in concentration level $4.5{\cdot}10^{-6}$ M. All electrochemical experiments were performed in 0.5 M KCl pH 6.00. The pH was adjusted to avoid the formation of other metal ion species, mainly hydroxides, in the solution aside from the free ion [65-67]. The selection of pH and an influence od electrolyte was previously described by the authors in review paper [68]. There was three well-defined peaks observed at anodic stripping voltammograms at –0.65 V, –0.44 V and –0.20 V confirming the presence of Cd^{2+}, Pb^{2+} and Cu^{2+} ion, respectively. Current

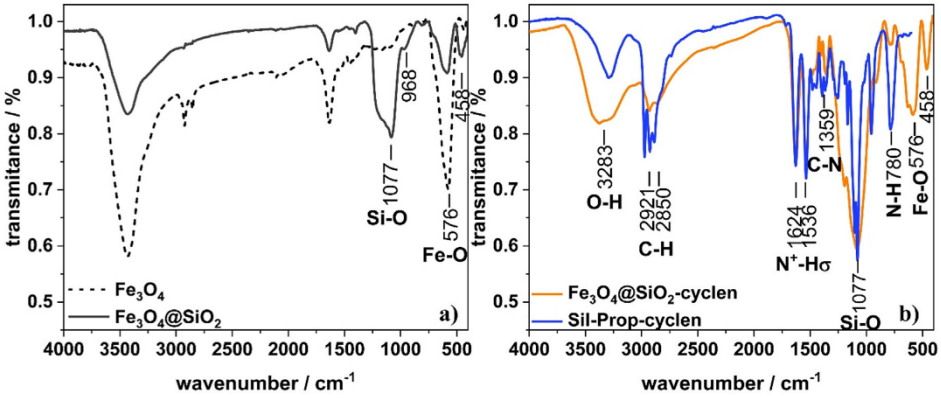

Fig. 4. FT-IR spectra for a) bare Fe_3O_4, silica coated Fe_3O_4@SiO_2 and b) functionalised Fe_3O_4@SiO_2-cyclen nanoparticles, modifier silane N-(3-(triethoxysilyl)propyl)-1,4,7,10-tetraazacyclododecane-1-carboxamide (Sil-Prop-cyclen).

intensities were multiplied by the dilution factor expressed by the equation (1):

$$DF = \frac{V_0 + V_s}{V_0} \quad (1)$$

where V_0 is initial volume and V_s is the volume of added nanoparticles suspension in a particular portion.

3.4.1. Cd^{2+}, Pb^{2+}, Cu^{2+} ions binding by Fe_3O_4@SiO_2-cyclen - kinetics examination

First, kinetic studies were performed to determine the effectual time to establish the equilibrium in the solution after adding the nanoparticles portion. All voltammograms were recorded immediately after adding 1 mg of Fe_3O_4@SiO_2-cyclen nanoparticles to the ion solution and after every 5 min of having mixed the solution. In the graph is shown the actual time that the nanoparticles stayed in the solution due to the length of the DPASV measurement (Fig. 5).

After adding one portion of nanoparticles to the ion solution, a decrease in the peak intensity in the case of only the Cu^{2+} ion was observed. It can be stated that the addition 1 mg of nanoparticles does not affect $Cd^{2+}$and Pb^{2+} ions binding. It can be assumed that the slight peaks intensity changes are within the limit of the measurement error. On the basis of the experiment it can be concluded that the equilibrium in the solution is established no more than 15 min after adding the portion of nanoparticles. A different phenomenon is observed in the case of an experiment in independent Cd^{2+}, Pb^{2+} and Cu^{2+} ion solutions (Figure S1. in the Supporting Information file). In such a case, one observes a decrease in the peaks intensity over time for both the Cd^{2+} and Cu^{2+} ion after adding 0.5 mg Fe_3O_4@SiO_2- cyclen nanoparticles. Functionalised nanomagnetite show no tendency to Pb^{2+} ions binding and it is certainly not influenced by the time of their presence in the solution. It can be assumed that in the case of Cd^{2+} and Cu^{2+} ions the equilibrium in the solution is established after about 50 min after adding the nanoparticles. After analysing the kinetics of ion binding by Fe_3O_4@SiO_2- cyclen nanoparticles, both in individual ion solutions and simultaneous analysis, it was found that the optimal time for adding the nanoparticles portion to the solution to the measurement is 20 min after mixing. Also, the conducted kinetics experiment suggests that the ion binding level may be influenced by the amount

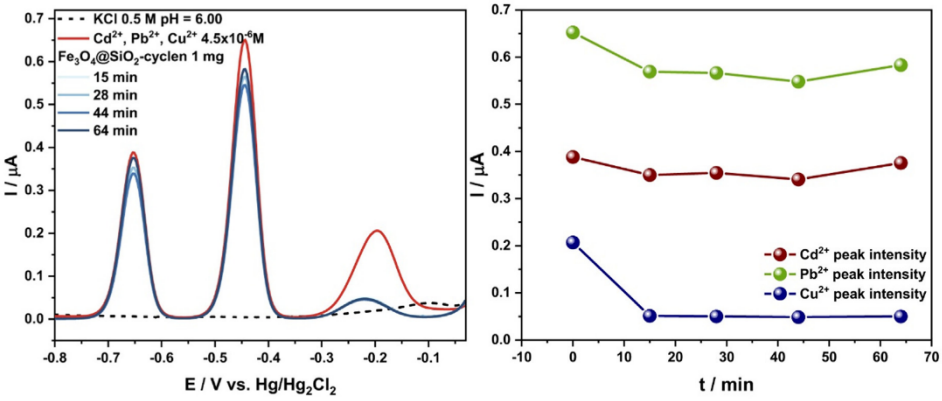

Fig. 5. Simultaneous differential pulse anodic stripping voltammograms for examination of kinetics Cd^{2+}, Pb^{2+} and Cu^{2+} ($4.5{\cdot}10^{-6}$M) ions binding – changes of peak intensities over time after addition of 1 mg Fe_3O_4@SiO_2-cyclen nanoparticles.

of added nanoparticles. Consequently, the observed dependencies lead to the study of the Fe_3O_4@SiO_2- cyclen nanoparticles binding capacity by titration of the Cd^{2+}, Pb^{2+} and Cu^{2+} ions solution.

3.4.2. Determination of Fe_3O_4@SiO_2-cyclen binding ability in Cd^{2+}, Pb^{2+} and Cu^{2+} ions solutions

In order to determine the ion Cd^{2+}, Pb^{2+} and Cu^{2+} binding capacity of Fe_3O_4@SiO_2- cyclen nanoparticles, both in individual solutions and in the mixture, titration with nanoparticles was performed. Used as the measurement analytical method was a two-stage DPASV analysis involving pre-concentration and metal ions stripping. In the first stage, the negative potential of −0.9 V was applied to Cd^{2+}, Pb^{2+} and Cu^{2+} ions electrodeposition on the working electrode. Subsequently, the faradic current obtained by oxidation was recorded during the potential sweep toward the positive potential direction from −0.8 V to −0.5 V, from −0.6 V to −0.3 V, from −0.4 V to −0.04 V and from −0.8 V to 0.0 V, for Cd^{2+}, Pb^{2+}, Cu^{2+} and simultaneous ions detection, respectively. A 0.25 mg portion of Fe_3O_4@SiO_2- cyclen nanoparticles was added into ion solution at each titration step and mixed for 20 min before

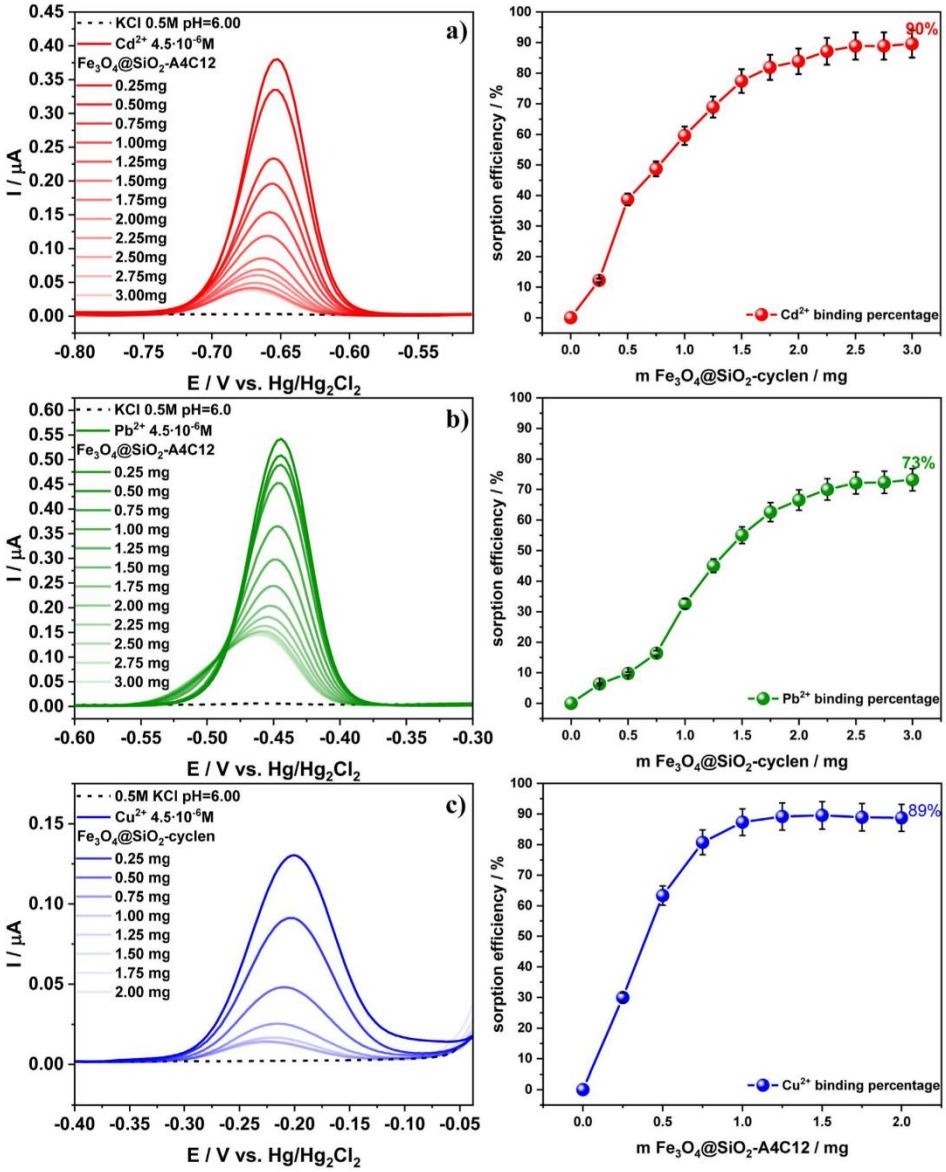

Fig. 6. Individual differential pulse anodic stripping voltammograms and calculated sorption efficiency for a) Cd^{2+}, b) Pb^{2+} and c) Cu^{2+} ions binding by Fe_3O_4@SiO_2-cyclen nanoparticles.

starting the DPASV measurement. The mixing time was determined by the equilibrium establishment experiment in time. Peaks intensity changes during the addition of further nanoparticles portions were recalculated into sorption efficiency $R_{\%}$ (%) at every measuring step based on the formula (2) [69]:

$$R_{\%} = \frac{(C_0 - C_f)}{C_0} \cdot 100\% \quad (2)$$

where C_0 (mg/L) is initial ion Me^{2+} concentration in the solution, C_f (C_e) (mg/L) is the final ion concentration remaining in the solution [69].

Fig. 6 shows an individual Cd^{2+}, Pb^{2+} and Cu^{2+} ions titration using Fe_3O_4@SiO_2- cyclen nanoparticles in portion of 0.25 mg added in every titration step. Fig. 6 a) shows Cd^{2+} ions binding capacity. While adding successive nanoparticles portions, the peak intensity decreases, thus the sorption efficiency increases. After adding about 2–2.5 mg of nanoparticles, the equilibrium is established and the next portions do not affect the peak intensity reduction. The sorption effectiveness reaches about 90% and remains at this level despite nanoparticles excess. A very similar phenomenon was observed during the titration of the Pb^{2+} ion (Fig. 6b). Initially, the peak intensity decreases with each subsequent Fe_3O_4@SiO_2- cyclen portion so that after the addition of about 2–2.5 mg of nanoparticles, it reaches equilibrium. The titration ending determines the Pb^{2+} ion sorption efficiency at a level of 73%. The Fe_3O_4@SiO_2- cyclen nanoparticles behaviour was very different in the Cu^{2+} solution. Similar as in the case of Cd^{2+} and Pb^{2+} ions titrations, a decrease in peak intensity during titration was observed. However, a much smaller amount of nanoparticles was needed to establish equilibrium in the solution. An equilibrium establishing was observed after the addition of about 1 mg of nanoparticles. The addition of excess nanoparticles did not increase the sorption efficiency, and its level reached about 89%.

Afterwards, to compare, all three ions were titrated simultaneously by Fe_3O_4@SiO_2- cyclen nanoparticles starting with 0.25 mg for the first portion and 0.5 mg in the final steps (Fig. 7).

In the initial titration steps, only a decrease in the intensity of the Cu^{2+} peak was observed. After adding about 1–1.5 mg of nanoparticles, the percentage of Cu^{2+} binding remained unchanged at a level of 83%. Then, after the Cu^{2+} binding equilibrium establishing, changes in the intensity of the Cd^{2+} and Pb^{2+} peaks were observed. As more Fe_3O_4@SiO_2- cyclen portions are added, the intensity of the Cd^{2+} and Pb^{2+} peaks was reduced and the binding efficiency increased. The Pb^{2+} binding equilibrium was established after adding about 3–3.5 mg of nanoparticles to the ions solution and the sorption efficiency reached 79%. As the last equilibrium was Cd^{2+} binding established after the addition stage of ion binding remains at a comparable level, however, it requires different amount of nanoparticles.

Table 2
Sorption efficiency parameters for individual and simultaneous Cd^{2+}, $Pb^{2+}$and Cu^{2+} ions binding by Fe_3O_4@SiO_2- cyclen nanoparticles.

	Individual $R_{\%}$	Simultaneous $R_{\%}$
Cd^{2+}	89.55%	88.37%
Pb^{2+}	73.20%	78.85%
Cu^{2+}	88.75%	83.08%

The exact calculated sorption efficiency parameters for individual (from Fig. 6) and simultaneous (from Fig. 7) is presented in Table 2. The sorption efficiency $R_{\%}$ calculated on the basis of the conducted DPASV experiments show that for Cd^{2+} this ion was detected at similar levels of 89–88% regardless as an individual ion in solution or in a mixture of studied ions. In the case of Pb^{2+}, the sorption level was higher for the simultaneous solution, while for Cu^{2+} sorption value was higher in the single-component. Nevertheless, the sorption efficiency are at very high levels for all analysed solutions, which confirms high efficiency of ions binding by Fe_3O_4@SiO_2-cyclen nanoparticles.

3.4.3. Magnetic separation of adsorbed Cd^{2+}, Pb^{2+} and Cu^{2+}

Finally, the separation effectiveness of nanoparticles with adsorbed heavy metal ions by external magnetic field was investigated. First, the necessary amount of nanoparticles to bind Cd^{2+}, Pb^{2+}, Cu^{2+} ions solution was added to them. After that, the reduction in the metal ions peaks intensity at the DPAS voltammograms was observed (from blue line to yellow line). Then the nanoparticles contained in the solution were isolated with the use of a magnet and the solution was separated and subjected to DPASV measurement. The obtained voltammogram, apart from slightly negatively shifted potentials, shows no deviation from that obtained directly after the adsorption process. This phenomenon indicates the separation of all bound ions along with the nanoparticles from the solution (Fig. 8).

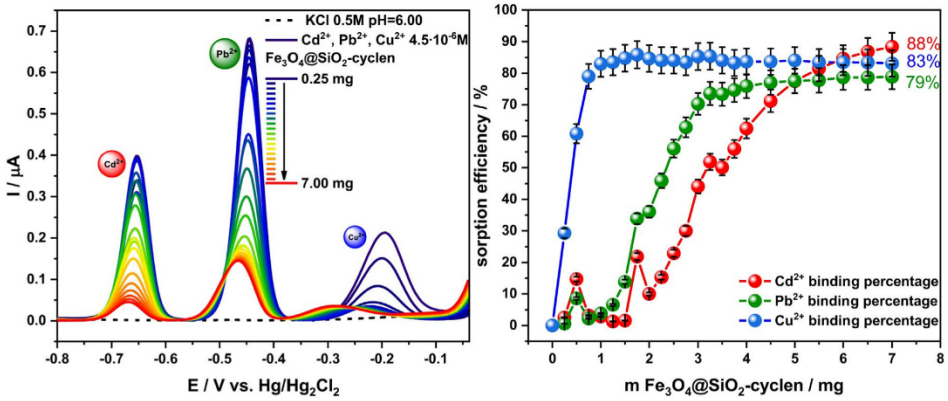

Fig. 7. Simultaneous differential pulse anodic stripping voltammograms and calculated sorption efficiency for Cd^{2+}, Pb^{2+}, Cu^{2+} ions binding by Fe_3O_4@SiO_2-cyclen nanoparticles.

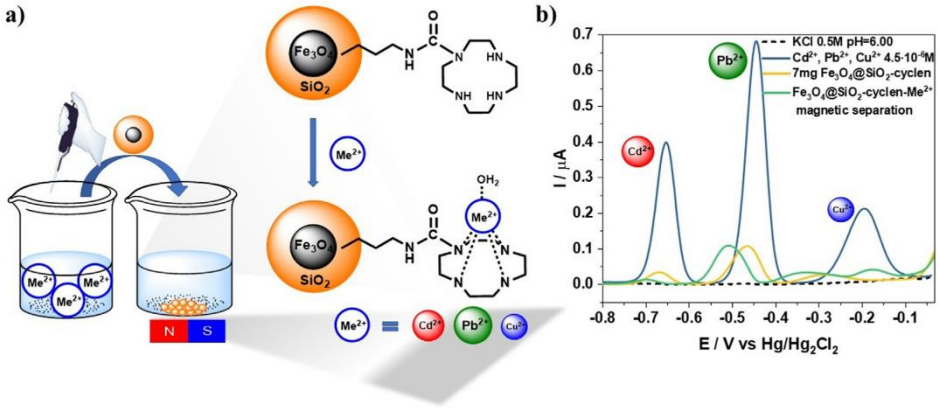

Fig. 8. a) Scheme of magnetic Me^{2+} ions binding and magnetic separation experiment. Ion binding model by aza-crown based on Subat et al. [46]. b) Simultaneous differential pulse anodic stripping voltammograms: of Cd^{2+}, Pb^{2+}, Cu^{2+} ions (blue line), after adsorption by 7 mg Fe_3O_4@SiO_2-cyclen nanoparticles (yellow line) and after magnetic isolation nanoparticles with adsorbed ions (green line).

4. Conclusions

In this work, new core–shell nanostructures were synthesised containing a magnetic Fe_3O_4 core and silane shell functionalised with 1,4,7,10-tetraazacyclododecane were synthesised and characterised and their binding capacity was investigated. The results of nanomaterial characteristics using SEM, XPS, pXRD and FT-IR confirmed the success of the three-stage synthesis process.

Moreover, Fe_3O_4@SiO_2- cyclen nanoparticles binding kinetics and the sorption efficiency of Cd^{2+}, Pb^{2+} and Cu^{2+} was investigated both in individual ions solutions and in an ions mixture. Electrochemical studies proved that nanoparticles can be effectively used as adsorbents in environment heavy metal ions pollution management, which can be easily collected using an external magnetic field.

The research showed that nanoparticles have a binding tendency to all selected ions Cd^{2+}, Pb^{2+} and Cu^{2+} in their individual solutions and their sorption efficiency remains at 90%, 73% and 89%, respectively. It is worth mentioning that the smallest amount of nanoparticles was needed to bind the Cu^{2+}. Simultaneous Cd^{2+}, Pb^{2+} and Cu^{2+} determination also indicates the ability of Fe_3O_4@-SiO_2-cyclen to bind of all ions. However, a clear order of ion binding was observed in the mixture during the addition of further nanoparticles portions. First, Cu^{2+} ions were bound, then Pb^{2+} and Cd^{2+} the sorption efficiency remains at 83%, 79% and 88% level, respectively. This phenomenon can be explained by the complexation constants value of these ions by 1,4,7,10-tetraazacyclodode cane. The fastest Cu^{2+} binding can be explained by the highest value of the complexation constant 23.9, 24.8 according to Antunes et al. [48], whereas the complexation constants of Pb^{2+} and Cd^{2+} are 15.9 and 14.3, respectively [48]. Additionally, the level of ion binding depends on the amount of added nanoparticles. On this basis, it can be concluded that the presence of cyclen functional groups on the surface of nanoparticles gives them the ability to bind ions. Furthermore, the Cd^{2+}, Pb^{2+}, Cu^{2+} ions adsorption and magnetic separation experiment confirms the effectiveness of ion binding and purification of water environments. On the basis of this work, it can be assumed that the new nanomaterials based on Fe_3O_4 and functionalised with N-(3-(triethoxysilyl)propyl)-1,4,7,10-tetraazacyclododecane-1-carboxamide can be successfully used as a universal Cd^{2+}, Pb^{2+}, Cu^{2+} ions magnetic adsorbent.

CRediT authorship contribution statement

Amanda Kulpa-Koterwa: Methodology, Formal analysis, Investigation, Data curation, Writing – original draft, Writing – review & editing, Visualization, Funding acquisition. **Jacek Ryl:** Investigation, Data curation, Writing – original draft. **Karolina Górnicka:** Investigation, Data curation, Writing – original draft. **Paweł Niedziałkowski:** Conceptualization, Resources, Writing – original draft, Writing – review & editing, Supervision.

Data availability

The data that has been used is confidential.

Declaration of Competing Interest

The authors declare the following financial interests/personal relationships which may be considered as potential competing interests: Pawel Niedzialkowski reports financial support was provided by University of Gdansk.

Acknowledgements

This work was created thanks to the University of Gdansk within the project supporting young scientists and PhD students (grant No. BMN 539-T050-B019-22).

Appendix A. Supplementary data

Supplementary data to this article can be found online at https://doi.org/10.1016/j.molliq.2022.120710.

References

[1] S.S. Kolluru, S. Agarwal, S. Sireesha, I. Sreedhar, S.R. Kale, Heavy metal removal from wastewater using nanomaterials-process and engineering aspects, Process Saf. Environ. Prot. 150 (2021) 323–355, https://doi.org/10.1016/j.psep.2021.04.025.

[2] T.K. Das, A. Poater, Review on the use of heavy metal deposits from water treatment waste towards catalytic chemical syntheses, Int. J. Mol. Sci. 22 (2021) 13383, https://doi.org/10.3390/ijms222413383.

[3] J. Briffa, E. Sinagra, R. Blundell, Heavy metal pollution in the environment and their toxicological effects on humans, Heliyon. 6 (9) (2020) e04691, https://doi.org/10.1016/j.heliyon.2020.e04691.
[4] R.K. Gautam, S.K. Sharma, S. Mahiya, M.C. Chattopadhyaya, CHAPTER 1 Contamination of Heavy Metals in Aquatic Media: Transport, Toxicity and Technologies for Remediation, (2014) 1–24. https://doi.org/10.1039/9781782620174-00001.
[5] R. Shrestha, S. Ban, S. Devkota, S. Sharma, R. Joshi, A.P. Tiwari, H.Y. Kim, M.K. Joshi, Technological trends in heavy metals removal from industrial wastewater: A review, J. Environ. Chem. Eng. 9 (4) (2021) 105688, https://doi.org/10.1016/j.jece.2021.105688.
[6] D.-Q. Cao, X. Song, X.-M. Fang, W.-Y. Yang, X.-D. Hao, E. Iritani, N. Katagiri, Membrane filtration-based recovery of extracellular polymer substances from excess sludge and analysis of their heavy metal ion adsorption properties, Chem. Eng. J. 354 (2018) 866–874, https://doi.org/10.1016/j.cej.2018.08.121.
[7] A. Saeedi-Jurkuyeh, A.J. Jafari, R.R. Kalantary, A. Esrafili, A novel synthetic thin-film nanocomposite forward osmosis membrane modified by graphene oxide and polyethylene glycol for heavy metals removal from aqueous solutions, React. Funct. Polym. 146 (2020), https://doi.org/10.1016/j.reactfunctpolym.2019.104397.
[8] Y. Ibrahim, E. Abdulkarem, V. Naddeo, F. Banat, S.W. Hasan, Synthesis of super hydrophilic cellulose-alpha zirconium phosphate ion exchange membrane via surface coating for the removal of heavy metals from wastewater, Sci. Total Environ. 690 (2019) 167–180, https://doi.org/10.1016/j.scitotenv.2019.07.009.
[9] S. Platzer, M. Kar, R. Leyma, S. Chib, A. Roller, F. Jirsa, R. Krachler, D.R. MacFarlane, W. Kandioller, B.K. Keppler, Task-specific thioglycolate ionic liquids for heavy metal extraction: Synthesis, extraction efficacies and recycling properties, J. Hazard. Mater. 324 (2017) 241–249, https://doi.org/10.1016/j.jhazmat.2016.10.054.
[10] Y. Deng, C. Feng, L. Tang, G. Zeng, Z. Chen, M. Zhang, Chapter 5 - Nanohybrid Photocatalysts for Heavy Metal Pollutant Control, in: L. Tang, Y. Deng, J. Wang, J. Wang, G. Zeng (Eds.), Nanohybrid and Nanoporous Materials for Aquatic Pollution Control, Elsevier, 2019, pp. 125–153, https://doi.org/10.1016/B978-0-12-814154-0.00005-0.
[11] X. Guan, X. Yuan, Y. Zhao, H. Wang, H. Wang, J. Bai, Y. Li, Application of functionalized layered double hydroxides for heavy metal removal: A review, Sci. Total Environ. 838 (2022) 155693, https://doi.org/10.1016/j.scitotenv.2022.155693.
[12] C. Yan, Z. Qu, J. Wang, L. Cao, Q. Han, Microalgal bioremediation of heavy metal pollution in water: Recent advances, challenges, and prospects, Chemosphere 286 (2022), https://doi.org/10.1016/j.chemosphere.2021.131870.
[13] J. He, J.P. Chen, A comprehensive review on biosorption of heavy metals by algal biomass: Materials, performances, chemistry, and modeling simulation tools, Bioresour. Technol. 160 (2014) 67–78, https://doi.org/10.1016/j.biortech.2014.01.068.
[14] L. Yang, J. Wang, Y. Yang, S. Li, T. Wang, P. Oleksak, Z. Chrienova, Q. Wu, E. Nepovimova, X. Zhang, K. Kuca, Phytoremediation of heavy metal pollution: Hotspots and future prospects, Ecotoxicol. Environ. Saf. 234 (2022), https://doi.org/10.1016/j.ecoenv.2022.113403.
[15] Q. Chen, Y. Yao, X. Li, J. Lu, J. Zhou, Z. Huang, Comparison of heavy metal removals from aqueous solutions by chemical precipitation and characteristics of precipitates, Journal of Water, Process Engineering. 26 (2018) 289–300, https://doi.org/10.1016/j.jwpe.2018.11.003.
[16] A.J. Bora, R.K. Dutta, Removal of metals (Pb, Cd, Cu, Cr, Ni, and Co) from drinking water by oxidation-coagulation-absorption at optimized pH, J. Water Process Eng. 31 (2019), https://doi.org/10.1016/j.jwpe.2019.100839.
[17] A. Jain, S. Rai, R. Srinivas, R.I. Al-Raoush, Bioinspired modeling and biogeography-based optimization of electrocoagulation parameters for enhanced heavy metal removal, J. Cleaner Prod. 338 (2022), https://doi.org/10.1016/j.jclepro.2022.130622.
[18] S. Shukla, R. Khan, A. Daverey, Synthesis and characterization of magnetic nanoparticles, and their applications in wastewater treatment: A review, Environ. Technol. Innovation 24 (2021), https://doi.org/10.1016/j.eti.2021.101924.
[19] R.M. Ali, H.A. Hamad, M.M. Hussein, G.F. Malash, Potential of using green adsorbent of heavy metal removal from aqueous solutions: Adsorption kinetics, isotherm, thermodynamic, mechanism and economic analysis, Ecol. Eng. 91 (2016) 317–332, https://doi.org/10.1016/j.ecoleng.2016.03.015.
[20] D. Saritha, A concise review on the removal of heavy metals from wastewater using adsorbents, Mater. Today:. Proc. 63 (2022) 3973–3977, https://doi.org/10.1016/j.matpr.2022.04.579.
[21] U. Haripriyan, K.P. Gopinath, J. Arun, Chitosan based nano adsorbents and its types for heavy metal removal: A mini review, Mater. Lett. 312 (2022), https://doi.org/10.1016/j.matlet.2022.131670.
[22] I. Ihsanullah, M. Sajid, S. Khan, M. Bilal, Aerogel-based adsorbents as emerging materials for the removal of heavy metals from water: Progress, challenges, and prospects, Sep. Purif. Technol. 291 (2022), https://doi.org/10.1016/j.seppur.2022.120923.
[23] Y. Yue, Y. Liu, W. Zhang, J. Guo, Y. Gong, Y. Yu, Amidoxime functionalized low-cost cellulose-based adsorbent derived from waste cigarette filters for efficient heavy metal removal, J. Environ. Chem. Eng. 10 (3) (2022) 107846, https://doi.org/10.1016/j.jece.2022.107846.
[24] H. Zhang, X. Hu, T. Li, Y. Zhang, H. Xu, Y. Sun, X. Gu, C. Gu, J. Luo, B. Gao, MIL series of metal organic frameworks (MOFs) as novel adsorbents for heavy metals in water: A review, J. Hazard. Mater. 429 (2022), https://doi.org/10.1016/j.jhazmat.2022.128271.
[25] C. Duan, T. Ma, J. Wang, Y. Zhou, Removal of heavy metals from aqueous solution using carbon-based adsorbents: A review, J. Water Process Eng. 37 (2020), https://doi.org/10.1016/j.jwpe.2020.101339.
[26] S. Cho, J.-H. Kim, K.S. Yang, M. Chang, Facile preparation of amino-functionalized polymeric microcapsules as efficient adsorbent for heavy metal ions removal, Chem. Eng. J. 425 (2021), https://doi.org/10.1016/j.cej.2021.130645.
[27] E. Vunain, A. Mishra, B. Mamba, Dendrimers, mesoporous silicas and chitosan-based nanosorbents for the removal of heavy-metal ions: A review, Int. J. Biol. Macromol. 86 (2016) 570–586, https://doi.org/10.1016/j.ijbiomac.2016.02.005.
[28] M.M. Al-Mahadeen, A.G. Jiries, S.A. Al-Trawneh, S.F. Alshahateet, A.S. Eldouhaibi, S. Sagadevan, Kinetics and equilibrium studies for the removal of heavy metal ions from aqueous solution using the synthesized C-4-bromophenylcalix[4]resorcinarene adsorbent, Chem. Phys. Lett. 783 (2021), https://doi.org/10.1016/j.cplett.2021.139053.
[29] Z. Cheng, J. Yang, L. Li, Y. Chen, X. Wang, Flocculation inspired combination of layered double hydroxides and fulvic acid to form a novel composite adsorbent for the simultaneous adsorption of anionic dye and heavy metals, J. Colloid Interface Sci. 618 (2022) 386–398, https://doi.org/10.1016/j.jcis.2022.03.097.
[30] R. Torkaman, F. Maleki, M. Gholami, M. Torab-Mostaedi, M. Asadollahzadeh, Assessing the radiation-induced graft polymeric adsorbents with emphasis on heavy metals removing: A systematic literature review, J. Water Process Eng. 44 (2021), https://doi.org/10.1016/j.jwpe.2021.102371.
[31] V. Vinayagam, S. Murugan, R. Kumaresan, M. Narayanan, M. Sillanpää, D.-V.-N. Vo, O.S. Kushwaha, Protein nanofibrils as versatile and sustainable adsorbents for an effective removal of heavy metals from wastewater: A review, Chemosphere 301 (2022), https://doi.org/10.1016/j.chemosphere.2022.134635.
[32] J. R., B. Gurunathan, S. K, S. Varjani, H.H. Ngo, E. Gnansounou, Advancements in heavy metals removal from effluents employing nano-adsorbents: Way towards cleaner production, Environ. Res. 203 (2022) 111815, https://doi.org/10.1016/j.envres.2021.111815.
[33] R. Bhateria, R. Singh, A review on nanotechnological application of magnetic iron oxides for heavy metal removal, J. Water Process Eng. 31 (2019), https://doi.org/10.1016/j.jwpe.2019.100845.
[34] A. Latif, D. Sheng, K. Sun, Y. Si, M. Azeem, A. Abbas, M. Bilal, Remediation of heavy metals polluted environment using Fe-based nanoparticles: Mechanisms, influencing factors, and environmental implications, Environ. Pollut. 264 (2020), https://doi.org/10.1016/j.envpol.2020.114728.
[35] F. Ghorbani, S. Kamari, Core–shell magnetic nanocomposite of Fe_3O_4@SiO_2@NH_2 as an efficient and highly recyclable adsorbent of methyl red dye from aqueous environments, Environ. Technol. Innovation 14 (2019), https://doi.org/10.1016/j.eti.2019.100333.
[36] S. Patil, R. Tandon, N. Tandon, A current research on silica coated ferrite nanoparticle and their application: Review, Curr. Res. Green Sustain. Chem. 4 (2021), https://doi.org/10.1016/j.crgsc.2021.100063.
[37] L. Wang, X. Huang, C. Wang, X. Tian, X. Chang, Y. Ren, S. Yu, Applications of surface functionalized Fe_3O_4 NPs-based detection methods in food safety, Food Chem. 342 (2021), https://doi.org/10.1016/j.foodchem.2020.128343.
[38] S. Jin, B.C. Park, W.S. Ham, L. Pan, Y.K. Kim, Effect of the magnetic core size of amino-functionalized Fe_3O_4-mesoporous SiO_2 core-shell nanoparticles on the removal of heavy metal ions, Colloids Surf., A 531 (2017) 133–140, https://doi.org/10.1016/j.colsurfa.2017.07.086.
[39] Y. Harinath, D.H.K. Reddy, L.S. Sharma, K. Seshaiah, Development of hyperbranched polymer encapsulated magnetic adsorbent (Fe_3O_4@SiO_2–NH_2-PAA) and its application for decontamination of heavy metal ions, Journal of Environmental, Chem. Eng. 5 (2017) 4994–5001, https://doi.org/10.1016/j.jece.2017.09.031.
[40] N. Naini, H. Sid Kalal, M.R. Almasian, D. Niknafs, M. Taghiof, H. Hoveidi, Phosphine-functionalized Fe_3O_4/SiO_2/composites as efficient magnetic nanoadsorbents for the removal of palladium ions from aqueous solution: Kinetic, thermodynamic and isotherm studies, Mater. Chem. Phys. 287 (2022), https://doi.org/10.1016/j.matchemphys.2022.126242.
[41] E. Ragheb, M. Shamsipur, F. Jalali, F. Mousavi, Modified magnetic-metal organic framework as a green and efficient adsorbent for removal of heavy metals, J. Environ. Chem. Eng. 10 (2) (2022) 107297, https://doi.org/10.1016/j.jece.2022.107297.
[42] W. Qin, S. Xu, G. Xu, Q. Xie, C. Wang, Z. Xu, Preparation of silica gel bound crown ether and its extraction performance towards zirconium and hafnium, Chem. Eng. J. 225 (2013) 528–534, https://doi.org/10.1016/j.cej.2013.03.127.
[43] M. Subat, K. Woinaroschy, S. Anthofer, B. Malterer, B. König, 1,4,7,10-Tetraazacyclododecane Metal Complexes as Potent Promoters of Carboxyester Hydrolysis under Physiological Conditions, Inorg. Chem. 46 (2007) 4336–4356, https://doi.org/10.1021/ic070101z.
[44] J.M. Park, O.J. Shon, H. Hong, J.S. Kim, Y. Kim, H.B. Lim, Development of a microchip metal ion sensor using dinitro-azocalix[4]azacrown, Microchem. J. 80 (2005) 139–144, https://doi.org/10.1016/j.microc.2004.07.017.
[45] B. König, M. Pelka, M. Subat, I. Dix, P.G. Jones, Urea Derivatives of 1,4,7,10-Tetraazacyclododecane – Synthesis and Binding Properties, European Journal of Organic Chemistry. 2001 (2001) 1943–1949. https://doi.org/10.1002/1099-0690(200105)2001:10<1943::AID-EJOC1943>3.0.CO;2-O.
[46] M. Subat, K. Woinaroschy, C. Gerstl, B. Sarkar, W. Kaim, B. König, 1,4,7,10-Tetraazacyclododecane Metal Complexes as Potent Promoters of Phosphodiester Hydrolysis under Physiological Conditions, Inorg. Chem. 47 (2008) 4661–4668, https://doi.org/10.1021/ic702413q.

[47] M. Regueiro-Figueroa, E. Ruscsák, L. Fra, G. Tircsó, I. Tóth, A. de Blas, T. Rodríguez-Blas, C. Platas-Iglesias, D. Esteban-Gómez, Highly Stable Complexes of Divalent Metal Ions (Mg2+, Ca^{2+}, Cu^{2+}, Zn^{2+}, Cd^{2+}, and Pb^{2+}) with a Dota-Like Ligand Containing a Picolinate Pendant, Eur. J. Inorg. Chem. 2014 (2014) 6165–6173, https://doi.org/10.1002/ejic.201402693.

[48] P. Antunes, P.M. Campello, R. Delgado, M.G.B. Drew, V. Félix, I. Santos, Metal complexes of a tetraazacyclophane: solution and molecular modelling studies, Dalton Trans. (2003) 1852–1860, https://doi.org/10.1039/B301033C.

[49] P. Niedziałkowski, D. Zarzeczańska, T. Ossowski, Synthesis and Characterization of 1,4,7,10-Tetraazacyclododecane Derivatives and Their Metal Complexes, Pol. J. Chem. 82 (2008) 1175–1197.

[50] A. Kulpa, J. Ryl, G. Skowierzak, A. Koterwa, G. Schroeder, T. Ossowski, P. Niedziałkowski, Comparison of Cadmium Cd^{2+} and Lead Pb^{2+} Binding by Fe_2O_3@SiO_2-EDTA Nanoparticles – Binding Stability and Kinetic Studies, Electroanalysis 32 (2020) 588–597, https://doi.org/10.1002/elan.201900616.

[51] A. Kulpa, J. Ryl, G. Schroeder, A. Koterwa, J. Sein Anand, T. Ossowski, P. Niedziałkowski, Simultaneous voltammetric determination of Cd^{2+}, Pb^{2+}, and Cu^{2+} ions captured by Fe_3O_4@SiO_2 core-shell nanostructures of various outer amino chain length, J. Mol. Liq. 314 (2020), 113677 https://doi.org/10.1016/j.molliq.2020.113677.

[52] S. Sawan, R. Maalouf, A. Errachid, N. Jaffrezic-Renault, Metal and metal oxide nanoparticles in the voltammetric detection of heavy metals: A review, TrAC, Trends Anal. Chem. 131 (2020), https://doi.org/10.1016/j.trac.2020.116014.

[53] T. Matsuoka, S. Yamamoto, O. Moriya, M. Kashio, T. Sugizaki, Synthesis of thermoresponsive polysilsesquioxane with methoxyethylamide group and crown ether, Polym J. 42 (2010) 313–318, https://doi.org/10.1038/pj.2010.7.

[54] M.C. Biesinger, B.P. Payne, A.P. Grosvenor, L.W.M. Lau, A.R. Gerson, R.St.C. Smart, Resolving surface chemical states in XPS analysis of first row transition metals, oxides and hydroxides: Cr, Mn, Fe, Co and Ni, Applied Surface Science. 257 (2011) 2717–2730. https://doi.org/10.1016/j.apsusc.2010.10.051.

[55] Š. Meškinis, A. Vasiliauskas, M. Andrulevičius, D. Peckus, S. Tamulevičius, K. Viskontas, Diamond Like Carbon Films Containing Si: Structure and Nonlinear Optical Properties, Materials. 13 (2020) 1003, https://doi.org/10.3390/ma13041003.

[56] F. Sirotti, M. De Santis, G. Rossi, Synchrotron-radiation photoemission and x-ray absorption of Fe silicides, Phys. Rev. B. 48 (1993) 8299–8306, https://doi.org/10.1103/PhysRevB.48.8299.

[57] R. Bywalez, H. Karacuban, H. Nienhaus, C. Schulz, H. Wiggers, Stabilization of mid-sized silicon nanoparticles by functionalization with acrylic acid, Nanoscale Res. Lett. 7 (2012) 76, https://doi.org/10.1186/1556-276X-7-76.

[58] A. Mohtasebi, T. Chowdhury, L.H.H. Hsu, M.C. Biesinger, P. Kruse, Interfacial Charge Transfer between Phenyl-Capped Aniline Tetramer Films and Iron Oxide Surfaces, J. Phys. Chem. C. 120 (2016) 29248–29263, https://doi.org/10.1021/acs.jpcc.6b09950.

[59] A. Tanver, M.-H. Huang, Y. Luo, Energetic interpenetrating polymer network (EIPN): enhanced thermo-mechanical properties of NCO-fMWCNTs/HTPB PU and alkyne-fMWCNTs/acyl-GAP based nanocomposite and its propellants, RSC Adv. 6 (2016) 49101–49112, https://doi.org/10.1039/C6RA07742K.

[60] Q. Li, C.W. Kartikowati, S. Horie, T. Ogi, T. Iwaki, K. Okuyama, Correlation between particle size/domain structure and magnetic properties of highly crystalline Fe_3O_4 nanoparticles, Sci Rep. 7 (2017) 9894, https://doi.org/10.1038/s41598-017-09897-5.

[61] F. Shalali, S. Cheraghi, M.A. Taher, A sensitive electrochemical sensor amplified with ionic liquid and N-CQD/Fe_3O_4 nanoparticles for detection of raloxifene in the presence of tamoxifen as two essentials anticancer drugs, Mater. Chem. Phys. 278 (2022), https://doi.org/10.1016/j.matchemphys.2021.125658.

[62] T. Yousofi, A. Rahmati, Fe_3O_4@SiO_2-BU core-shell as a new nanomagnetic gelator for oil recovery from water, Polyhedron 180 (2020), https://doi.org/10.1016/j.poly.2020.114363.

[63] T. Akbarpour, J. Yousefi Seyf, A. Khazaei, N. Sarmasti, Synthesis of Pyrano [2,3-c] Pyrazole Derivatives Using a Novel Ionic-Liquid Based Nano-Magnetic Catalyst (Fe_3O_4@SiO_2@$(CH_2)_3$NH@CC@Imidazole@$SO_3H^+Cl^-$), Polycyclic Aromat. Compd. 42 (6) (2022) 3844–3864, https://doi.org/10.1080/10406638.2021.1873152.

[64] D. Chen, T. Awut, B. Liu, Y. Ma, T. Wang, I. Nurulla, Functionalized magnetic Fe_3O_4 nanoparticles for removal of heavy metal ions from aqueous solutions, E-Polymers. 16 (2016) 313–322, https://doi.org/10.1515/epoly-2016-0043.

[65] Q. Kong, C. Wei, S. Preis, Y. Hu, F. Wang, Facile preparation of nitrogen and sulfur co-doped graphene-based aerogel for simultaneous removal of Cd^{2+} and organic dyes, Environ Sci Pollut Res Int. 25 (2018) 21164–21175, https://doi.org/10.1007/s11356-018-2195-8.

[66] T. Chen, H. Li, H. Wang, X. Zou, H. Liu, D. Chen, Y. Zhou, Removal of Pb(II) from Aqueous Solutions by Periclase/Calcite Nanocomposites, Water Air Soil Pollut. 230 (2019) 299, https://doi.org/10.1007/s11270-019-4354-z.

[67] J. Liu, D. Luo, L. Huang, Y. Wang, S. Wen, Copper adsorption reaction rate and ion exchange ratio during the copper activation of sphalerite, Physicochem. Probl. Miner. Process. 54 (2017) 377–385, https://doi.org/10.5277/ppmp1832.

[68] A. Kulpa-Koterwa, T. Ossowski, P. Niedziałkowski, Functionalized Fe_3O_4 Nanoparticles as Glassy Carbon Electrode Modifiers for Heavy Metal Ions Detection—A Mini Review, Materials. 14 (2021) 7725, https://doi.org/10.3390/ma14247725.

[69] C. Zeng, P. Liu, Z. Xiao, Y. Li, L. Song, Z. Cao, D. Wu, Y.-F. Zhang, Highly Selective Adsorption and Recovery of Palladium from Spent Catalyst Wastewater by 1,4,7,10-Tetraazacyclododecane-Modified Mesoporous Silica, ACS Sustainable Chem. Eng. 10 (2022) 1103–1114, https://doi.org/10.1021/acssuschemeng.1c05915.

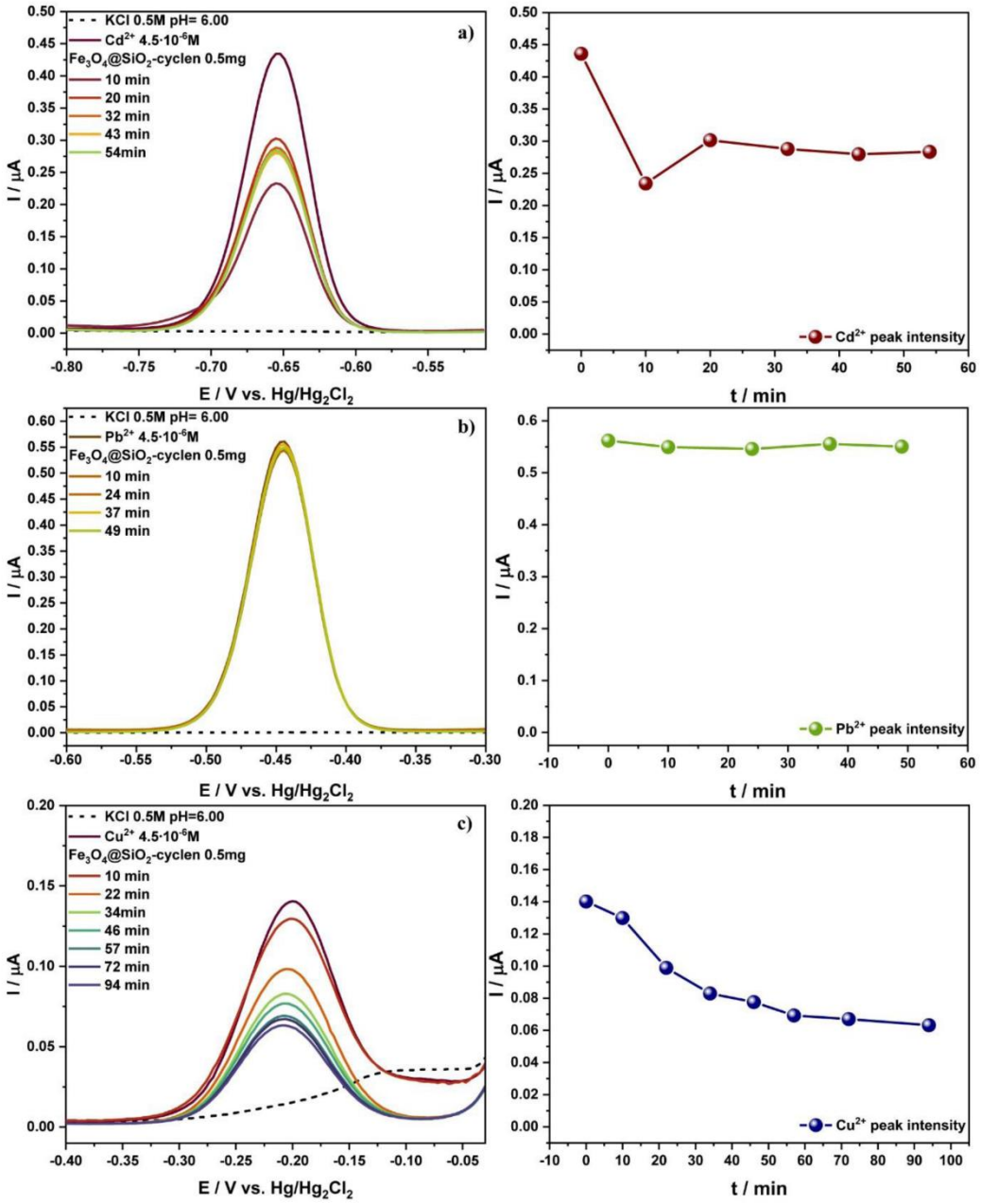

Figure S1. Individual differential pulse anodic stripping voltammograms for examination of kinetics a) Cd^{2+}, b) Pb^{2+} and c) Cu^{2+} ($4.5 \cdot 10^{-6}$M) ions binding – changes of peak intensities over time after addition of 0.5 mg Fe_3O_4@SiO_2-cyclen nanoparticles.

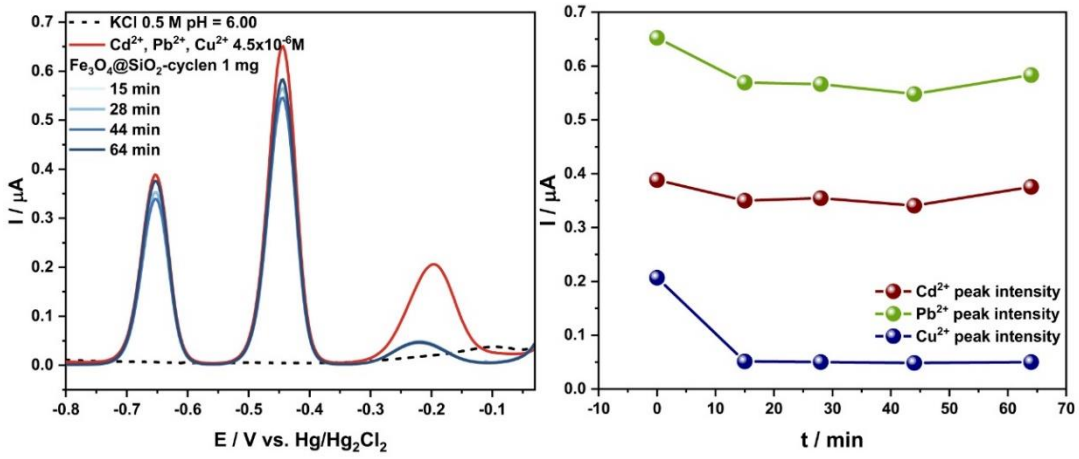

Fig. 5. Simultaneous differential pulse anodic stripping voltammograms for examination of kinetics Cd^{2+}, Pb^{2+} and Cu^{2+} ($4.5 \cdot 10^{-6}$M) ions binding – changes of peak intensities over time after addition of 1 mg Fe_3O_4@SiO_2-cyclen nanoparticles.

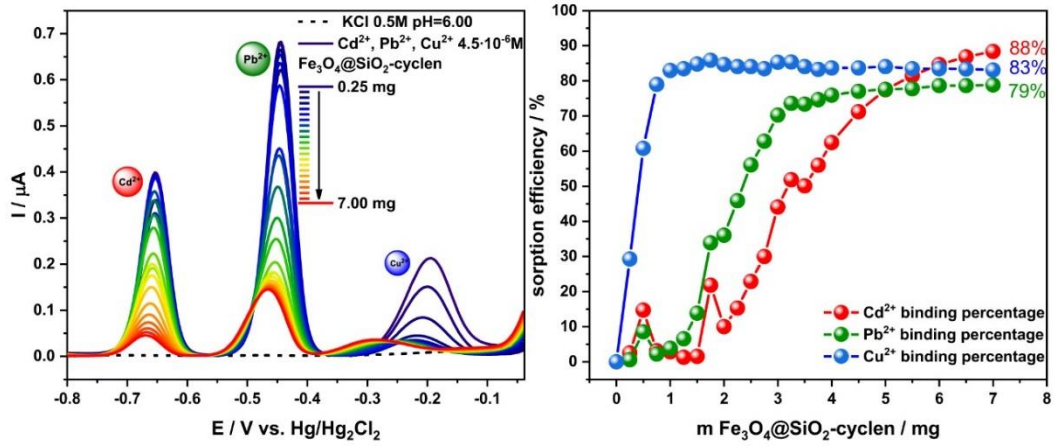

Fig. 7. Simultaneous differential pulse anodic stripping voltammograms and calculated sorption efficiency for Cd^{2+}, Pb^{2+}, Cu^{2+} ions binding by Fe_3O_4@SiO_2-cyclen nanoparticles.

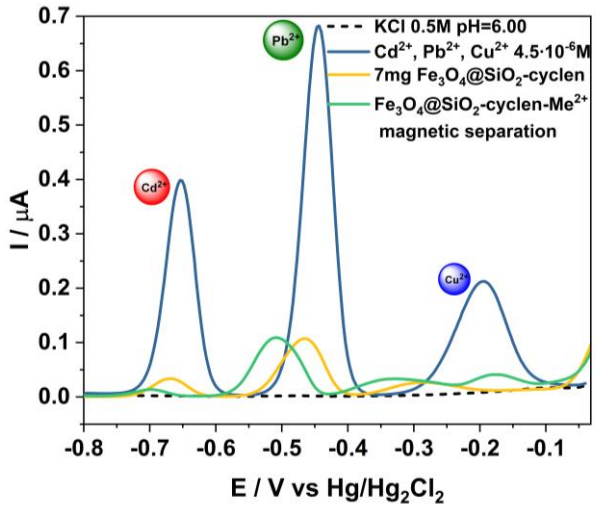

Fig. 8. b) Simultaneous differential pulse anodic stripping voltammograms: of Cd^{2+}, Pb^{2+}, Cu^{2+} ions (blue line), after adsorption by 7 mg Fe_3O_4@SiO_2-cyclen nanoparticles (yellow line) and after magnetic isolation nanoparticles with adsorbed ions (green line).

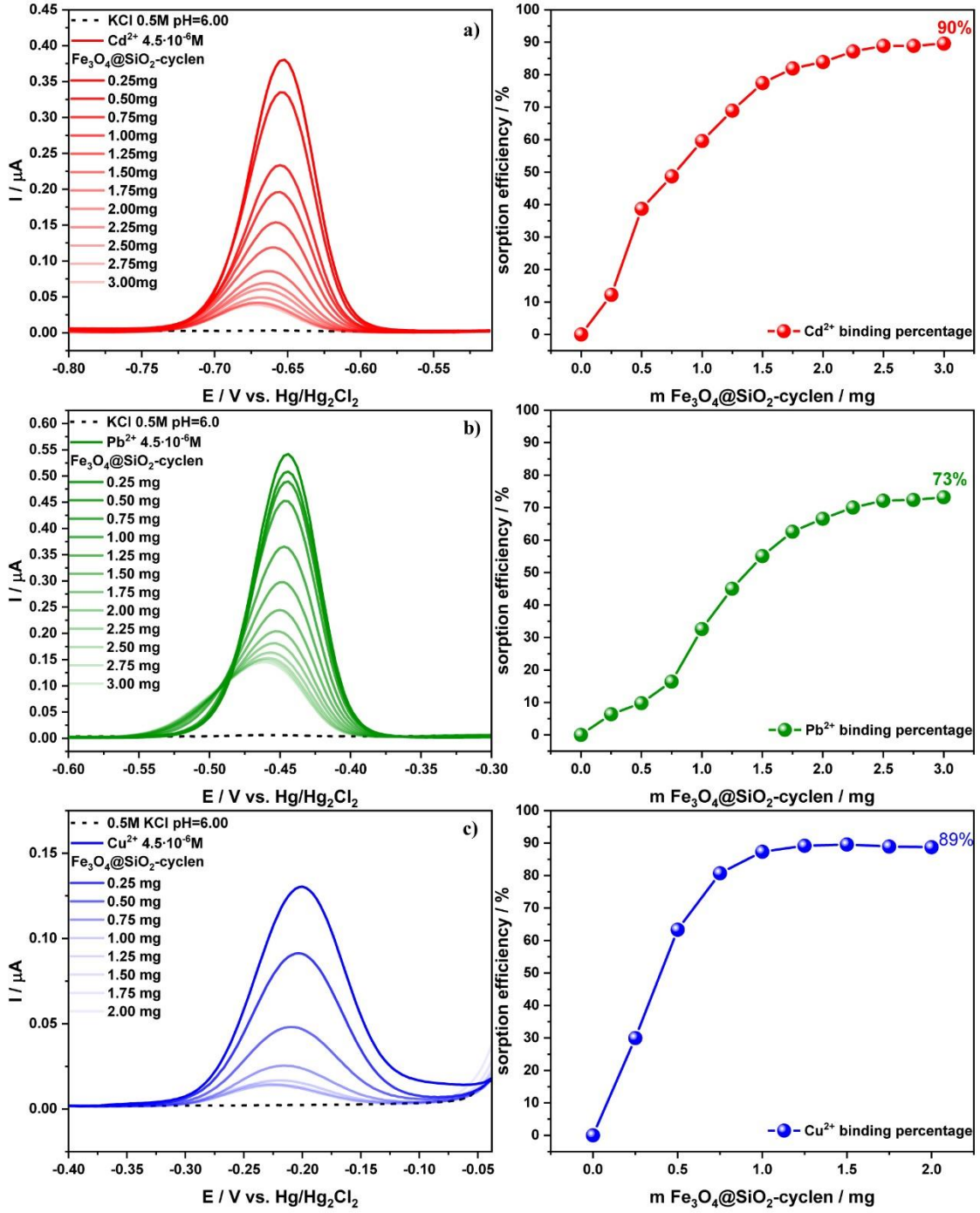

Fig. 6. Individual differential pulse anodic stripping voltammograms and calculated sorption efficiency for a) Cd^{2+}, b) Pb^{2+} and c) Cu^{2+} ions binding by $Fe_3O_4@SiO_2$-cyclen nanoparticles.

4. Załącznik 4

Kopernikańskie Seminarium Doktoranckie
NA POGRANICZU CHEMII, BIOLOGII I FIZYKI – ROZWÓJ NAUK
TOM 3
TORUŃ 2022

Nanostruktury magnetyczne typu *core-shell* Fe_3O_4@SiO_2-Nn jako nowe adsorbenty jonów metali ciężkich Cd^{2+}, Pb^{2+} oraz Cu^{2+} – badania elektrochemiczne

Amanda Kulpa-Koterwa[1], Grzegorz Schroeder[2], Tadeusz Ossowski[1], Adrian Koterwa[1], Paweł Niedziałkowski[1]

[1]Zespół Chemii Supramolekularnej, Katedra Chemii Analitycznej, Wydział Chemii, Uniwersytet Gdański
[2]Zakład Chemii Supramolekularnej, Wydział Chemii, Uniwersytet im. Adama Mickiewicza w Poznaniu
email: amanda.kulpa@phdstud.ug.edu.pl

Streszczenie: W ostatnich latach nanostruktury zyskały duże znaczenie jako adsorbenty jonów metali. W prezentowanej pracy przedstawiono badania zdolności wiązania nanocząstek typu rdzeń – otoczka zawierających różną liczbę grup aminowych w łańcuchu zewnętrznym Fe_3O_4@SiO_2-N_n wobec jonów Cd^{2+}, Pb^{2+} oraz Cu^{2+}. Badania elektrochemiczne przeprowadzono z wykorzystaniem różnicowej woltamperometrii pulsowej i kroplowej elektrody rtęciowej metodą zatężania analitu w kropli (DPASV – *Differential Pulse Anodic Stripping Voltammetry*). Przeprowadzone eksperymenty wskazują na wysoką pojemność sorpcyjną nanostruktur. Bardzo silne wiązania na poziomie ≥ 94% występują pomiędzy Fe_3O_4@SiO_2-N_1 – Pb^{2+} (98%), Fe_3O_4@SiO_2-N_1 – Cu^{2+} (94%), Fe_3O_4@SiO_2-N_2 – Pb^{2+} (98%) oraz Fe_3O_4@SiO_2-N_3 – Cu^{2+} (95%). Wszystkie ze wskazanych rodzajów nanocząstek

wykazują słabe powinowactwo wobec jonów Cd^{2+}. Procent związania jonów kadmu waha się w granicach od 10 do 39%. Natomiast żadnych oddziaływań nie zaobserwowano pomiędzy strukturami $Fe_3O_4@SiO_2$-N_3 a jonami Pb^{2+}. Na podstawie otrzymanych wyników badań można dokładnie określić selektywność nanocząstek wobec badanych jonów. Nanostruktury $Fe_3O_4@SiO_2$-N_2 najsilniej wiążą jony Pb^{2+}, natomiast $Fe_3O_4@SiO_2$-N_3 – jony Cu^{2+}. Dobra pojemność jonowa użytych nanostruktur oraz możliwość ich separacji za pomocą zewnętrznego pola magnetycznego sprawia, że mogą być one z powodzeniem wykorzystywane jako nowa klasa nanoadsorbentów do remediacji jonów metali ciężkich ze środowiska.

Słowa kluczowe: nanocząstki Fe_3O_4, amino funkcjonalizacja, usuwanie jonów Cd^{2+}, Pb^{2+}, Cu^{2+}, DPASV

1. Wstęp

Wraz z szybkim rozwojem gospodarki znacznie wzrosło zanieczyszczenie środowiska, co stało się globalnym problemem całego świata. Szczególnie obserwowany jest wzrost obecności metali ciężkich w środowisku, generowany przez procesy produkcyjne, takie jak: rafinacja, stosowanie nawozów i pestycydów, produkcja baterii, garbarstwo, produkcja chemiczna czy też górnictwo [1]. Skażenie środowiska metalami ciężkimi generuje poważne obawy ze względu na ich niską biodegradowalność, tendencję do bioakumulacji, mutagenność i rakotwórczość [2, 3]. Ponadto jony kadmu, ołowiu i miedzi znajdują się na liście 129 priorytetowych zanieczyszczeń (Priority Pollutant List) Amerykańskiej Agencji Ochrony Środowiska (United States Environmental Protection Agency).

Wiele grup badawczych chemików i ekologów na całym świecie poszukuje metod analizy oraz usuwania zanieczyszczeń jonami metali ciężkich ze środowiska. Najczęściej wykorzystywanymi metodami są: współstrącanie, proces koagulacji, flotacji, filtracja membranowa, ekstrakcja cieczami jonowymi, wymiana jonowa, elektroliza czy procesy odwróconej osmozy [4–11]. Wszystkie one wykazują pewne wady, takie jak: niska wydajność procesu, złożoność analizy, wysoki koszt, a także możliwość powstawania odpadów wtórnych. Dlatego też coraz większym zainteresowaniem cieszy się zastosowanie nanoadsorbcji, głównie ze względu na doskonałe właściwości

nanocząstek, tj. duża powierzchnia właściwa oraz dobre właściwości sorpcyjne. Mały rozmiar cząstek powoduje również trudność w oddzieleniu ich od roztworów, co ogranicza ich zastosowanie, np. w uzdatnianiu wody [12]. W związku z tym przewagę w tej dziedzinie zyskują nanomateriały o właściwościach magnetycznych, które dają się łatwo wyodrębnić za pomocą zewnętrznego pola magnetycznego [13, 14].

W prezentowanej pracy przebadano serię nanocząstek magnetycznych $Fe_3O_4@SiO_2$ funkcjonalizowanych łańcuchami alkiloaminowymi różniącymi się liczbą grup aminowych: $Fe_3O_4@SiO_2$-N_1, $Fe_3O_4@SiO_2$-N_2 oraz $Fe_3O_4@SiO_2$-N_3. Powyższe nanomateriały wykorzystano do wiązania i usuwania jonów metali ciężkich w postaci Cd^{2+}, Pb^{2+} oraz Cu^{2+} z roztworów wodnych. Na podstawie wykonanych badań elektrochemicznych z wykorzystaniem techniki różnicowej woltamperometrii pulsowej i kroplowej elektrody rtęciowej obliczono procent związania jonów w roztworze wodnym. Otrzymane wyniki pozwoliły na porównanie powinowactwa analizowanych nanocząstek do określonych jonów.

2. Materiały i metody

2.1 Reagenty

Syntezę oraz funkcjonalizację nanocząstek przeprowadzono z wykorzystaniem następujących odczynników: sześciowodnego chlorku żelaza(III) ($FeCl_3 \cdot 6H_2O$) i tetrahydratu chlorku żelaza(II) ($FeCl_2 \cdot 4H_2O$), amoniaku (25%) (NH_3), ortokrzemianu tetraetylu (98%) (TEOS), 3-(aminopropylo) trietoksysilanu (APTES) (99%), N-(2-aminoetylo)-3-amino-propylotrimetoksysilanu oraz N^1-(3-trimetoksysililopropylo) dietylenotriaminy, firmy Sigma-Aldrich (Polska). Natomiast użyte rozpuszczalniki organiczne i sole nieorganiczne: chlorek potasu KCl (99,9%), tetrahydrat azotanu(V) kadmu $Cd(NO_3)_2 \cdot 4H_2O$ (99,9%), azotan(V) ołowiu $Pb(NO_3)_2$ oraz trzywodny azotan(V) miedzi $Cu(NO_3)_2 \cdot 3H_2O$ (99,9%) zakupiono w POCh (Polska).

2.2. Synteza i charakterystyka nanomateriałów

Nanocząstki magnetytu otrzymano metodą współstrącania w warunkach beztlenowych poprzez zmieszanie dwóch roztworów zawierających jony Fe^{2+} i Fe^{3+} w stosunku molowym 1:2. Następnie przeprowadzono proces strącania poprzez wkraplanie roztworu amoniaku, uzyskując pH 11. Na kolejnym etapie otrzymane nanocząstki powleczono krzemionką, wykorzystując metodę Ströbera, w etanolowym roztworze tetraetylokrzemianu (TEOS). Ostatnim etapem syntezy była funkcjonalizacja powierzchni otrzymanych nanocząstek $Fe_3O_4@SiO_2$ z wykorzystaniem następujących reagentów: 3-amino propylotrietoksysilanu (APTES), N-(2-aminoetylo)-3-aminopropylotrimetoksysilanu i N^1-(3-trimetoksysililopropylo) dietylenotriaminy. Reakcję przeprowadzono w toluenie, otrzymując serię nanokompozytów z różną liczbą grup aminowych w łańcuchu zewnętrznym, znajdujących się na powierzchni nanocząstki: $Fe_3O_4@SiO_2$-N_1, $Fe_3O_4@SiO_2$- N_2 oraz $Fe_3O_4@SiO_2$-N_3 (ryc. 1).

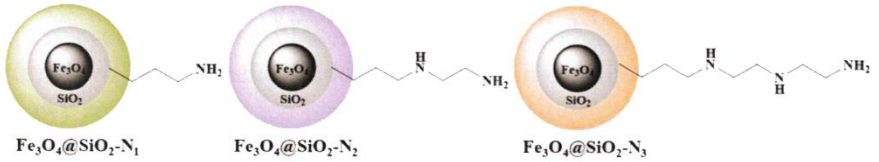

Ryc. 1. Schemat budowy otrzymanych nanostruktur typu $Fe_3O_4@SiO_2$-N_n

Następnie wykonano charakterystykę otrzymanego materiału z wykorzystaniem skaningowego mikroskopu elektronowego (SEM – *Scanning Electron Microscopy*), transmisyjnego mikroskopu elektronowego (TEM – *Transmission Electron Microscopy*), mikroskopu konfokalnego, spektroskopii w podczerwieni (FT-IR – *Fourier-Transform Infrared Spectroscopy*) oraz spektroskopii fotoelektronów w zakresie promieniowania X (XPS – *X-ray Photoelectron Spectroscopy*) [15].

2.3. Pomiary elektrochemiczne

Pomiary elektrochemiczne przeprowadzono z zastosowaniem kroplowej elektrody rtęciowej Metrohm 663 VA Stand zintegrowanej z potencjostatem/galwanostatem Autolab PGSTAT-128 N, który kontrolowany był przez program NOVA 2.1.4. Trzyelektrodowy system pomiarowy zawierał statyczną elektrodę rtęciową (SDME – Static Drop Mercury Electrode) użytą jako elektroda robocza, elektrodę kalomelową $Hg|Hg_2Cl_2|KCl_{(nasycony)}$ jako elektrodę odniesienia oraz przeciwelektrodę w postaci pręta z węgla szklistego (GC – Glassy Carbon).

Pomiary elektrochemiczne wykonano z zastosowaniem różnicowej woltamperometrii pulsowej (DPV – *Differential Pulse Voltammetry*). Detekcję jonów przeprowadzono z wykorzystaniem metody zatężania analitu w kropli (ASV – *Anodic Stripping Voltammetry*) w zoptymalizowanych warunkach eksperymentalnych. Wszystkie pomiary przeprowadzono w naczynku teflonowym w celu uniknięcia adsorpcji jonów metali na powierzchni szkła.

Roztwory jonów metali przygotowano w 0,5 M KCl o pH 6,5, użytym jako elektrolit podstawowy. W celu zbadania zdolności wiązania jonów przez nanocząstki $Fe_3O_4@SiO_2\text{-}N_1$, $Fe_3O_4@SiO_2\text{-}N_2$ i $Fe_3O_4@SiO_2\text{-}N_3$ wykonano serię pomiarów w roztworze zawierającym jony Cd^{2+}, Pb^{2+} oraz Cu^{2+} o stężeniu 4,5 μM. Wszystkie eksperymenty elektrochemiczne przeprowadzono w roztworze elektrolitu podstawowego 0,5 M KCl o pH 6,5. Naważkę nanocząstek przygotowano przez dyspersję w kąpieli ultradźwiękowej w elektrolicie podstawowym przez 30 minut przed każdym pomiarem. Po każdej porcji nanocząstek dodanej do celki pomiarowej po upływie 5 minut rejestrowano pomiar elektrochemiczny. Na uzyskanych woltamogramach uwidoczniły się dobrze zdefiniowane piki przy potencjałach -0,63 V, -0,42 V i 0,17 V, które przypisano odpowiednio jonom Cd^{2+}, Pb^{2+} i Cu^{2+}. Następnie wysokość pików została przeliczona na procent związania danego jonu.

3. Wyniki i dyskusja

3.1. Charakterystyka nanomateriałów

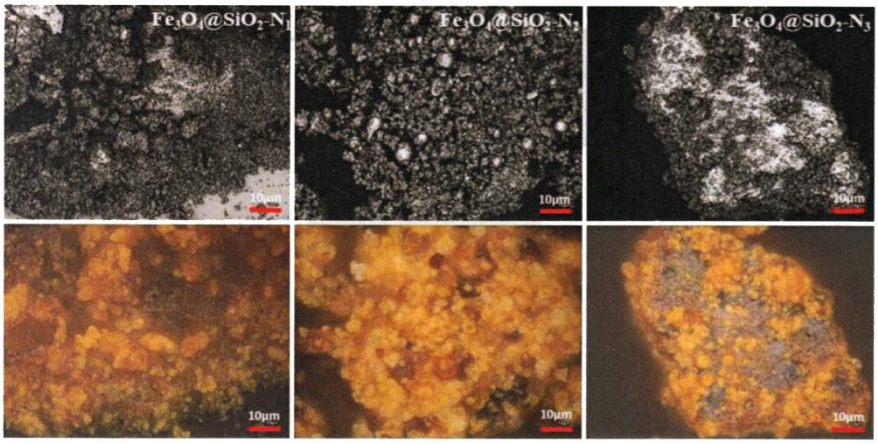

Ryc. 2. Fotografie z mikroskopu konfokalnego dla nanocząstek $Fe_3O_4@SiO_2$-N_1, $Fe_3O_4@SiO_2$-N_2 oraz $Fe_3O_4@SiO_2$-N_3

W celu charakterystyki morfologicznej otrzymanych materiałów wykonano fotografie za pomocą mikroskopu konfokalnego (ryc. 2), natomiast zdjęcia SEM oraz TEM zamieszczono w pracy [15]. Otrzymane wyniki pozwalają na stwierdzenie, że badane nanostruktury są materiałem wysoce jednorodnym w swoim kształcie oraz rozmiarze. Wszystkie nanostruktury obserwowano w zaglomeryzowanym stanie, ze względu na ich naturalną skłonność wynikającą z magnetycznego charakteru. Na podstawie otrzymanych zdjęć określono sferyczny kształt nanocząstek oraz rozmiar zawierający się w zakresie od 30 do 50 nm. Dodatkowo na podstawie fotografii TEM można rozróżnić obecność magnetycznego rdzenia oraz krzemionkowej otoczki w strukturze nanocząstek. Na tej podstawie otrzymane materiały można zakwalifikować do grupy nanocząstek typu rdzeń-otoczka (z ang. *core-shell*).

Obecność charakterystycznych pasm na widmach FT-IR pozwoliła na potwierdzenie obecności grup funkcyjnych na powierzchni otrzymanych

struktur, co dowodzi ich poprawnej funkcjonalizacji w procesie syntezy [15].

Dokładny opis wykorzystywanych narzędzi, metod i wyników dotyczących syntezy oraz charakterystyki nanomateriałów magnetycznych Fe_3O_4@SiO_2-N_1, Fe_3O_4@SiO_2-N_2, Fe_3O_4@SiO_2-N_3 umieszczono w innej pracy autorów pt. „Simultaneous voltammetric determination of Cd^{2+}, Pb^{2+}, and Cu^{2+} ions captured by Fe_3O_4@SiO_2 core-shell nanostructures of various outer amino chain length" [15].

3.2. Badanie zdolności wiązania jonów metali przez sfunkcjonalizowane nanocząstki magnetyczne

Jednoczesne woltamperometryczne oznaczanie jonów Cd^{2+}, Pb^{2+} oraz Cu^{2+} związane przez nanostruktury typu rdzeń-otoczka Fe_3O_4@SiO_2-N_n o różnej liczbie grup aminowych w łańcuchu zewnętrznym zostało opisane wcześniej [15]. W prezentowanej pracy przedstawiono wyniki oznaczenia wyżej wymienionych jonów w indywidualnych roztworach z wykorzystaniem tej samej serii nanocząstek.

W celu weryfikacji wpływu grup funkcyjnych obecnych na powierzchni nanocząstek Fe_3O_4 na wiązanie jonów przeprowadzono miareczkowanie mieszaniny jonów za pomocą niezmodyfikowanych nanocząstek magnetytu (ryc. 3). Na przedstawionych woltamogramach intensywności pików pozostają o stałej intensywności mimo dodawania kolejnych porcji nanocząstek, co wskazuje na brak powinowactwa Fe_3O_4 do badanych jonów.

Na ryc. 4 przedstawiono woltamogramy otrzymane dla miareczkowania roztworów zawierających odpowiednio jony Cd^{2+}, Pb^{2+} i Cu^{2+} za pomocą nanocząstek z jedną grupą aminową w łańcuchu zewnętrznym Fe_3O_4@SiO_2-N_1. Warto zauważyć, że po dodaniu kolejnych porcji nanocząstek obserwowano spadek intensywności pików jonów metali aż do ustalenia stanu równowagi. Najsilniejsze oddziaływanie zaobserwowano w przypadku wiązania jonów Pb^{2+}. Około 4 mg nanocząstek Fe_3O_4@SiO_2-N_1 wystarczyło na niemal 100% związanie jonów Pb^{2+} w badanej próbce (ryc. 4B). Nieco słabsze wiązanie obserwowano w parze Fe_3O_4@SiO_2-N_1 – Cu^{2+}. W tym

przypadku około 6 mg nanocząstek jest w stanie związać do 95% jonów Cu^{2+} z roztworu (ryc. 4C). Najniższe powinowactwo nanocząstek Fe_3O_4@SiO_2-N_1 zanotowano wobec jonów Cd^{2+}. Powyższy wniosek sformułowano na podstawie wyniku eksperymentu, dodając do próbki aż 25 mg nanocząstek, po czym nadal nie uzyskano wygaszenia badanego piku jonu metalu (ryc. 4A).

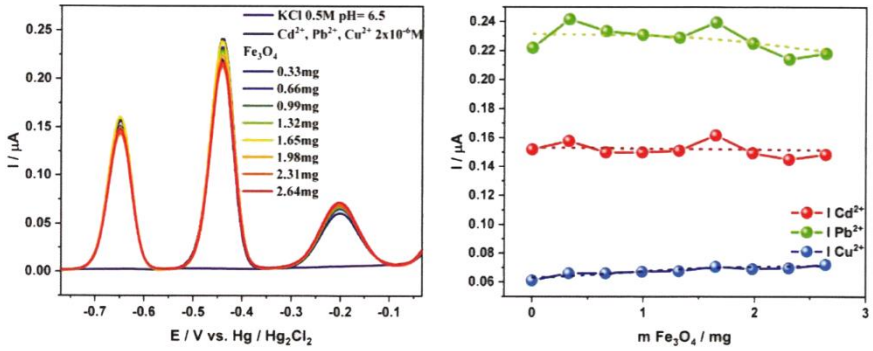

Ryc. 3. Woltamogram oraz wykres zależności intensywności piku jonu Cd^{2+}, Pb^{2+} oraz Cu^{2+} od masy dodanych nanocząstek Fe_3O_4

Następnie przeprowadzono eksperymenty w celu oceny zdolności wiązania nanocząstek zawierających dwie grupy aminowe w łańcuchu zewnętrznym Fe_3O_4@SiO_2-N_2 (ryc. 5). Uzyskane wyniki pomiarowe pozwalają na stwierdzenie, że w przypadku badania jonów Pb^{2+} obserwowano całkowity zanik piku, co wskazuje na silne ich wiązanie. Około 9 mg nanocząstek wiąże niemal całą zawartość jonów w roztworze (ryc. 5B). W przypadku badań z zastosowaniem jonów Cd^{2+} zmiany intensywności piku były nieznaczne, co wskazuje na bardzo niskie powinowactwo nanocząstek Fe_3O_4@SiO_2-N_2 do tego jonu. W tym przypadku 13 mg nanocząstek jest w stanie związać zaledwie 10% zawartości jonów Cd^{2+} (ryc. 5A). W przypadku miareczkowania jonów Cu^{2+} efekt spadku intensywności sygnału obserwuje się tylko w pierwszych krokach z jednoczesnym przesunięciem maksimum piku w kierunku ujemnych potencjałów. Zjawisko to wynika prawdopodobnie z adsorpcji nanocząstek i ich kompleksów z jonami miedzi do kropli rtęci [16]. Nieregularne zmiany intensywności piku Cu^{2+} wskazują na brak ustalającej się równowagi po dodaniu łącznie 15 mg nanocząstek

Fe_3O_4@SiO_2-N_2. Niemniej na podstawie obliczeń procentu związania jonów z roztworu można przyjąć, że utrzymuje się on na poziomie około 17% (ryc. 5C).

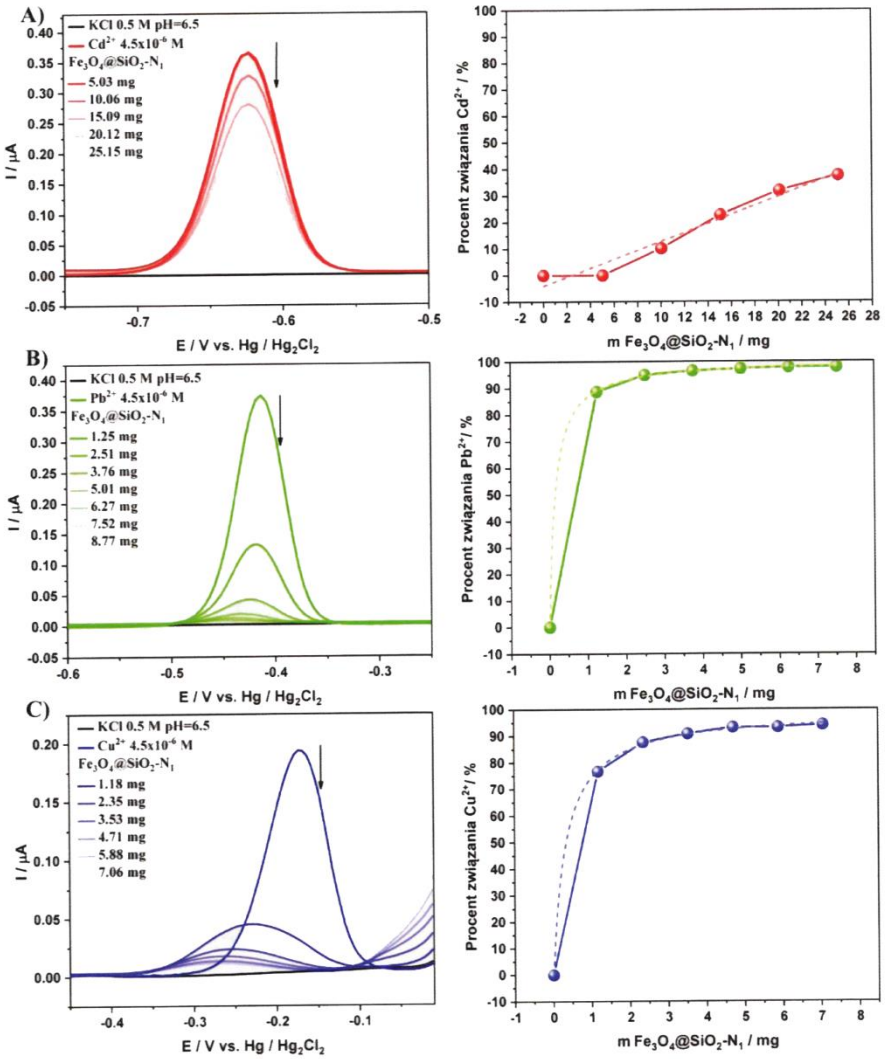

Ryc. 4. Zestawienie otrzymanych woltamogramów oraz wykresów zależności procentu związania jonów A) Cd^{2+}, B) Pb^{2+}, C) Cu^{2+} od masy dodanych nanocząstek Fe_3O_4@SiO_2-N_1

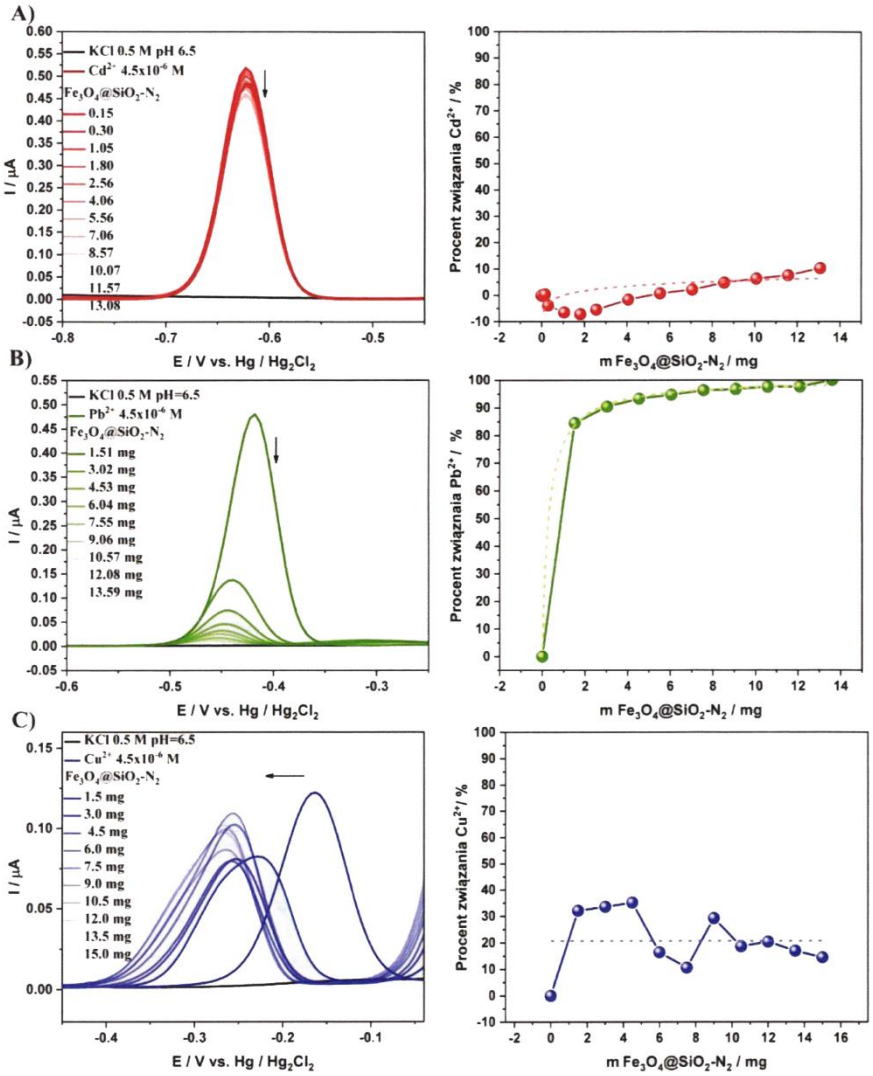

Ryc. 5. Zestawienie woltamogramów oraz wykresów zależności procentu związania jonów A) Cd^{2+}, B) Pb^{2+}, C) Cu^{2+} od masy dodanych nanocząstek $Fe_3O_4@SiO_2$-N_2

Na podstawie woltamogramów pokazanych na ryc. 6, które przedstawiają miareczkowanie jonów Cd^{2+}, Pb^{2+} i Cu^{2+} za pomocą nanocząstek z trzema grupami aminowymi w łańcuchu zewnętrznym $Fe_3O_4@SiO_2$-N_3, można stwierdzić, że spadek intensywności pików, po dodaniu nanocząstek, obserwowany jest w przypadku jonów Cd^{2+} i Cu^{2+}. Jednak najsilniejsze oddziaływania rejestrowane są w przypadku wiązania Cu^{2+} przez $Fe_3O_4@SiO_2$-N_3, gdzie widoczne jest całkowite wygaszenie piku już po dodaniu około 0,5 mg nanocząstek (ryc. 6C), a procent związania jonów Cu^{2+} utrzymuje się na poziomie około 95%. Nieznaczny spadek intensywności piku obserwuje się po dodaniu około 0,8 mg nanocząstek do roztworu jonów Cd^{2+} (ryc. 6A), co odpowiada 17% związania jonów. Natomiast żadne oddziaływania nie występują pomiędzy wiązaniem jonów Pb^{2+} z zastosowaniem $Fe_3O_4@SiO_2$-N_3. Nieznaczne zmiany intensywności piku Pb^{2+} występują w granicach błędu pomiarowego (ryc. 6B).

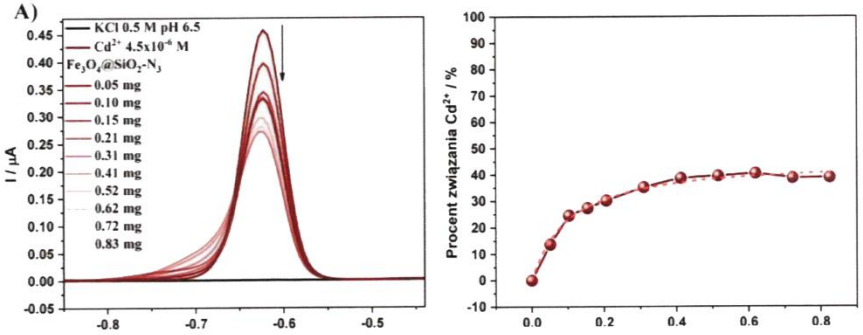

Ryc. 6. Zestawienie woltamogramów oraz wykresów zależności procentu związania jonów A) Cd^{2+}, B) Pb^{2+}, C) Cu^{2+} od masy dodanych nanocząstek $Fe_3O_4@SiO_2$-N_3

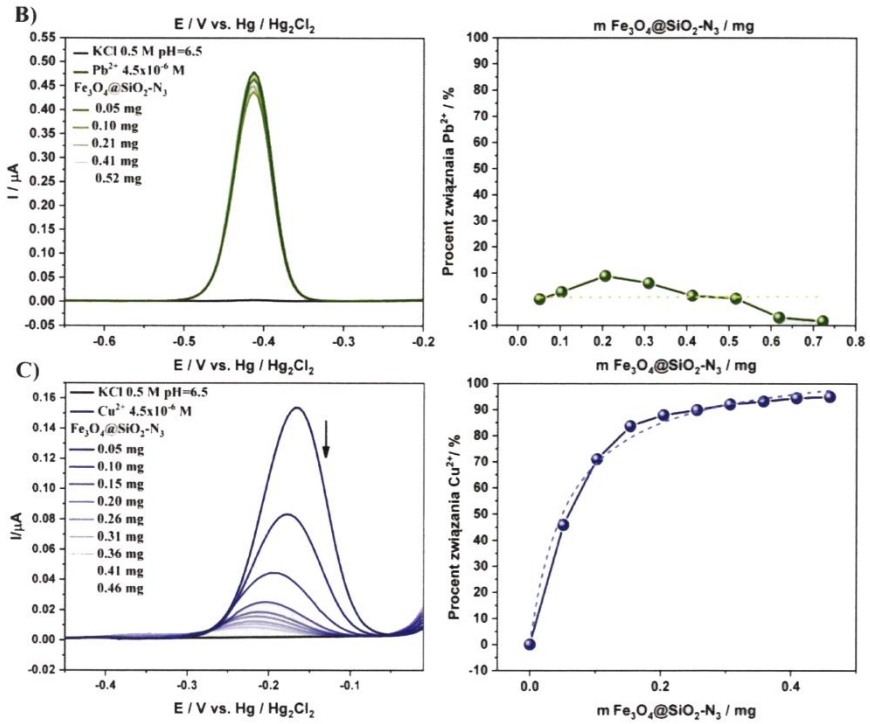

Ryc. 6 cd. Zestawienie woltamogramów oraz wykresów zależności procentu związania jonów B) Pb^{2+}, C) Cu^{2+} od masy dodanych nanocząstek $Fe_3O_4@SiO_2-N_3$

4. Podsumowanie

W niniejszej pracy zbadano szereg funkcjonalizowanych nanocząstek magnetytu typu rdzeń-otoczka $Fe_3O_4@SiO_2-N_n$ użytych jako nowy nanoadsorbent wybranych jonów metali ciężkich Cd^{2+}, Pb^{2+}, Cu^{2+} w wodnym roztworze 0,5 M KCl. Grupę analizowanych nanocząstek stanowiły cząstki o magnetycznym rdzeniu F_3O_4 pokryte krzemionką i w następnej kolejności modyfikowane grupami funkcyjnymi o różnej liczbie grup amionowych w łańcuchu zewnętrznym. W celu porównania zdolności wiązania serii

nanocząstek w 4,5 μM roztworach jonów Cd^{2+}, Pb^{2+}, Cu^{2+} przeliczono procent wiązania dla określonej masy użytych nanocząstek (ryc. 7).

Między niesfunkcjonalizowanymi nanocząstkami magnetytu Fe_3O_4 a wskazanymi jonami nie obserwowano żadnych oddziaływań. Wskazuje to na konieczność obecności grup funkcyjnych na powierzchni wybranych magnetycznych nanoadsorbentów.

Najsłabsze oddziaływania występują pomiędzy każdym rodzajem nanocząstek $Fe_3O_4@SiO_2\text{-}N_n$ a jonami Cd^{2+}. Po dodaniu znacznych ilości nanocząstek, dochodzących aż do 25 mg, stopień związania jonów osiąga zaledwie niecałe 40%. Jony kadmu najsilniej były wiązane przez nanocząstki typu $Fe_3O_4@SiO_2\text{-}N_3$, ponieważ 0,8 mg nanocząstek wystarczyło na związanie 39% zawartości jonów. Jony Pb^{2+} natomiast są silnie wiązane przez nanocząstki $Fe_3O_4@SiO_2\text{-}N_1$ oraz $Fe_3O_4@SiO_2\text{-}N_2$, gdzie stopień związania jonów dochodzi do 98%. Jednak potrzeba dużych ilości, od 8 do 13 mg nanocząstek, do osiągnięcia tak wysokiego poziomu wiązania.

W przypadku jonów Cu^{2+} najsilniejsze powinowactwo zaobserwowano wobec nanocząstek $Fe_3O_4@SiO_2\text{-}N_1$ i $Fe_3O_4@SiO_2\text{-}N_3$. Należy jednak zauważyć, że do związania około 95% jonów miedzi potrzeba 14-krotnie mniejszej masy nanocząstek $Fe_3O_4@SiO_2\text{-}N_3$ niż $Fe_3O_4@SiO_2\text{-}N_1$.

Nanocząstki typu $Fe_3O_4@SiO_2\text{-}N_1$ o masie 7–mg wykazują zbliżony stopień związania jonów Pb^{2+} i Cu^{2+} odpowiednio na poziomie 98 i 94%. Podczas gdy struktury $Fe_3O_4@SiO_2\text{-}N_2$ silnie wiążą jeden rodzaj jonów, około 14 mg nanocząstek wiąże 98% procent jonów Pb^{2+}, nanoadsorbenty $Fe_3O_4@SiO_2\text{-}N_3$ najsilniej oddziałują z jonami miedzi, ponieważ zaledwie 0,8 mg nanocząstek wystarcza do niemalże całkowitego związania jonów. Na podstawie procentu związania danych jonów można domniemywać selektywność nanocząstek $Fe_3O_4@SiO_2\text{-}N_2$ wobec jonów Pb^{2+} oraz $Fe_3O_4@SiO_2\text{-}N_3$ wobec jonów Cu^{2+}.

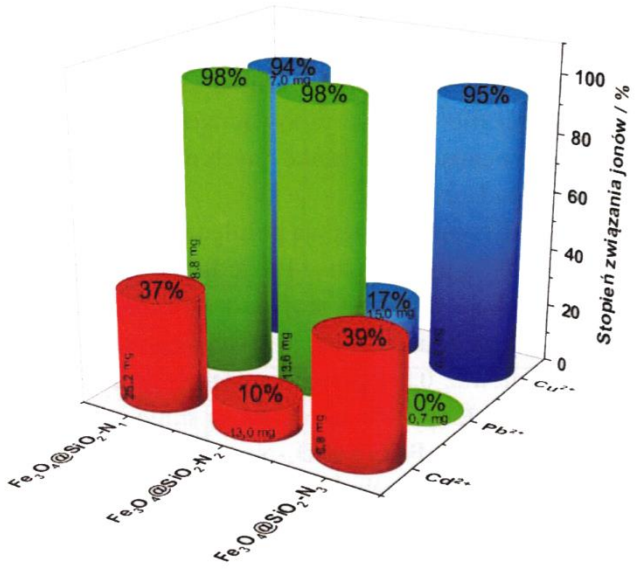

Ryc. 7. Diagram obrazujący zdolność wiązania jonów Cd^{2+}, Pb^{2+} oraz Cu^{2+} przez określoną ilość nanocząstek $Fe_3O_4@SiO_2$-N_n

Na podstawie przeprowadzonych badań można stwierdzić, że badane nanocząstki typu $Fe_3O_4@SiO_2$-N_n są obiecującymi nanoadsorbentami jonów metali ciężkich ze względu na ich wysoką pojemność jonową oraz łatwość separacji za pomocą zewnętrznego pola magnetycznego. Ponadto wykazana selektywność nanocząstek może stanowić podstawę tworzenia sensorów na wybrane jony.

5. Podziękowania

Podziękowania dla Uniwersytetu Gdańskiego za sfinansowanie projektu służącego rozwojowi Młodych Naukowców oraz Doktorantów. Decyzja nr BMN 539-T050-B890-21.

Literatura

[1] D. Chen, T. Awut, B. Liu, Y. Ma, T. Wang, I. Nurulla, Functionalized magnetic Fe_3O_4 nanoparticles for removal of heavy metal ions from aqueous solutions, E-Polym. 16 (2016) 313–322.

[2] H. Ali, E. Khan, I. Ilahi, Environmental Chemistry and Ecotoxicology of Hazardous Heavy Metals: Environmental Persistence, Toxicity, and Bioaccumulation, J. Chem. 2019 (2019) e6730305.

[3] B.E. Igiri, S.I.R. Okoduwa, G.O. Idoko, E.P. Akabuogu, A.O. Adeyi, I.K. Ejiogu, Toxicity and Bioremediation of Heavy Metals Contaminated Ecosystem from Tannery Wastewater: A Review, J. Toxicol. 2018 (2018) e2568038.

[4] H. Bai, D. Liu, W. Zheng, L. Ma, S. Yang, J. Cao, X. Lu, H. Wang, N. Mehta, Microbially-induced calcium carbonate precipitation by a halophilic ureolytic bacterium and its potential for remediation of heavy metal-contaminated saline environments, Int. Biodeterior. Biodegrad. 165 (2021) 105311.

[5] Z. Liao, Z. Zhao, J. Zhu, H. Chen, D. Meng, Complexing characteristics between Cu(II) ions and dissolved organic matter in combined sewer overflows: Implications for the removal of heavy metals by enhanced coagulation, Chemosphere 265 (2021) 129023.

[6] M. Taseidifar, F. Makavipour, R.M. Pashley, A.F.M.M. Rahman, Removal of heavy metal ions from water using ion flotation, Environ. Technol. Innov. 8 (2017) 182–190.

[7] D.-Q. Cao, X. Song, X.-M. Fang, W.-Y. Yang, X.-D. Hao, E. Iritani, N. Katagiri, Membrane filtration-based recovery of extracellular polymer substances from excess sludge and analysis of their heavy metal ion adsorption properties, Chem. Eng. J. 354 (2018) 866–874.

[8] J.M. Reyna-González, G. Santos-Jurado, G. López-Reyes, M. Aguilar-Martínez, Effect of SCN^- and NO_3^- ions on the extraction of heavy metals from aqueous solutions with the ionic liquid trihexylammonium octanoate, Sep. Purif. Technol. 247 (2020) 116920.

[9] R.-E. Dong, P. Kang, X.-L. Xu, L.-X. Cai, Z. Guo, Cation-exchange strategy for a colorimetric paper sensor: Belt-like ZnSe nanoframes toward visual determination of heavy metal ions, Sens. Actuators B Chem. 312 (2020) 128013.

[10] I. Chakraborty, S.M. Sathe, C.N. Khuman, M.M. Ghangrekar, Bioelectrochemically powered remediation of xenobiotic compounds and heavy metal toxicity using microbial fuel cell and microbial electrolysis cell, Mater. Sci. Energy Technol. 3 (2020) 104–115.

[11] K.W. Soo, K.C. Wong, P.S. Goh, A.F. Ismail, N. Othman, Efficient heavy metal removal by thin film nanocomposite forward osmosis membrane modified with geometrically different bimetallic oxide, J. Water Process Eng. 38 (2020) 101591.

[12] V. Dhiman, N. Kondal, ZnO Nanoadsorbents: A potent material for removal of heavy metal ions from wastewater, Colloid Interface Sci. Commun. 41 (2021) 100380.

[13] S. Xue, Y. Xiao, G. Wang, J. Fan, K. Wan, Q. He, M. Gao, Z. Miao, Adsorption of heavy metals in water by modifying Fe_3O_4 nanoparticles with oxidized humic acid, Colloids Surf. Physicochem. Eng. Asp. 616 (2021) 126333.

[14] A. Kulpa, J. Ryl, G. Skowierzak, A. Koterwa, G. Schroeder, T. Ossowski, P. Niedziałkowski, Comparison of Cadmium Cd^{2+} and Lead Pb^{2+} Binding by $Fe_3O_4@SiO_2$-EDTA Nanoparticles – Binding Stability and Kinetic Studies, Electroanalysis 32 (2020) 588–597.

[15] A. Kulpa, J. Ryl, G. Schroeder, A. Koterwa, J. Sein Anand, T. Ossowski, P. Niedziałkowski, Simultaneous voltammetric determination of Cd^{2+}, Pb^{2+}, and Cu^{2+} ions captured by $Fe_3O_4@SiO_2$ core-shell nanostructures of various outer amino chain length, J. Mol. Liq. 314 (2020) 113677.

[16] W.H.M. Abdelraheem, Z.R. Komy, N.M. Ismail, Electrochemical determination of Cu^{2+} complexation in the extract of E crassipes by anodic stripping voltammetry, Arab. J. Chem. 10 (2017) S1105–S1110.

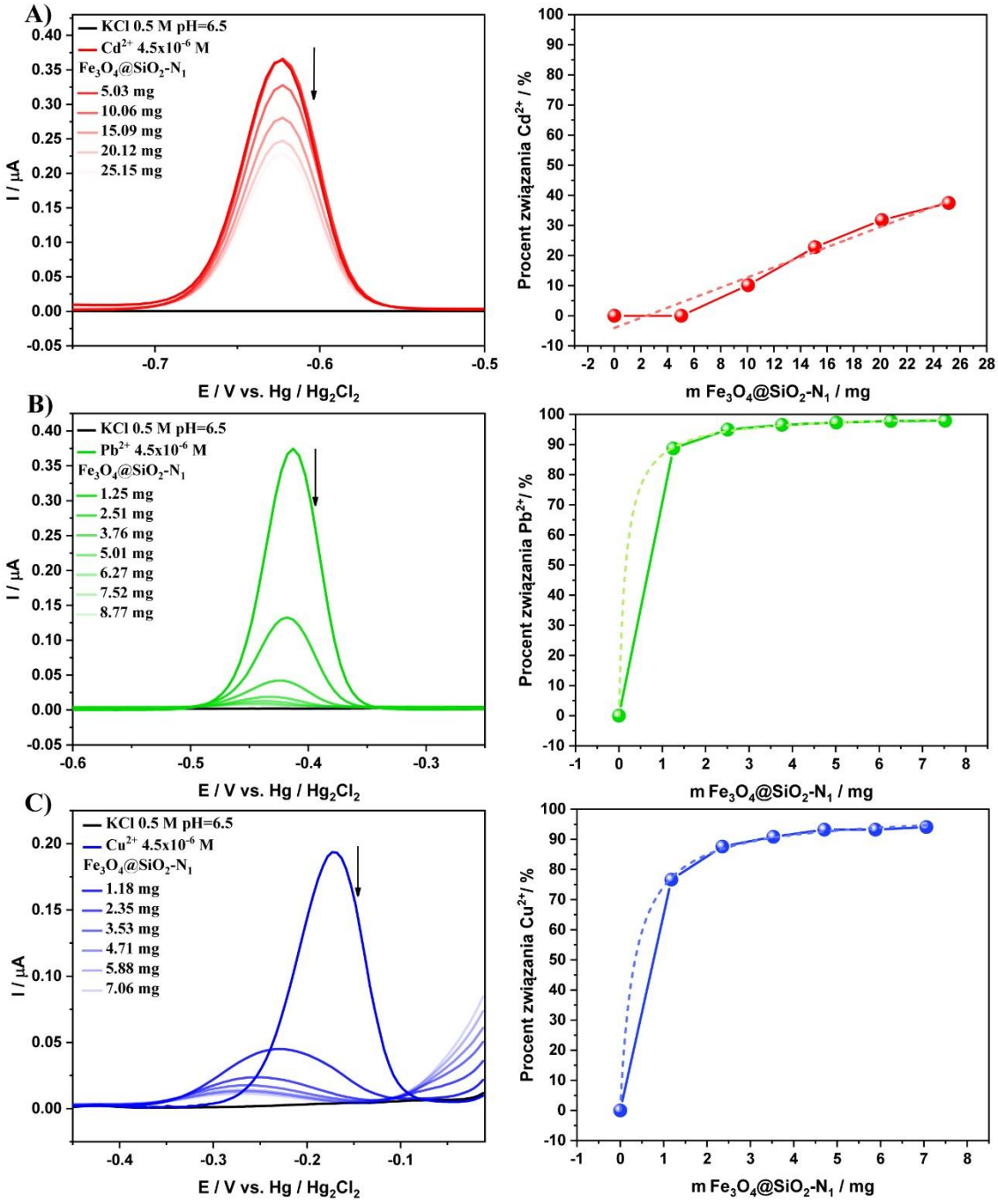

Rys. 1. Zestawienie otrzymanych woltamogramów oraz wykresów zależności procentu związania jonów A) Cd^{2+}, B) Pb^{2+}, C) Cu^{2+} od masy dodanych nanocząstek $Fe_3O_4@SiO_2$-N_1.

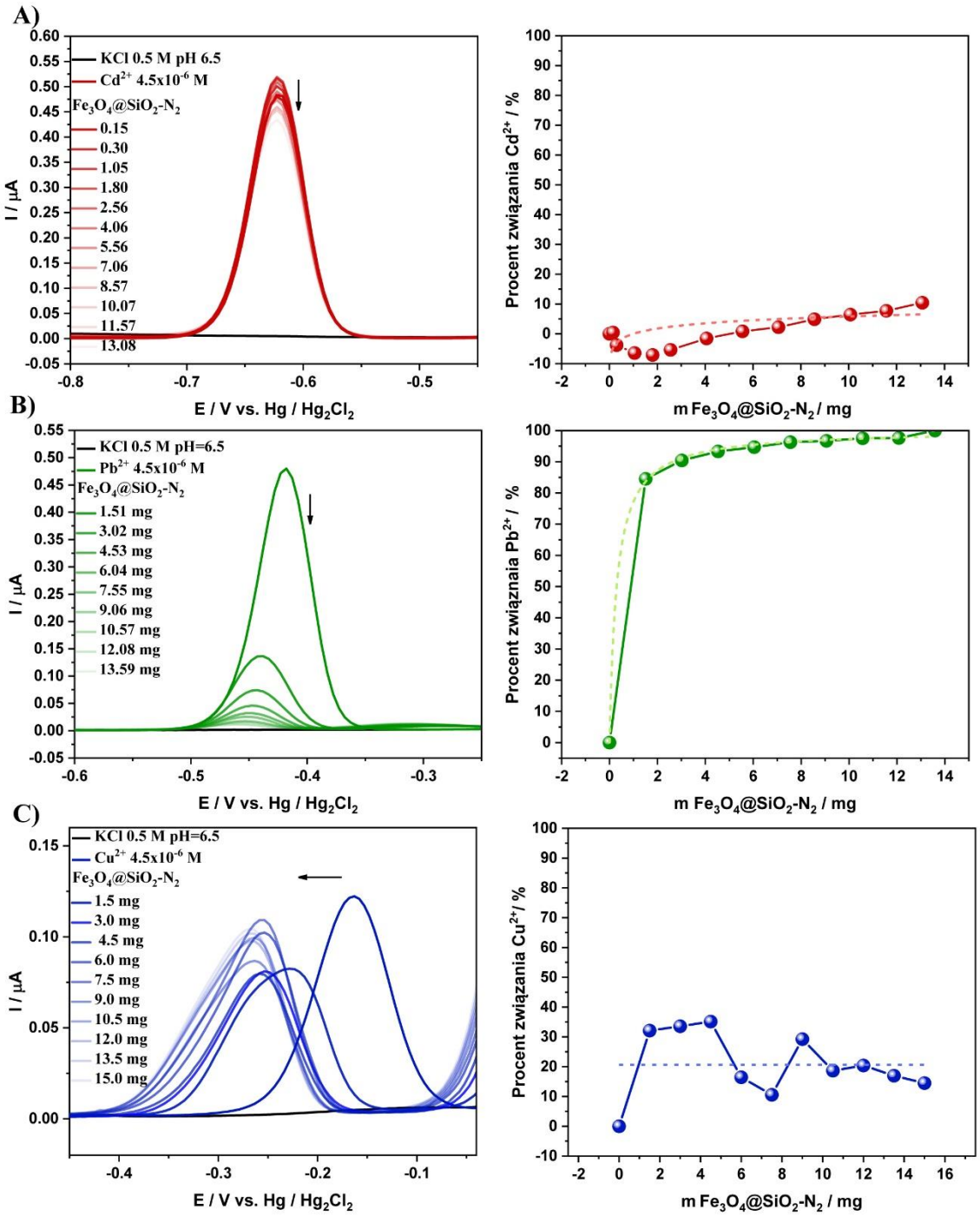

Rys. 2. Zestawienie woltamogramów oraz wykres*ów* zależności procentu związania jonów A) Cd^{2+}, B) Pb^{2+}, C) Cu^{2+} od masy dodanych nanocząstek $Fe_3O_4@SiO_2$-N_2.

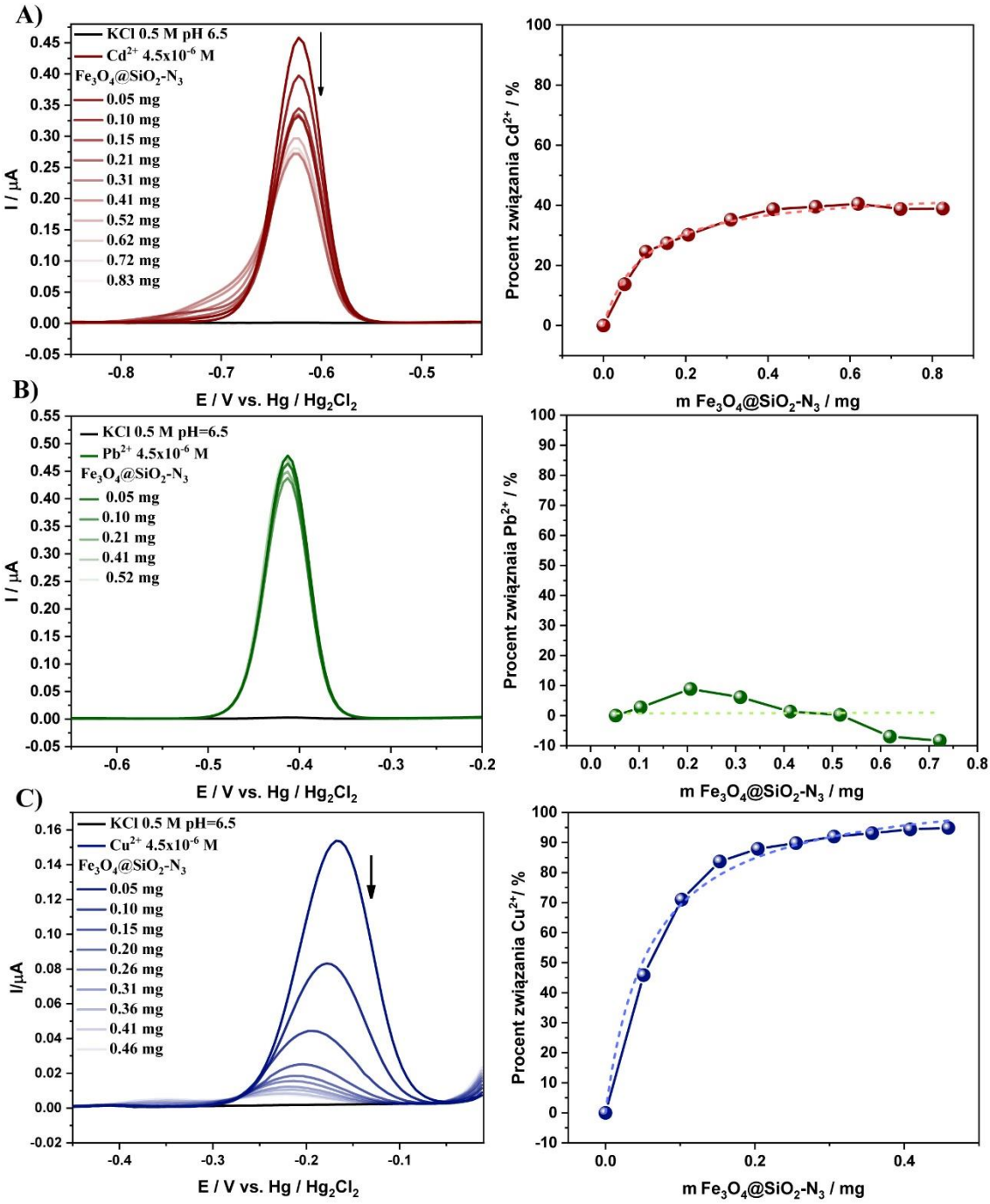

Rys. 3. Zestawienie woltamogramów oraz wykresów zależności procentu związania jonów A) Cd^{2+}, B) Pb^{2+}, C) Cu^{2+} od masy dodanych nanocząstek $Fe_3O_4@SiO_2$-N_3.

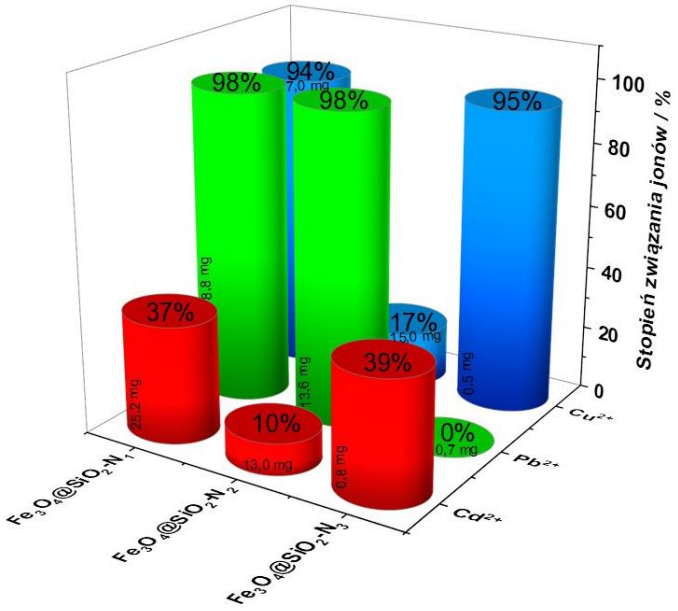

Rys. 4. Diagram obrazujący zdolność wiązania jonów Cd^{2+}, Pb^{2+} oraz Cu^{2+} przez określoną ilość nanocząstek $Fe_3O_4@SiO_2$-N_n.

DOROBEK NAUKOWY I DZIAŁALNOŚĆ POZANAUKOWA

1. Publikacje z listy filadelfijskiej

1. **Kulpa-Koterwa A**., Ryl J., Górnicka K., Niedziałkowski P.: New nanoadsorbent based on magnetic iron oxide containing 1,4,7,10-tetraazacyclododecane in outer chain (Fe_3O_4@SiO_2- cyclen) for adsorption and removal of selected heavy metal ions Cd^{2+}, Pb^{2+}, Cu^{2+}, Journal of Molecular Liquids, vol. 368, nr pt. B, 2022, s. 1–11, DOI:10.1016/j.molliq.2022.120710, 100 punktów, IF (6,633)

2. **Kulpa-Koterwa A.**, Ossowski T., Niedziałkowski P.: Functionalized Fe_3O_4 nanoparticles as glassy carbon electrode modifiers for heavy metal ions detection – a mini review, Materials, vol. 14, nr 24, 2021, s. 1–15, DOI:10.3390/ma14247725, 140 punktów, IF (3,748)

3. **Kulpa A.**, Ryl J., Skowierzak G., Koterwa A., Schroeder G., Ossowski T., Niedziałkowski P.: Comparison of cadmium Cd^{2+} and lead Pb^{2+} binding by Fe_3O_4@SiO_2- EDTA nanoparticles – binding stability and kinetic studies, Electroanalysis, vol. 32, nr 3, 2020, s. 588–597, DOI:10.1002/elan.201900616, 70 punktów, IF (3,223)

4. **Kulpa A.**, Ryl J., Schroeder G., Koterwa A., Sein Anand J., Ossowski T., Niedziałkowski P.: Simultaneous voltammetric determination of Cd^{2+}, Pb^{2+}, and Cu^{2+} ions captured by Fe_3O_4@SiO_2 core-shell nanostructures of various outer amino chain length, Journal of Molecular Liquids, vol. 314, 2020, s. 1–11, DOI:10.1016/j.molliq.2020.113677, 100 punktów, IF (6,633)

5. Szczepańska E., Grobelna B., Ryl J., **Kulpa A**., Ossowski T., Niedziałkowski P.: Efficient method for the concentration determination of Fmoc groups incorporated in the core-shell materials by Fmoc–glycine, Molecules, vol. 25, nr 17, 2020, s. 1–17, DOI:10.3390/molecules25173983, 140 punktów, IF (4,927)

6. Zarzeczańska D., Adamczyk-Woźniak A., **Kulpa A.**, Ossowski T., Sporzyński A.: Fluorinated boronic acids: acidity and hydrolytic stability of fluorinated phenylboronic acids, European Journal of Inorganic Chemistry, vol. 2017, nr 38–39, 2017, s. 4493–4498, DOI:10.1002/ejic.201700546, 35 punktów, IF (2,524)

2. Rozdziały w monografii

1. **Kulpa-Koterwa A.**, Schroeder G., Ossowski T., Koterwa A., Niedziałkowski P.: Nanostruktury magnetyczne typu core-shell Fe_3O_4@SiO_2-N_n jako nowe adsorbenty jonów metali ciężkich Cd^{2+}, Pb^{2+} oraz Cu^{2+} – badania elektrochemiczne, Na pograniczu chemii, biologii i fizyki, vol. 3, 2022, Wydawnictwo Naukowe Uniwersytetu Mikołaja Kopernika, ISBN 978-83-231-4836-4, s. 121–136, 20 punktów

2. **Kulpa A.,** Zarzeczańska D., Niedziałkowski P., Koterwa A., Ossowski T.: Kwasowość oraz trwałość w roztworze dipodstawionych pochodnych kwasu fenyloboronowego, Na pograniczu chemii i biologii, vol. 39, 2019, Wydawnictwo Naukowe Uniwersytetu im. Adama Mickiewicza, ISBN 978-83-232-3593-4, s. 171–182, 20 punktów

3. Inne prace opublikowane

1. **Kulpa A**.: Dezynfekcja w dobie pandemii COVID-19, Chemia w Szkole, vol. 65, nr 6, 2020, s. 19–21, 5 punktów

2. **Kulpa A.,** Szczepańska E., Koterwa A.: Nanocząstki magnetyczne w oczyszczaniu środowisk wodnych z jonów metali ciężkich, Laborant, nr 14, 2020

3. Szczepańska E., **Kulpa A.**, Grobelna B.: Właściwości optyczne nanocząstek, Laborant, nr 14, 2020

4. Wystąpienia konferencyjne

4.1. Referaty

Współautorka 18 komunikatów ustnych na konferencjach krajowych, w tym prezentowałam:

1. **Kulpa-Koterwa A.**, Koterwa A., Niedziałkowski P.: Nowe nanoadsorbenty jonów metali ciężkich na bazie magnetycznego tlenku żelaza i cyklenu Fe_3O_4@SiO_2-A4C12, IV Konferencja Naukowa "Chemia-Biznes-Środowisko", 2022

2. **Kulpa-Koterwa A.**, Adamska E., Koterwa A., Ossowski T., Niedziałkowski P.: Optymalizacja warunków modyfikacji elektrody GC sfunkcjonalizowanymi nanocząstkami Fe_3O_4 w celu efektywnej detekcji wybranych analitów, II Pomorskie Studenckie Sympozjum Chemiczne, 2021

3. **Kulpa-Koterwa A.**, Koterwa A., Ossowski T., Niedziałkowski P.: Wykorzystanie nanostruktur opartych na nanocząstkach Fe_3O_4 w celu stworzenia sensora elektrochemicznego – optymalizacja warunków modyfikacji elektrody, XIV Kopernikańskie Seminarium Doktoranckie, 2021

4. **Kulpa-Koterwa A.**, Koterwa A., Ossowski T., Niedziałkowski P.: Elektroda GC modyfikowana nanocząstkami magnetycznymi typu rdzeń-otoczka opartymi na Fe_3O_4 – charakterystyka, VI Interdyscyplinarna Akademicka Konferencja Ochrony Środowiska, 2021

5. **Kulpa A**., Koterwa A., Szczepańska E., Ossowski T., Niedziałkowski P.: Nanoadsorbenty typu core-shell oparte na magnetycznym rdzeniu tlenku żelaza, I Pomorskie Studenckie Sympozjum Chemiczne, 2020

6. **Kulpa A.**, Koterwa A., Szczepańska E., Ossowski T., Niedziałkowski P.: Elektrochemiczne badania zdolności wiążących nanomateriałów magnetycznych, I Ogólnopolskie Sympozjum Studentów Chemii "UWiedzeni Chemią", 2020

7. **Kulpa A.**, Zarzeczańska D., Ramotowska S., Ossowski T.: Kwasowość oraz trwałość w roztworze dipodstawionych pochodnych kwasu fenyloboronowego, XVII Ogólnopolskie Seminarium Doktorantów "Na Pograniczu Chemii i Biologii", 2019

8. **Kulpa A.**, Zarzeczańska D., Ossowski T.: Właściwości kwasowo-zasadowe fluoropochodnych kwasu fenyloboronowego – badania spektroskopowe i potencjometryczne,VI Ogólnopolskie Seminarium "Postępy w chemii boru", 2019

9. **Kulpa A.**, Koterwa A., Zarzeczańska D., Ossowski T., Niedziałkowski P.: Nanocząstki magnetyczne Fe_3O_4@SiO_2-EDTA jako adsorbenty jonów Cd^{2+} – badania elektrochemiczne, II Konferencja Naukowa " Chemia-Biznes-Środowisko", 2019

4.2. Postery

Współautorka 21 posterów na konferencjach krajowych i 2 posterów na konferencjach międzynarodowych, w tym prezentowałam:

1. **Kulpa-Koterwa A.**, Koterwa A., Ossowski T., Niedziałkowski P.: Wykorzystanie nanostruktur Fe_3O_4@SiO_2-N_X o różnej ilości grup aminowych w łańcuchu zewnętrznym do oznaczania jonów Cd^{2+}, Pb^{2+} i Cu^{2+}, VI Interdyscyplinarna Akademicka Konferencja Ochrony Środowiska, 2021

2. **Kulpa-Koterwa A.**, Koterwa A., Ossowski T., Niedziałkowski P.: Modyfikacja elektrody GC z wykorzystaniem magnetycznych nanostruktur Fe_3O_4, III Konferencja Naukowa "Chemia-Biznes-Środowisko", 2021

3. **Kulpa-Koterwa A.**, Niedziałkowski P., Koterwa A., Ossowski T.: Modyfikacja powierzchni elektrody GC magnetycznymi nanostrukturami typu core-shell – badania elektrochemiczne, e-Zjazd Zimowy Sekcji Studenckiej Polskiego Towarzystwa Chemicznego, 2020

4. **Kulpa A.**, Koterwa A., Ossowski T., Niedziałkowski P.: Nanomateriały magnetyczne Fe_3O_4 jako adsorbenty jonów metali ciężkich, XVI Wrocławskie Studenckie Sympozjum Chemiczne, 2020

5. **Kulpa A.**, Zarzeczańska D., Ossowski T., Niedziałkowski P.: Badanie właściwości wiążących magnetycznych nanocząstek tlenku żelaza modyfikowanych grupami aminowymi, XIII Kopernikańskie Seminarium Doktoranckie, 2019

6. **Kulpa A.**, Zarzeczańska D., Szczepańska E., Ramotowska S., Ossowski T., Niedziałkowski P.: Nanocząstki magnetyczne tlenku żelaza jako kompleksony jonów kadmu(II), VII Łódzkie Sympozjum Doktorantów Chemii, 2019

7. **Kulpa A.**, Niedziałkowski P., Szczepańska E., Ossowski T.: Nowe nanomateriały magnetyczne o potencjalnych zastosowaniach sensorycznych, XXII Zjazd Zimowy Sekcji Studenckiej Polskiego Towarzystwa Chemicznego, 2019

8. **Kulpa A.**, Cirocka A., Zarzeczańska D., Ossowski T., Niedziałkowski P.: Zastosowanie magnetycznych nanocząstek (Fe_3O_4) w celu jednoczesnego oznaczenia jonów Cd^{2+} i Pb^{2+} metodami elektrochemicznym, IV Interdyscyplinarna Akademicka Konferencja Ochrony Środowiska, 2019

9. **Kulpa A.**, Zarzeczańska D., Ramotowska S., Ossowski T.: Nanocząstki w kosmetyce, I Konferencja Naukowa "Chemia-Biznes-Środowisko", 2018

10. **Kulpa A.**, Zarzeczańska D., Koterwa A., Ossowski T.: Stabilność w roztworze tetrafluoropochodnych kwasu fenyloboronowego, II Konferencja Doktorantów Pomorza "BioMed Session", 2018

5. Uczestnictwo w projektach i grantach

1. Stypendystka grantu NCN SonataBis 10 pt. „Technologia addytywnego wytwarzania elektroaktywnych przestrzennych struktur z kompozytów polilaktydu wzmacnianego diamentem”, UMO-2020/38/E/ST8/00409, marzec 2022-czerwiec 2022

2. Kierowanie projektami badawczymi w ramach badań młodych naukowców oraz doktorantów na Wydziale Chemii Uniwersytetu Gdańskiego BMN:

- pt. „Nanocząstki magnetyczne typu rdzeń-otoczka Fe_3O_4@SiO_2-A12C4 jako adsorbenty jonów metali ciężkich Cd^{2+}, Pb^{2+}, Cu^{2+} – otrzymywanie, modyfikacja oraz badania elektrochemiczne”, nr 539-T050-B019-22, 2022
- pt. „Detekcja wybranych jonów metali ciężkich oraz antybiotyków na elektrodzie GC modyfikowanej magnetycznymi nanostrukturami typu rdzeń-otoczka Fe_3O_4@SiO_2- N_n”, nr 539-T050-B890-21, 2021
- pt. „Modyfikacja i charakterystyka materiałów elektrodowych za pomocą nanostruktur typu rdzeń-otoczka opartych na magnetycznym tlenku żelaza w celu detekcji wybranych analitów”, nr 539-T050-B460-20, 2020
- pt. „Otrzymywanie, modyfikacja i charakterystyka właściwości magnetycznych nanocząstek tlenku żelaza (Fe_3O_4)”, nr 538-8210-B281-18, 2019

3. Opiekunka warsztatów chemicznych w ramach projektu „Z CHEMIĄ NA PRZÓD – rozwój kompetencji podopiecznych placówek wsparcia dziennego poprzez udział w działaniach dydaktycznych realizowanych na Wydziale Chemii Uniwersytetu Gdańskiego” w roku akademickim 2018/19

6. Nagrody i osiągnięcia

1. III miejsce w konkursie na najlepszy komunikat ustny z badań własnych wygłoszony podczas konferencji naukowej "Chemia-Biznes-Środowisko" w dniach 24–25 czerwca 2022 r. w Gdańsku.
2. I miejsce w kategorii plakat naukowy podczas VI Interdyscyplinarnej Akademickiej Konferencji Ochrony Środowiska w dniach 22–24 września 2021 r. w Gdańsku.
3. Nagroda Gdańskiego Polskiego Towarzystwa Chemicznego za najlepszą pracę magisterską obronioną na Wydziale Chemii Uniwersytetu Gdańskiego w roku akademickim 2017/18.
4. Zajęcie 3 lokaty ze względu na osiągnięte w toku studiów wyniki w nauce absolwentów Kierunku Chemia, Wydziału Chemii Uniwersytetu Gdańskiego w roku akademickim 2017/18.

7. Działalność pozanaukowa

1. Przewodnicząca Rady Doktorantów Wydziału Chemii Uniwersytetu Gdańskiego w latach 2021–2024.
2. Współautorka artykułu w Gazecie Uniwersyteckiej (wydanie nr 3 (176) marzec 2022, ISSN 1689–4723) przedstawiającego działalność Katedry Chemii Analitycznej Wydziału Chemii Uniwersytetu Gdańskiego.
3. Członek Rady Wydziału w grupie doktorantów w latach 3.11.2021 r. – 31.08.2024 r.
4. Członek Uczelnianej Komisji Stypendialnej ds. Doktorantów na Wydziale Chemii w latach 2021–2024.
5. Udział w organizacji części laboratoryjnej II etapu Ogólnopolskiej Olimpiady Chemicznej w Okręgu Gdańskim w latach 2019–2022.
6. Udział w organizacji Dnia Otwartego Wydziału Chemii Uniwersytetu Gdańskiego w latach 2019–2021.
7. Prowadząca warsztaty chemiczne z chemii ogólnej i nieorganicznej pt. „Reakcje chemiczne w laboratorium” oraz „Pierwiastki chemiczne i ich rodzaje” dla uczniów liceów w roku 2019.

OŚWIADCZENIA

dr hab. Paweł Niedziałkowski, prof. UG
Uniwersytet Gdański
Wydział Chemii
Katedra Chemii Analitycznej
Pracowania Chemii Supramolekularnej
ul. Wita Stwosza 63
80-308 Gdańsk
pawel.niedzialkowski@ug.edu.pl

Gdańsk, 28.11.2023

OŚWIADCZENIE

Jako współautor publikacji wchodzącej w skład rozprawy doktorskiej mgr Amandy Magdaleny Kulpa-Koterwa oświadczam, że mój wkład w publikację:

Kulpa A., Ryl J., Skowierzak G., Koterwa A., Schroeder G., Ossowski T., Niedziałkowski P.: Comparison of cadmium Cd^{2+} and lead Pb^{2+} binding by Fe_3O_4@SiO_2– EDTA nanoparticles – binding stability and kinetic studies, *Electroanalysis*, vol. 32, nr 3, 2020, s. 588–597, DOI:10.1002/elan.201900616

polegał na konceptualizacji, pomocy w planowaniu badań oraz redakcji manuskryptu.

Paweł Niedziałkowski

dr hab. Paweł Niedziałkowski
profesor Uniwersytetu Gdańskiego
Uniwersytet Gdański
Wydział Chemii
Katedra Chemii Analitycznej

prof. dr hab. inż. Tadeusz Ossowski
Uniwersytet Gdański
Wydział Chemii
Katedra Chemii Analitycznej
Pracowania Chemii Supramolekularnej
ul. Wita Stwosza 63
80-308 Gdańsk
tadeusz.ossowski@ug.edu.pl

Gdańsk, 28.11.2023

OŚWIADCZENIE

Jako współautor publikacji wchodzącej w skład rozprawy doktorskiej mgr Amandy Magdaleny Kulpa-Koterwa oświadczam, że mój wkład w publikację:

Kulpa A., Ryl J., Skowierzak G., Koterwa A., Schroeder G., Ossowski T., Niedziałkowski P.: Comparison of cadmium Cd^{2+} and lead Pb^{2+} binding by Fe_3O_4@SiO_2– EDTA nanoparticles – binding stability and kinetic studies, *Electroanalysis*, vol. 32, nr 3, 2020, s. 588–597, DOI:10.1002/elan.201900616

polegał na konsultacji przy planowaniu badań elektrochemicznych.

KIEROWNIK
KATEDRY CHEMII ANALITYCZNEJ
prof. dr hab. inż. Tadeusz Ossowski

dr hab. inż. Jacek Ryl, prof. PG
Politechnika Gdańska
Instytut Nanotechnologii i Inżynierii Materiałowej
Zakład Elektrochemii i Fizykochemii Powierzchni
ul. Narutowicza 11/12,
80-233 Gdańsk
jacryl@pg.edu.pl

Gdańsk, 28.11.2023

OŚWIADCZENIE

Jako współautor publikacji wchodzącej w skład rozprawy doktorskiej mgr Amandy Magdaleny Kulpa-Koterwa oświadczam, że mój wkład w publikację:

Kulpa A., Ryl J., Skowierzak G., Koterwa A., Schroeder G., Ossowski T., Niedziałkowski P.: Comparison of cadmium Cd^{2+} and lead Pb^{2+} binding by $Fe_3O_4@SiO_2$– EDTA nanoparticles – binding stability and kinetic studies, *Electroanalysis*, vol. 32, nr 3, 2020, s. 588–597, DOI:10.1002/elan.201900616

polegał na wykonaniu badań techniką spektroskopii fotoelektronów w zakresie promieniowania X (XPS), interpretacji otrzymanych wyników oraz ich opisaniu w manuskrypcie.

prof. dr hab. Grzegorz Schroeder
Uniwersytet im Adama Mickiewicza w Poznaniu
Wydział Chemii
Zakład Chemii Supramolekularnej
ul. Uniwersytetu Poznańskiego 8
61-614 Poznań
schroede@amu.edu.pl

Gdańsk, 28.11.2023

OŚWIADCZENIE

Jako współautor publikacji wchodzącej w skład rozprawy doktorskiej mgr Amandy Magdaleny Kulpa-Koterwa oświadczam, że mój wkład w publikację:

1. **Kulpa A.**, Ryl J., Skowierzak G., Koterwa A., **Schroeder G.**, Ossowski T., Niedziałkowski P.: Comparison of cadmium Cd^{2+} and lead Pb^{2+} binding by $Fe_3O_4@SiO_2$– EDTA nanoparticles – binding stability and kinetic studies, *Electroanalysis*, vol. 32, nr 3, 2020, s. 588–597, DOI:10.1002/elan.201900616

polegał na syntezie badanych nanocząstek oraz napisaniu części manuskryptu w tym zakresie.

2. **Kulpa A.**, Ryl J., Schroeder G., Koterwa A., Sein Anand J., Ossowski T., Niedziałkowski P.: Simultaneous voltammetric determination of Cd^{2+}, Pb^{2+}, and Cu^{2+} ions captured by $Fe_3O_4@SiO_2$ core-shell nanostructures of various outer amino chain length, *Journal of Molecular Liquids*, vol. 314, 2020, s. 1–11, DOI:10.1016/j.molliq.2020.113677

polegał na syntezie badanych nanocząstek oraz napisaniu części manuskryptu w tym zakresie.

3. **Kulpa-Koterwa A.**, Schroeder G., Ossowski T., Koterwa A., Niedziałkowski P.: Nanostruktury magnetyczne typu core-shell $Fe_3O_4@SiO_2$-N_n jako nowe adsorbenty jonów metali ciężkich Cd^{2+}, Pb^{2+} oraz Cu^{2+} – badania elektrochemiczne, Na pograniczu chemii, biologii i fizyki /Szłyk Edward [i in.] (red.), vol. 3, 2022, *Wydawnictwo Naukowe Uniwersytetu Mikołaja Kopernika*, ISBN 978-83-231-4836-4, s. 121–136

polegał na syntezie badanych nanocząstek.

Grzegorz Schroeder

mgr Adrian Koterwa
Uniwersytet Gdański
Wydział Chemii
Katedra Chemii Analitycznej
Pracowania Chemii Supramolekularnej
ul. Wita Stwosza 63
80-308 Gdańsk
adrian.koterwa@ug.edu.pl

Gdańsk, 28.11.2023

OŚWIADCZENIE

Jako współautor publikacji wchodzącej w skład rozprawy doktorskiej mgr Amandy Magdaleny Kulpa-Koterwa oświadczam, że mój wkład w publikację:

Kulpa A., Ryl J., Skowierzak G., Koterwa A., Schroeder G., Ossowski T., Niedziałkowski P.: Comparison of cadmium Cd^{2+} and lead Pb^{2+} binding by Fe_3O_4@SiO_2– EDTA nanoparticles – binding stability and kinetic studies, *Electroanalysis*, vol. 32, nr 3, 2020, s. 588–597, DOI:10.1002/elan.201900616

polegał na współudziale w opracowaniu części danych pomiarowych.

Koterwa Adrian

mgr Grzegorz Skowierzak
Uniwersytet Gdański
Wydział Chemii
Katedra Chemii Analitycznej
Pracowania Chemii Supramolekularnej
ul. Wita Stwosza 63,
80-308 Gdańsk
grzegorz.skowierzak@phdstud.ug.edu.pl

Gdańsk, 28.11.2023

OŚWIADCZENIE

Jako współautor publikacji wchodzącej w skład rozprawy doktorskiej mgr Amandy Magdaleny Kulpa-Koterwa oświadczam, że mój wkład w publikację:

Kulpa A., Ryl J., Skowierzak G., Koterwa A., Schroeder G., Ossowski T., Niedziałkowski P.: Comparison of cadmium Cd^{2+} and lead Pb^{2+} binding by Fe_3O_4@SiO_2– EDTA nanoparticles – binding stability and kinetic studies, *Electroanalysis*, vol. 32, nr 3, 2020, s. 588–597, DOI:10.1002/elan.201900616

polegał na współudziale w opracowaniu części danych pomiarowych.

Grzegorz Skowierzak

dr hab. Paweł Niedziałkowski, prof. UG
Uniwersytet Gdański
Wydział Chemii
Katedra Chemii Analitycznej
Pracowania Chemii Supramolekularnej
ul. Wita Stwosza 63
80-308 Gdańsk
pawel.niedzialkowski@ug.edu.pl

Gdańsk, 28.11.2023

OŚWIADCZENIE

Jako współautor publikacji wchodzącej w skład rozprawy doktorskiej mgr Amandy Magdaleny Kulpa-Koterwa oświadczam, że mój wkład w publikację:

Kulpa A., Ryl J., Schroeder G., Koterwa A., Sein Anand J., Ossowski T., Niedziałkowski P.: Simultaneous voltammetric determination of Cd^{2+}, Pb^{2+}, and Cu^{2+} ions captured by Fe_3O_4@SiO_2 core-shell nanostructures of various outer amino chain length, *Journal of Molecular Liquids*, vol. 314, 2020, s. 1–11, DOI:10.1016/j.molliq.2020.113677

polegał na konceptualizacji, pomocy w planowaniu badań oraz redakcji manuskryptu.

Paweł Niedziałkowski

dr hab. Paweł Niedziałkowski
profesor Uniwersytetu Gdańskiego

Uniwersytet Gdański
Wydział Chemii
Katedra Chemii Analitycznej

prof. dr hab. inż. Tadeusz Ossowski
Uniwersytet Gdański
Wydział Chemii
Katedra Chemii Analitycznej
Pracowania Chemii Supramolekularnej
ul. Wita Stwosza 63
80-308 Gdańsk
tadeusz.ossowski@ug.edu.pl

Gdańsk, 28.11.2023

OŚWIADCZENIE

Jako współautor publikacji wchodzącej w skład rozprawy doktorskiej mgr Amandy Magdaleny Kulpa-Koterwa oświadczam, że mój wkład w publikację:

Kulpa A., Ryl J., Schroeder G., Koterwa A., Sein Anand J., Ossowski T., Niedziałkowski P.: Simultaneous voltammetric determination of Cd^{2+}, Pb^{2+}, and Cu^{2+} ions captured by Fe_3O_4@SiO_2 core-shell nanostructures of various outer amino chain length, Journal of Molecular Liquids, vol. 314, 2020, s. 1–11, DOI:10.1016/j.molliq.2020.113677

polegał na konsultacji w planowaniu badań elektrochemicznych.

KIEROWNIK
KATEDRY CHEMII ANALITYCZNEJ
Prof. dr hab. inż. Tadeusz Ossowski

dr hab. inż. Jacek Ryl, prof. PG
Politechnika Gdańska
Instytut Nanotechnologii i Inżynierii Materiałowej
Zakład Elektrochemii i Fizykochemii Powierzchni
ul. Narutowicza 11/12,
80-233 Gdańsk
jacryl@pg.edu.pl

Gdańsk, 28.11.2023

OŚWIADCZENIE

Jako współautor publikacji wchodzącej w skład rozprawy doktorskiej mgr Amandy Magdaleny Kulpa-Koterwa oświadczam, że mój wkład w publikację:

Kulpa A., **Ryl J.**, Schroeder G., Koterwa A., Sein Anand J., Ossowski T., Niedziałkowski P.: Simultaneous voltammetric determination of Cd^{2+}, Pb^{2+}, and Cu^{2+} ions captured by Fe_3O_4@SiO_2 core-shell nanostructures of various outer amino chain length, *Journal of Molecular Liquids*, vol. 314, 2020, s. 1–11, DOI:10.1016/j.molliq.2020.113677

polegał na wykonaniu badań techniką spektroskopii fotoelektronów w zakresie promieniowania X (XPS), interpretacji otrzymanych wyników oraz ich opisaniu w manuskrypcie.

mgr Adrian Koterwa
Uniwersytet Gdański
Wydział Chemii
Katedra Chemii Analitycznej
Pracowania Chemii Supramolekularnej
ul. Wita Stwosza 63
80-308 Gdańsk
adrian.koterwa@ug.edu.pl

Gdańsk, 28.11.2023

OŚWIADCZENIE

Jako współautor publikacji wchodzącej w skład rozprawy doktorskiej mgr Amandy Magdaleny Kulpa-Koterwa oświadczam, że mój wkład w publikację:

Kulpa A., Ryl J., Schroeder G., Koterwa A., Sein Anand J., Ossowski T., Niedziałkowski P.: Simultaneous voltammetric determination of Cd^{2+}, Pb^{2+}, and Cu^{2+} ions captured by Fe_3O_4@SiO_2 core-shell nanostructures of various outer amino chain length, *Journal of Molecular Liquids*, vol. 314, 2020, s. 1–11, DOI:10.1016/j.molliq.2020.113677

polegał pomocy w analizie oraz części wizualizacji wyników badań.

Koterwa Adrian

dr hab. Paweł Niedziałkowski, prof. UG
Uniwersytet Gdański
Wydział Chemii
Katedra Chemii Analitycznej
Pracowania Chemii Supramolekularnej
ul. Wita Stwosza 63
80-308 Gdańsk
pawel.niedzialkowski@ug.edu.pl

Gdańsk, 28.11.2023

OŚWIADCZENIE

Jako współautor publikacji wchodzącej w skład rozprawy doktorskiej mgr Amandy Magdaleny Kulpa-Koterwa oświadczam, że mój wkład w publikację:

Kulpa-Koterwa A., Ryl J., Górnicka K., Niedziałkowski P.: New nanoadsorbent based on magnetic iron oxide containing 1,4,7,10-tetraazacyclododecane in outer chain (Fe_3O_4@SiO_2– cyclen) for adsorption and removal of selected heavy metal ions Cd^{2+}, Pb^{2+}, Cu^{2+}, Journal of Molecular Liquids, vol. 368, nr pt. B, 2022, s. 1–11, DOI:10.1016/j.molliq.2022.120710

polegał na konceptualizacji, syntezie nanocząstek, pomocy w planowaniu badań oraz redakcji manuskryptu.

Paweł Niedziałkowski

dr hab. Paweł Niedziałkowski
profesor Uniwersytetu Gdańskiego

Uniwersytet Gdański
Wydział Chemii
Katedra Chemii Analitycznej

dr hab. inż. Jacek Ryl, prof. PG
Politechnika Gdańska
Instytut Nanotechnologii i Inżynierii Materiałowej
Zakład Elektrochemii i Fizykochemii Powierzchni
ul. Narutowicza 11/12,
80-233 Gdańsk
jacryl@pg.edu.pl

Gdańsk, 28.11.2023

OŚWIADCZENIE

Jako współautor publikacji wchodzącej w skład rozprawy doktorskiej mgr Amandy Magdaleny Kulpa-Koterwa oświadczam, że mój wkład w publikację:

Kulpa-Koterwa A., Ryl J., Górnicka K., Niedziałkowski P.: New nanoadsorbent based on magnetic iron oxide containing 1,4,7,10-tetraazacyclododecane in outer chain (Fe_3O_4@SiO_2– cyclen) for adsorption and removal of selected heavy metal ions Cd^{2+}, Pb^{2+}, Cu^{2+}, *Journal of Molecular Liquids*, vol. 368, nr pt. B, 2022, s. 1–11, DOI:10.1016/j.molliq.2022.120710

polegał na wykonaniu badań techniką spektroskopii fotoelektronów w zakresie promieniowania X (XPS), interpretacji otrzymanych wyników oraz ich opisaniu w manuskrypcie.

dr inż. Karolina Górnicka
Politechnika Gdańska
Instytut Nanotechnologii i Inżynierii Materiałowej
ul. Narutowicza 11/12,
80-233 Gdańsk
karolina.gornicka@pg.edu.pl

Gdańsk, 28.11.2023

OŚWIADCZENIE

Jako współautor publikacji wchodzącej w skład rozprawy doktorskiej mgr Amandy Magdaleny Kulpa-Koterwa oświadczam, że mój wkład w publikację:

Kulpa-Koterwa A., Ryl J., Górnicka K., Niedziałkowski P.: New nanoadsorbent based on magnetic iron oxide containing 1,4,7,10-tetraazacyclododecane in outer chain (Fe_3O_4@SiO_2– cyclen) for adsorption and removal of selected heavy metal ions Cd^{2+}, Pb^{2+}, Cu^{2+}, *Journal of Molecular Liquids*, vol. 368, nr pt. B, 2022, s. 1–11, DOI:10.1016/j.molliq.2022.120710

polegał na wykonaniu badań techniką XRD, interpretacji otrzymanych wyników oraz ich opisaniu w manuskrypcie.

Górnicka Karolina

dr hab. Paweł Niedziałkowski, prof. UG
Uniwersytet Gdański
Wydział Chemii
Katedra Chemii Analitycznej
Pracowania Chemii Supramolekularnej
ul. Wita Stwosza 63
80-308 Gdańsk
pawel.niedzialkowski@ug.edu.pl

Gdańsk, 28.11.2023

OŚWIADCZENIE

Jako współautor publikacji wchodzącej w skład rozprawy doktorskiej mgr Amandy Magdaleny Kulpa-Koterwa oświadczam, że mój wkład w publikację:

Kulpa-Koterwa A., Schroeder G., Ossowski T., Koterwa A., Niedziałkowski P.: Nanostruktury magnetyczne typu core-shell Fe_3O_4@SiO_2-N_n jako nowe adsorbenty jonów metali ciężkich Cd^{2+}, Pb^{2+} oraz Cu^{2+} – badania elektrochemiczne, Na pograniczu chemii, biologii i fizyki /Szłyk Edward [i in.] (red.), vol. 3, 2022, Wydawnictwo Naukowe Uniwersytetu Mikołaja Kopernika, ISBN 978-83-231-4836-4, s. 121–136

polegał na konceptualizacji, pomocy w planowaniu badań oraz redakcji manuskryptu.

Paweł Niedziałkowski

dr hab. Paweł Niedziałkowski
profesor Uniwersytetu Gdańskiego
Uniwersytet Gdański
Wydział Chemii
Katedra Chemii Analitycznej

prof. dr hab. inż. Tadeusz Ossowski
Uniwersytet Gdański
Wydział Chemii
Katedra Chemii Analitycznej
Pracowania Chemii Supramolekularnej
ul. Wita Stwosza 63
80-308 Gdańsk
tadeusz.ossowski@ug.edu.pl

Gdańsk, 28.11.2023

OŚWIADCZENIE

Jako współautor publikacji wchodzącej w skład rozprawy doktorskiej mgr Amandy Magdaleny Kulpa-Koterwa oświadczam, że mój wkład w publikację:

Kulpa-Koterwa A., Schroeder G., Ossowski T., Koterwa A., Niedziałkowski P.: Nanostruktury magnetyczne typu core-shell Fe_3O_4@SiO_2-N_n jako nowe adsorbenty jonów metali ciężkich Cd^{2+}, Pb^{2+} oraz Cu^{2+} – badania elektrochemiczne, Na pograniczu chemii, biologii i fizyki /Szłyk Edward [i in.] (red.), vol. 3, 2022, Wydawnictwo Naukowe Uniwersytetu Mikołaja Kopernika, ISBN 978-83-231-4836-4, s. 121–136

polegał na konsultacji w planowaniu badań elektrochemicznych.

KIEROWNIK
KATEDRY CHEMII ANALITYCZNEJ
Prof. dr hab. inż. Tadeusz Ossowski

mgr Adrian Koterwa
Uniwersytet Gdański
Wydział Chemii
Katedra Chemii Analitycznej
Pracowania Chemii Supramolekularnej
ul. Wita Stwosza 63
80-308 Gdańsk
adrian.koterwa@ug.edu.pl

Gdańsk, 28.11.2023

OŚWIADCZENIE

Jako współautor publikacji wchodzącej w skład rozprawy doktorskiej mgr Amandy Magdaleny Kulpa-Koterwa oświadczam, że mój wkład w publikację:

Kulpa-Koterwa A., Schroeder G., Ossowski T., Koterwa A., Niedziałkowski P.: Nanostruktury magnetyczne typu core-shell Fe_3O_4@SiO_2-N_n jako nowe adsorbenty jonów metali ciężkich Cd^{2+}, Pb^{2+} oraz Cu^{2+} – badania elektrochemiczne, Na pograniczu chemii, biologii i fizyki /Szłyk Edward [i in.] (red.), vol. 3, 2022, *Wydawnictwo Naukowe Uniwersytetu Mikołaja Kopernika*, ISBN 978-83-231-4836-4, s. 121–136

polegał na współudziale w opracowaniu części danych pomiarowych.

Koterwa Adrian